

Electronic Thesis and Dissertation Repository

---

11-24-2014 12:00 AM

## Studies In Small Scale Thermal Convection

Daniel F. Stranges

*The University of Western Ontario*

Supervisor

Dr. Roger E. Khayat

*The University of Western Ontario*

Graduate Program in Mechanical and Materials Engineering

A thesis submitted in partial fulfillment of the requirements for the degree in Doctor of Philosophy

© Daniel F. Stranges 2014

Follow this and additional works at: <https://ir.lib.uwo.ca/etd>



Part of the [Other Mechanical Engineering Commons](#)

---

### Recommended Citation

Stranges, Daniel F., "Studies In Small Scale Thermal Convection" (2014). *Electronic Thesis and Dissertation Repository*. 2548.

<https://ir.lib.uwo.ca/etd/2548>

This Dissertation/Thesis is brought to you for free and open access by Scholarship@Western. It has been accepted for inclusion in Electronic Thesis and Dissertation Repository by an authorized administrator of Scholarship@Western. For more information, please contact [wlsadmin@uwo.ca](mailto:wlsadmin@uwo.ca).

STUDIES IN SMALL SCALE THERMAL CONVECTION

(Thesis Format: Integrated Article)

by

Daniel F. Stranges

Graduate Program in Engineering Science,  
Department of Mechanical and Materials Engineering

A thesis submitted in partial fulfillment  
of the requirements for the degree of  
Doctor of Philosophy

The School of Graduate and Postdoctoral Studies  
The University of Western Ontario  
London, Ontario, Canada

© Daniel Stranges 2015

## Abstract

The effect of non-Fourier heat transfer and partial-slip boundary conditions in Rayleigh-Bénard are analyzed theoretically. Non-Fourier fluids possess a relaxation time that reflects the delay in the response of the heat flux to a change in the temperature gradient while the partial slip boundary condition assumes that the fluid velocity and temperature are not equal to that of the wall. Both non-Fourier and partial-slip effects become important when small-scale heat transfer applications are investigated such as convection around micro- and nano-devices as suggested by the extended heat transport equations from kinetic theory. Other applications are also known to exhibit one or both of these effects such as low-temperature liquids, nanofluids, granular flows, rarefied gases and polymer flows. Small scale effects are measured by the Knudsen number. From this, non-Fourier effects can be estimated, measured non-dimensionally by the Cattaneo number and modelled using the frame indifferent Cattaneo-Vernotte equation which is derived from Oldroyd's upper-convected derivative. Linear stability of non-Fourier fluids shows that the neutral stability curve possesses a stationary Fourier branch and an oscillatory branch intersecting at some wave number, where for small relaxation time, no change in stability is expected from that of a Fourier fluid. As the relaxation time increases to a critical value, both stationary and oscillatory convection become equally probable. Past this value, oscillatory instability is expected to occur at a smaller Rayleigh number and larger wave number than for a Fourier fluid. Non-linear analysis of weakly non-Fourier fluids shows that near the onset of convection, the convective roll intensity is stronger than for a Fourier fluid. The bifurcation to convection changes from subcritical to supercritical as the Cattaneo number increases and the instability of the convection state for a non-Fourier fluid is shown to occur via a Hopf bifurcation at lower Rayleigh number and higher Nusselt number than for a Fourier fluid. When hydrodynamic slip and temperature jump boundary conditions are considered, a significant reduction in the minimum critical Rayleigh number and corresponding wave number are found. Depending on the sign used for second-order coefficients, critical conditions can be greater than or less than that for first-order boundary conditions.

## Keywords

Rayleigh-Bénard, non-Fourier, partial slip, small scale, Rayleigh number, Knudsen number, Lorenz model, nanofluids

## Co-Authorship Statement

I hereby declare co-authorship in the following chapters:

Chapter 2 is the journal article published by the International Journal of Thermal Science. D.F. Stranges wrote the article, R.E. Khayat played a supervisory and editing role, and B. Albaalbaki solely wrote chapter 2.5.4. The complete reference is:

D.F. Stranges, R.E. Khayat and B. Albaalbaki, “Thermal convection of non-Fourier fluids. Linear Stability,” *Int. J. Thermal Sci.*, vol. 74, pp. 14-23, 2013.

Chapter 3 will be submitted for publication under the co-authorship D.F. Stranges, John R. de Bruyn and R.E. Khayat.

Chapter 4 will be submitted for publication under the co-authorship D.F. Stranges, John R. de Bruyn and R.E. Khayat.

## Acknowledgments

I would like to express my gratitude and appreciation to my supervisor Dr. Roger Khayat for his assistance and support, as well as pushing me to expand my knowledge and experience past what I thought myself capable. Special thanks is due to Dr. John de Bruyn who graciously took the time to offer valuable guidance and fresh perspective. Many thanks are also given to my colleagues for their encouragement and for making the office as enjoyable a place as possible. Finally, to my friends and family, who, without their immense patience and reinforcement, I would not have had the strength to complete this PhD.

# Table of Contents

Abstract .....	ii
Co-Authorship Statement.....	iv
Acknowledgments.....	v
Table of Contents .....	vi
List of Tables .....	ix
List of Figures .....	x
Nomenclature .....	xiv
Chapter 1 .....	1
1 Introduction .....	1
1.1 Objective .....	1
1.2 Heat Transport .....	1
1.3 Rayleigh-Bénard Convection.....	3
1.4 Fourier vs non-Fourier behaviour .....	5
1.5 Breakdown of Fourier's law and the generalized non-Fourier equation for fluids	11
1.6 Breakdown of the No-Slip Boundary Condition .....	16
1.7 Linear Stability and Steady State Analysis .....	19
1.8 Motivation.....	22
1.9 Thesis Summary.....	22
1.10References .....	23
Chapter 2.....	32
2 Thermal convection of non-Fourier fluids. Linear stability.....	32
2.1 Introduction.....	32
2.2 Constitutive equation for heat.....	34
2.3 Governing equations and boundary conditions.....	35

2.4	Linear stability analysis .....	39
2.5	Results and discussion .....	44
2.5.1	Stability of the conduction state.....	45
2.5.2	Further influence of the Prandtl number.....	52
2.5.3	Overstability threshold.....	54
2.5.4	Mechanism behind oscillatory convection in non-Fourier fluids .....	58
2.6	Concluding remarks .....	60
2.7	Acknowledgements.....	60
2.8	References.....	61
Chapter 3.....		67
3	Thermal convection of fluids with non-Fourier heat transport .....	67
3.1	Introduction.....	67
3.2	The Mathematical Model.....	69
3.2.1	Governing equations and boundary conditions.....	69
3.2.2	Development of the Dynamical System .....	72
3.3	Linear Stability Analysis of the Conduction State.....	74
3.4	Steady State Solutions.....	78
3.5	Linear Stability Analysis of the Steady State Convection .....	84
3.6	Heat Transport .....	88
3.7	Discussion.....	91
3.8	Conclusion .....	95
3.9	Acknowledgements.....	96
3.10	References.....	96
Chapter 4.....		101
4	The influence of second order partial slip boundary conditions on thermal convection .....	101



4.1 Introduction.....	101
4.2 Governing equations and boundary conditions.....	104
4.2.1 Development of the Dynamical System .....	109
4.3 Linear Stability Analysis of the Conduction State.....	110
4.4 Results and Discussion .....	114
4.4.1 First-Order Slip.....	114
4.4.2 Second-Order Slip.....	123
4.5 Conclusion .....	129
4.6 Acknowledgements.....	130
4.7 References.....	130
Chapter 5.....	133
5 Conclusions .....	133
5.1 Conclusion .....	133
5.2 Future Work .....	135
5.3 References.....	136
Curriculum Vitae .....	138

## List of Tables

Table 1 - Cattaneo number for some common gases (mean free paths are from [42]).....	94
Table 2 - Slip coefficients developed by [8] and [12] for second-order hydrodynamic slip and first-order temperature jump. ....	113

## List of Figures

Figure 1.1 – 2D Rayleigh-Benard convection diagram showing the roll pattern formed after the loss of stability of the conduction state. Image from [6]. .....	3
Figure 1.2 – Temperature $t$ vs position $x$ for Fourier heat transfer in a 1D rod.....	7
Figure 1.3 - Temperature, $t$ vs position, $x$ for non-Fourier heat transfer in a 1D rod. The temperature distribution propagates outward with a finite speed.....	9
Figure 1.4 - Temperature $T$ vs time $t$ for $x = 0.5$ with varying $C$ . As $C$ increases, damped oscillations appear, eventually reaching the steady state.....	10
Figure 1.5 - Comparison of first- and second-order slip effects with the no slip boundary condition. Bold lines denote the upper and lower surface. $l_{s1}$ and $l_{s2}$ denote the slip length for first- and second-order effects, respectively. ....	18
Figure 2.1 - Schematic illustrating notations used in the $(Ra-k)$ plane, qualitatively showing various marginal stability curves and corresponding regimes with respect to the critical Cattaneo number, $C_H$ . The curves 1, 2, 3, 4 and 5 correspond to $C \ll C_H$ , $C < C_H$ , $C = C_H$ , $C > C_H$ , $C \gg C_H$ . ....	45
Figure 2.2 - Influence of the Cattaneo number on (a) the marginal stability curves in the $Ra-k$ plane and (b) corresponding oscillation frequency for a $Pr = 10$ .....	46
Figure 2.3 - Influence of $Pr$ and $C$ on (a) the minimum critical Rayleigh number, $Ra_m$ , (b) corresponding wave number, $k_m$ , and (c) frequency, $\omega_m$ , in the absence of retardation.....	49
Figure 2.4 - Influence of the Cattaneo and Prandtl numbers on (a) the Rayleigh number, $Ra_i$ , and (b) wave number, $k_i$ , at the intersection between the steady and oscillatory marginal stability branches. ....	54
Figure 2.5 - Influence of the Prandtl number on (a) the critical Cattaneo number, $C_H$ , (b) the corresponding wave number, $k_H$ , and (c) the oscillation frequency, $\omega_H$ .....	56

Figure 2.6 - Distribution of $j$ at $z = 0.5$ for a Fourier ( $C = 0$ ) and a non-Fourier fluid ( $C = 0.5$ ). .....	59
Figure 3.1 - Marginal stability curves for the onset of convection in a non-Fourier fluid for several values of the Cattaneo number $C$ . $Pr = 10$ in all cases. The Fourier stability boundary ( $C = 0$ ) is shown by a heavier line. The weakly non-Fourier region corresponds to $C < 0.0651$ , and the strongly non-Fourier region to $C > 0.0651$ . .....	77
Figure 3.2 – Steady state convection amplitude as a function of $Ra$ . The heavier curve represents $C = 0$ , and the fine curves are, from right to left: $C = 0.01, 0.02, 0.03, 0.04$ and $0.05$ . Solid lines are linearly stable states, and dashed lines are linearly unstable. The stars indicate the point of at which the steady convection state becomes unstable, as discussed in the text.....	80
Figure 3.3 - The limiting amplitude of the steady state convection branch as $Ra$ goes to infinity plotted as a function of $C$ . .....	81
Figure 3.4 – a) The minimum value of $X$ and b) $Ra_m$ on the subcritical bifurcation curves for values of $C$ in the weakly non-Fourier regime.....	84
Figure 3.5 – $Ra^*$ vs $C$ . The solid line represents the region in which the bifurcation from conduction to convection is supercritical and dotted line represents the subcritical bifurcation regime. The horizontal line represents $Ra_{cF}$ . The inset shows the same data, but with a logarithmic x-axis. ....	85
Figure 3.6 – The convection amplitude, $X$ , for a Fourier and a non-Fourier fluid at the Rayleigh number $Ra^*$ at which the steady convection state becomes unstable. The inset shows the difference $X_{NF}-X_F$ at $Ra^*$ .....	86
Figure 3.7 – $\sigma_r$ vs $Ra$ near the loss of stability of the steady convection state at $Ra^*$ for $C = 0.01$ . The vertical line shows $Ra^*$ , at which $\sigma_r = 0$ . .....	87
Figure 3.8 - $Ra^*$ as a function of $C$ for two values of $Pr$ . The inset is a log-log plot of the same data.....	88
Figure 3.9 - $Nu$ vs $Ra$ showing the point of instability for $Pr = 10$ ( $\bullet$ ) and $Pr = 1$ ( $\times$ ). .....	90

Figure 4.1 - Slip length for no-slip and first-order partial slip boundary conditions..... 102

Figure 4.2 - Comparison of first- and second-order slip effects on Poiseuille flow.  $l_{s1}$  and  $l_{s2}$  denote the slip length for first- and second-order slip, respectively. .... 104

Figure 4.3 – The influence of first-order hydrodynamic slip on the Rayleigh number,  $Ra_c$ , vs wave number,  $k_c$ , for varying Kn and  $a_1 = 1$ . From top to bottom, Kn = 0.001, 0.01, 0.1, 1 and 10..... 114

Figure 4.4 – The effect of first-order hydrodynamic slip with  $a_1 = 1$  on a) the minimum critical Rayleigh number and b) the corresponding critical wave number vs Kn. The inset to (a) shows the same results for  $Ra_{cm}$  but with a linear scale on the Knudsen axis. .... 116

Figure 4.5 – The influence of first-order temperature jump on the Rayleigh number,  $Ra_c$ , vs wave number,  $k_c$ , for varying Kn and  $b_1 = 1$ . From top to bottom, Kn = 0.001, 0.01, 0.1, 1 and 10..... 117

Figure 4.6 - Real convection cell (solid horizontal lines) and no-slip linear temperature profile (solid line). Temperature profile with jump (dashed line) is extrapolated by a slip length  $l_s$  to either side such that it has no temperature jump at the extrapolated cell (dashed horizontal lines). .... 118

Figure 4.7 - Onset of convection for the extrapolated cell. The temperature is shown by the dashed line and the infinitesimal velocity profile is shown by the solid line. Both temperature and velocity profile are no-slip for the extrapolated cell but not the real fluid cell..... 119

Figure 4.8 – The effect of first-order temperature jump on a) the minimum critical Rayleigh number and b) the corresponding critical wave number vs Kn for  $b_1 = 1$ . .... 120

Figure 4.9 – The effect of both first-order hydrodynamic slip and first-order temperature jump (solid line) on a) the minimum critical Rayleigh number and b) the corresponding critical wave number vs Kn. The short dashed line shows the results for first-order hydrodynamic slip only and the long dashed line is for a first-order temperature jump only. .... 122

Figure 4.10 – The influence of second-order hydrodynamic slip effects on the critical Rayleigh number,  $R_{ac}$ , vs wave number,  $kc$ , for varying  $Kn$  with  $a_1 = 1$  and  $a_2 = -9/8$ . From top to bottom,  $Kn = 0.001, 0.01, 0.1, 1$  and  $10$ . ..... 123

Figure 4.11 – The effect of second-order hydrodynamic slip effects (solid line) with coefficients proposed by [12] on a) the minimum critical Rayleigh number and b) the corresponding critical wave number vs  $Kn$  with  $a_1 = 1$  and  $a_2 = -9/8$ . Dashed line indicates solution for first-order hydrodynamic slip. .... 125

Figure 4.12 – The effect of second-order hydrodynamic slip effects with coefficients proposed by [8] where  $a_1 = 1$  and  $a_2 = 0.5$  on a) the minimum critical Rayleigh number and b) the corresponding critical wave number vs  $Kn$ . .... 126

Figure 4.13 - For the combined effects of  $a_1 = 1, a_2 = -9/8$  and  $b_1 = 1$  (solid line), the a) minimum critical Rayleigh number vs  $Kn$  and b) corresponding critical wave number vs  $Kn$ . Dashed curve represents combined contribution from first-order velocity slip and temperature jump where  $a_1 = 1$  and  $b_1 = 1$ . .... 128

## Nomenclature

$a$	Simplification parameter proportional to $1/C$
$a_n$	Hydrodynamic slip coefficient
$b_n$	Temperature jump coefficient
$b$	Simplification parameter
$C$	Cattaneo number
$D$	Gap size, m
$f$	Particle distribution function
$g$	Gravitational acceleration, $m/s^2$
$c_p$	Specific heat at constant pressure, $J/kg\ K$
$Gr$	Grashof number, $Ra/Pr$
$i$	Imaginary number, $\sqrt{-1}$
$j$	Divergence of heat flux (dimensionless)
$k$	Horizontal wave number, $1/m$
$K$	Thermal conductivity, $W/m^2\ K$
$Kn$	Knudsen number
$l_s$	Slip length, m
$m$	Particle mass, kg
$Nu$	Nusselt number
$P$	Pressure, Pa

Pr	Prandtl number, $\nu/\kappa$
Q	Heat flux, W/m K
$q_n$	Vertical wave numer, 1/m
Ra	Rayleigh number, $\delta T \alpha_T g D^3 / \nu \kappa$
t	Time, s
T	Temperature, K
$\delta T$	Temperature difference between upper and lower boundaries, K
V	Velocity, m/s
u	Horizontal velocity
U	Internal energy
w	Vertical velocity, m/s
x	Horizontal direction
X	Scaled $\psi_1$ , $m^2/s$
Y	Scaled $\theta_1$ , K
Z	Scaled $\theta_2$ , K
z	Vertical direction

### Greek Symbols

$\alpha_T$	Thermal expansion coefficient, 1/K
$\beta$	$\pi^2 + k^2$
$\theta$	Temperature deviation from steady state, K



$\zeta$	Tangential momentum accommodation coefficient
$\gamma$	Specific heat ratio
$\kappa$	Thermal diffusivity, $\text{m}^2/\text{s}$
$\lambda$	Mean free path, $\text{m}$
$\mu$	Dynamic viscosity, $\text{kg}/\text{ms}$
$\nu$	Kinematic viscosity, $\text{m}^2/\text{s}$
$\rho$	Density, $\text{kg}/\text{m}^3$
$\sigma$	Eigenvalue
$\tau$	Relaxation time, $\text{s}$
$\psi$	Stream function, $\text{m}^2/\text{s}$
$\omega$	Imaginary part of $\sigma$

#### Subscripts

c	Critical
B	Base state
F	Fourier condition
H	Hopf condition
i	Intersection
inf	Infinity, asymptotic condition
m	Minimum
n	Mode number
NF	Non-Fourier condition
o	Reference
sub	Subcritical
w	Wall
r	Real

# Chapter 1

## 1 Introduction

### 1.1 Objective

The main objective of this thesis is to investigate thermal convection in fluids in a small gap, particularly in a Rayleigh-Bénard configuration. As the gap size decreases, both non-Fourier heat transfer and partial slip boundary conditions are expected to be important. The main questions to be answered are how the onset of convection and the critical wave number will be affected by the small length scale. The properties of the steady state convective flow for a fluid with non-Fourier character will also be explored. Emphasis will be put on the deviation of the flow properties and heat transfer from that of a fluid that possesses Fourier heat transfer.

### 1.2 Heat Transport

The interaction between energy and matter is a complex area of study, having an effect on all aspects of day-to-day life, nature and engineering applications. Energy can take many different forms including thermal, kinetic, potential, and chemical, to name only a few. Thermal energy is one of the most interesting types of energy, especially to mechanical engineers. Thermal energy from the sun drives our weather systems and is part of the by-product of nearly every invention man has created. Thermal energy can be detrimental to functionality if not removed properly and thus the topic of its transport is studied vigorously.

The most basic method of heat transport is conduction. Pure conduction (diffusion) results in a medium with no bulk motion. Here, the microscopic collisions of particles due to a temperature gradient transfer energy from more energetic particles, to less energetic particles [1], [2]. Translational, internal rotational and vibrational motions are all related to the measure of energy of a given particle. High energy particles are associated with high temperatures and as a result, energy is always transferred from hot

to cold. Heat transfer via conduction is typically described by Fourier's law, which is given by

$$\mathbf{Q} = -K\nabla T. \quad (1.2.1)$$

Here,  $\mathbf{Q}$  is the heat flux,  $K$  is the thermal conductivity of the medium, and  $T$  is the temperature. Conduction is the primary method of heat transport within solids where the net motion of the particles within the medium is zero.

Thermal energy can also be transported due to the bulk motion of the medium. When this method of energy transport is considered exclusive of the microscopic collisions of the particles, it is known as advection. Advection is only theoretically possible within a fluid medium since these microscopic collisions will always occur. Thus, researchers are primarily interested in the combination of conduction and advection, known as convection. In the presence of a velocity field, the equation for the conservation of energy is

$$\rho c_p (T_t + \mathbf{V} \cdot \nabla T) = -\nabla \cdot \mathbf{Q}, \quad (1.2.2)$$

where  $\rho$  is the density,  $c_p$  is the specific heat at constant pressure,  $\mathbf{V}$  is the velocity vector and a subscript  $t$  denotes a partial differentiation with time. The second term on the left hand side is the advection term, and the right hand side describes pure conduction when Eq. (1.2.1) is substituted for  $\mathbf{Q}$ . As a result of the particles ability to travel more freely, convection heat transfer is commonly explored in fluids. The applications here are endless, for example cooling of mechanical and electrical devices, the human body, weather systems, ocean currents and more.

Finally, heat transfer can also occur via radiation. Radiation is special in that it needs no material medium in order to transport energy since it uses electromagnetic waves, or photons [1]. The Stefan-Boltzmann law describes the radiation emitted from a surface, given by Eq. (1.2.3),

$$q = \epsilon \sigma_R T_s^4, \quad (1.2.3)$$

where  $\varepsilon$  is the emissivity of the medium,  $\sigma_R$  is the Stefan-Boltzmann constant ( $5.67 \times 10^{-8}$ ), and  $T_s$  is the absolute temperature of the surface. All objects above absolute zero transfer heat to their surroundings through radiation and also absorb thermal energy due to thermal radiation from other bodies. Consequently, radiation is technically a part of every heat transfer problem, however its effects may be negligible and are often ignored unless temperature differences are high [3].

### 1.3 Rayleigh-Bénard Convection

Convection heat transfer exists in two forms: forced and natural. Forced convection exists when an external force such as a pump drives fluid flow. Natural convection is a buoyancy-driven phenomena caused by density variations induced by a temperature gradient. Natural convection is convenient to study due to its theoretical and experimental simplicity [4], as well its importance in everyday natural phenomena [5]. The most common natural convection configuration is known as Rayleigh-Bénard, shown in Fig. 1.1.

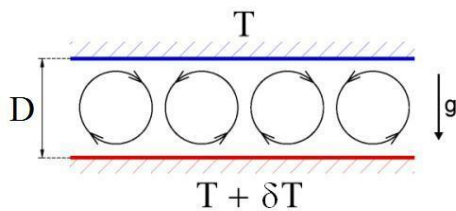


**Figure 1.1 – 2D Rayleigh-Benard convection diagram showing the roll pattern formed after the loss of stability of the conduction state. Image from [6].**

This configuration is defined by a thin layer of fluid confined between two infinite horizontal plates maintained at fixed temperatures where the lower plate is maintained at a temperature difference  $\delta T$  higher than the upper plate. If  $\delta T$  is low enough, viscous effects keep the fluid layer motionless despite the fact that the lower fluid layers are lighter due to gravity and thermal expansion. This is defined as the steady conduction state and a linear temperature profile develops between the upper and lower boundaries. As the temperature difference between the plates increases through a critical limit, the buoyancy effects overcome the viscous effects and some form of convection sets in.

The equations governing Rayleigh-Bénard convection of a two dimensional incompressible fluid in the  $x,z$ -plane are the equations of continuity and Navier-Stokes, respectively given by

$$\nabla \cdot \mathbf{V} = 0, \quad (1.3.1)$$

$$\rho(\mathbf{V}_t + \mathbf{V} \cdot \nabla \mathbf{V}) = -\nabla P - \rho g \hat{\mathbf{z}} + \mu \Delta \mathbf{V}, \quad (1.3.2)$$

along with the energy equation and Fourier's law given by Eqs. (1.2.1-1.2.2). Here,  $P$  is the pressure,  $g$  is the acceleration due to gravity,  $\hat{\mathbf{z}}$  is a unit vector in the vertical direction and  $\mu$  is the dynamic viscosity. The Navier-Stokes equation assumes that the fluid stresses are Newtonian in nature, where the viscous stresses vary linearly with the rate of strain [7].

As previously stated, variations in density drive the convective flow. This is generally modeled by the Boussinesq approximation, which states that the temperature induced density variations are negligible everywhere in the conservation equations except in the buoyancy term in the Navier-Stokes equation [8].

To study this form of convection, boundary conditions are required on the upper and lower surfaces. Mathematically, free-free boundary conditions can be used on the velocity, where the normal derivative of the tangential fluid velocity is zero, physically corresponding to zero shear stress at the fluid-solid interface. Although this is the least physical boundary condition, free-free conditions are mathematically convenient and no qualitative change in behaviour is expected if one set of boundary conditions is used over another [5]. Practically, no-slip boundary conditions are used, where the fluid velocity at the fluid-solid interface is equal to that of the solid surface. The same boundary condition is generally used for the temperature, where the temperature of the fluid immediately in contact with the boundary is assumed to be the same temperature as the boundary.

The simplest model of Rayleigh-Bénard convection is the Lorenz model [9]. Using stress-free boundary conditions and the Boussinesq approximation, Lorenz solved Eqs. (1.2.1-1.2.2) and Eqs. (1.3.1-1.3.2) by using a truncated Fourier series to represent the

velocity and temperature fields. A minimum of one Fourier mode was kept related to the velocity, along with two modes for the temperature in order to preserve non-linearities. After a Galerkin projection to eliminate the dependence of  $x$  and  $z$ , the resulting system is

$$\begin{aligned} X_t &= -\text{Pr}(X + \text{Ra}Y) \\ Y_t &= -XZ - \frac{X}{\text{Ra}_{\text{cF}}} - Y \\ Z_t &= XY - bZ \end{aligned} \quad (1.3.3)$$

where the non-dimensional Rayleigh number and Prandtl number are  $\text{Ra} = \frac{\delta T g \alpha_T D^3}{\nu \kappa}$  and

$\text{Pr} = \frac{\nu}{\kappa}$ , respectively.  $b$  is a strictly positive scaling coefficient,  $\text{Ra}_{\text{cF}}$  is the critical

Rayleigh number for the loss of stability of the steady conduction state, and  $X$ ,  $Y$  and  $Z$  are the Fourier modes related to the velocity and temperature. In the Rayleigh number,  $\nu = \mu / \rho$  is the kinematic viscosity and  $\alpha_T$  is the thermal expansion coefficient. This system of ordinary differential equations is a simplified model for atmospheric convection. It also possesses chaotic solutions, which under the right conditions, produces the Lorenz attractor, otherwise known as the butterfly effect.

As with any mathematical model, assumptions are made that are normally highly accurate. Two assumptions that are commonly made, which we will seek to implement more accurately, are Fourier's law and the no-slip boundary condition on the velocity and temperature.

## 1.4 Fourier vs non-Fourier behaviour

When Fourier's law is combined with the conservation of energy equation Eq. (1.2.2) for zero flow, the diffusion equation

$$\frac{\partial T}{\partial t} = \kappa \frac{\partial^2 T}{\partial x^2} \quad (1.4.1)$$

is generated where  $\kappa = K/\rho c_p$  is the thermal diffusivity. Eq. (1.4.1) may be cast into non-dimensional form by scaling length, time and temperature by  $L$ ,  $L^2/\kappa$ , and  $T_0$ ,

respectively, where  $T_0$  is a reference temperature. The resulting non-dimensional equation is

$$\frac{\partial T}{\partial t} = \frac{\partial^2 T}{\partial x^2}. \quad (1.4.2)$$

In order to illustrate the properties of Fourier heat conduction, consider a rod of length  $L = 1$  subject to the following conditions:

$$\begin{aligned} T(0, t) &= 1 \\ T(1, t) &= 0 \\ T(x < 0.1, t = 0) &= \cos(5\pi x) \\ T(x > 0.1, t = 0) &= 0 \end{aligned} \quad (1.4.3)$$

Using the method of separation of variables [10], the solution to Eq. (1.4.2) is

$$T(x, t) = 1 - x + \sum_{n=0}^{\infty} \left[ \frac{1 - \cos\left(\frac{n+5}{10}\pi\right)}{\pi(n+5)} + \frac{1 - \cos\left(\frac{n-5}{10}\pi\right)}{\pi(n-5)} - \frac{2}{n\pi} \right] \sin(n\pi x) e^{-n^2\pi^2 t} \quad (1.4.4)$$

where  $n$  is the mode number of the Fourier series. This is depicted by Fig. 1.2, which shows the solution  $T$  vs  $x$  for different times,  $t$ . Here, the non-zero heat profile diffuses out to the rest of the rod, eventually achieving a linear profile between the  $x = [0, 1]$ .

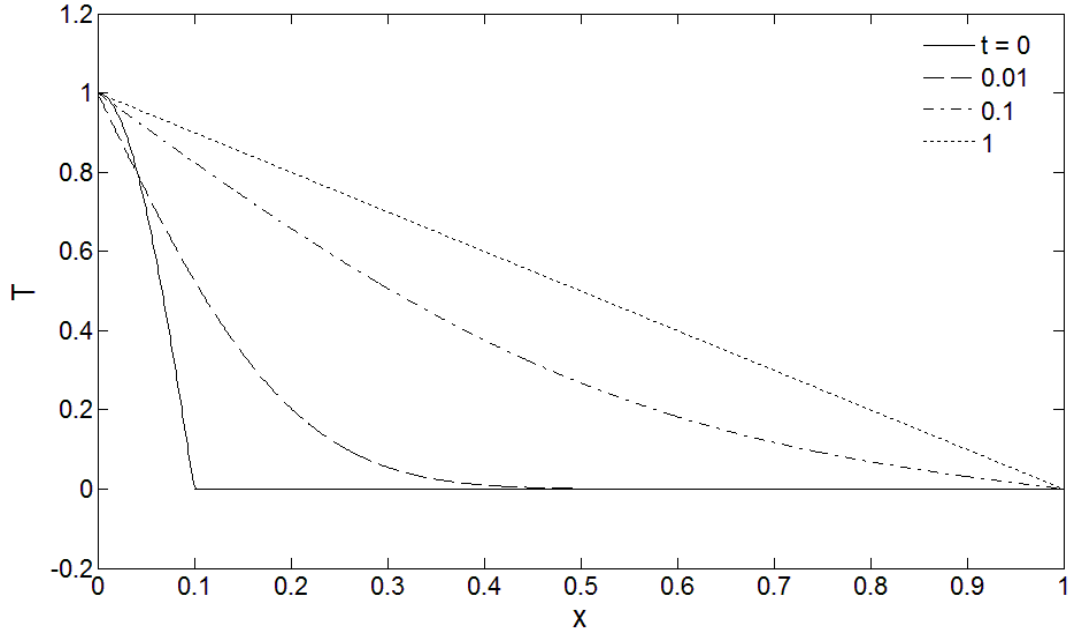


**Figure 1.2 – Temperature  $t$  vs position  $x$  for Fourier heat transfer in a 1D rod,  $n = 1000$**

Although difficult to see, this solution unrealistically predicts an infinite speed of heat propagation since even for small times,  $T > 0$  everywhere. This implies that some energy from  $x = 0.1$  instantaneously travels to the rest of the bar. Physically, a temperature disturbance propagates by molecular interaction, and thus should possess a finite speed [2].

The most basic characterization of the finite speed is given by the Maxwell-Cattaneo Eq. (1.4.5) [11], where a partial time derivative has been added to the left-hand side of Eq. (1.2.1):

$$\tau \frac{\partial \mathbf{Q}}{\partial t} + \mathbf{Q} = -K \nabla T. \quad (1.4.5)$$

$\tau$  is the thermal relaxation time of the medium and characterizes the temporal relaxation of the heat flux to a new steady state after a perturbation to the temperature field. This results in a hyperbolic differential equation that yields a wave-like heat transport equation when combined with Eq. (1.2.2), shown in non-dimensional form by



$$C \frac{\partial^2 T}{\partial t^2} + \frac{\partial T}{\partial t} = \frac{\partial^2 T}{\partial x^2}. \quad (1.4.6)$$

Here,  $C = \frac{\tau \kappa}{L^2}$  is the Cattaneo number which is proportional to the relaxation time. For a

hyperbolic equation such as Eq. (1.4.6), the speed of the temperature propagation is  $\sqrt{\frac{\kappa}{\tau}}$

[2], [12] which will decrease for increasing relaxation time. Again, using the method of separation of variables and adding the initial condition

$$\frac{\partial T}{\partial t}(x, t=0) = 0, \quad (1.4.7)$$

the following solution is obtained,

$$T(x, t) = 1 - x + \sum_{n=0}^{\infty} \sin(n\pi x) \frac{1}{r_2 - r_1} \left[ \frac{1 - \cos\left(\frac{n+5}{10}\pi\right)}{\pi(n+5)} + \frac{1 - \cos\left(\frac{n-5}{10}\pi\right)}{\pi(n-5)} - \frac{2}{n\pi} \right] \left[ r_2 e^{r_1 t} - r_1 e^{r_2 t} \right] \quad (1.4.8)$$

$$r_{1,2} = \frac{-1 \pm \sqrt{1 - 4n^2 \pi^2 C}}{2C}$$

where  $r_1$  and  $r_2$  are the characteristic values of the temporal solution in the method of separation of variables. Due to the definition of  $r_1$  and  $r_2$ , there will always be some oscillatory or wave-like behaviour for  $C > 0$ . For small  $C$ , oscillatory effects will not appear until  $n$  becomes large, at which point the effect on the solution will be small. When  $C$  is large, the low-order modes will contain oscillatory effects and their influence in the solution will be large.

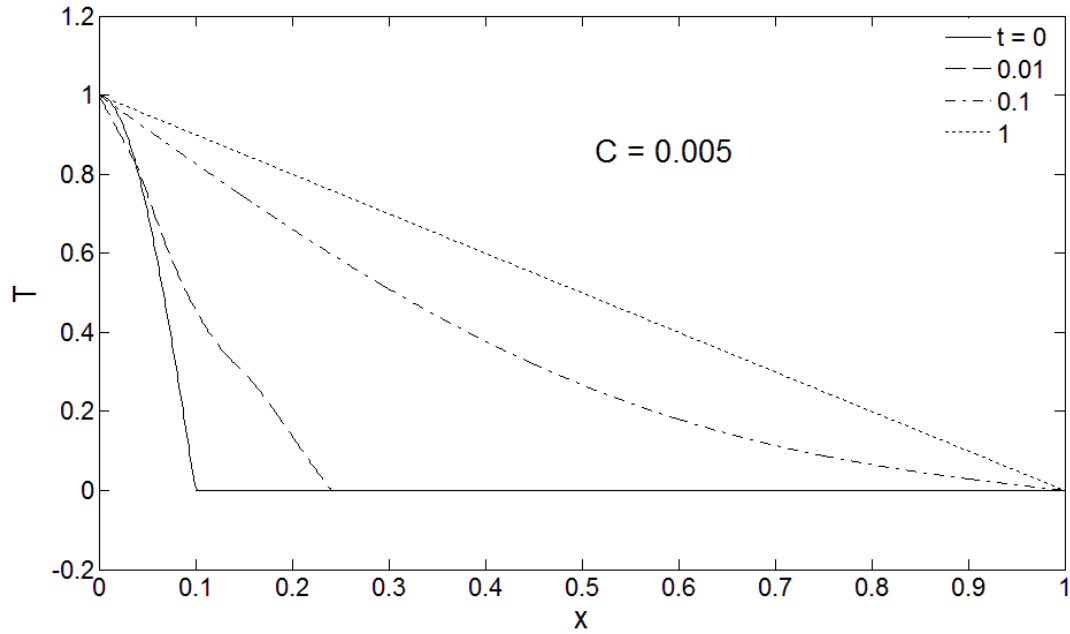


**Figure 1.3 - Temperature,  $t$  vs position,  $x$  for non-Fourier heat transfer in a 1D rod. The temperature distribution propagates outward with a finite speed,  $n = 1000$ .**

The solution to the wave equation shown by Fig. 1.3 for  $\tau > 0$  characterizes the physical response more realistically. The temperature far from  $x = 0.1$  is not immediately greater than zero. The non-zero initial condition travels outward as a wave, showing the effect of molecular interaction.

Non-Fourier heat transfer can also lead to oscillatory solutions. Consider, again, a 1D rod of length 1, subject to the following boundary and initial conditions:

$$T(0, t) = 1$$

$$T(1, t) = 0$$

$$T(x, t = 0) = \cos\left(\frac{\pi x}{2}\right) \quad . \quad (1.4.9)$$

$$\frac{\partial T}{\partial t}(x, t = 0) = -\frac{\pi^2}{4} \cos\left(\frac{\pi x}{2}\right)$$

The solution to Eq. (1.4.6) subject to these boundary conditions is

$$T(x, t) = 1 - x + \sum_{n=0}^{\infty} \sin(n\pi x) \left[ A_n e^{r_1 t} + B_n e^{r_2 t} \right]$$

$$A_n = \left[ \frac{r_2}{r_2 - r_1} \right] \left[ \frac{\pi - 4r_2}{\pi(n+0.5)} + \frac{\pi - 4r_2}{\pi(n-0.5)} - \frac{2}{n\pi} \right]$$

$$B_n = \frac{-1}{\pi(n+0.5)} - \frac{1}{\pi(n-0.5)} - \frac{2}{n\pi} - B_n$$
(1.4.10)

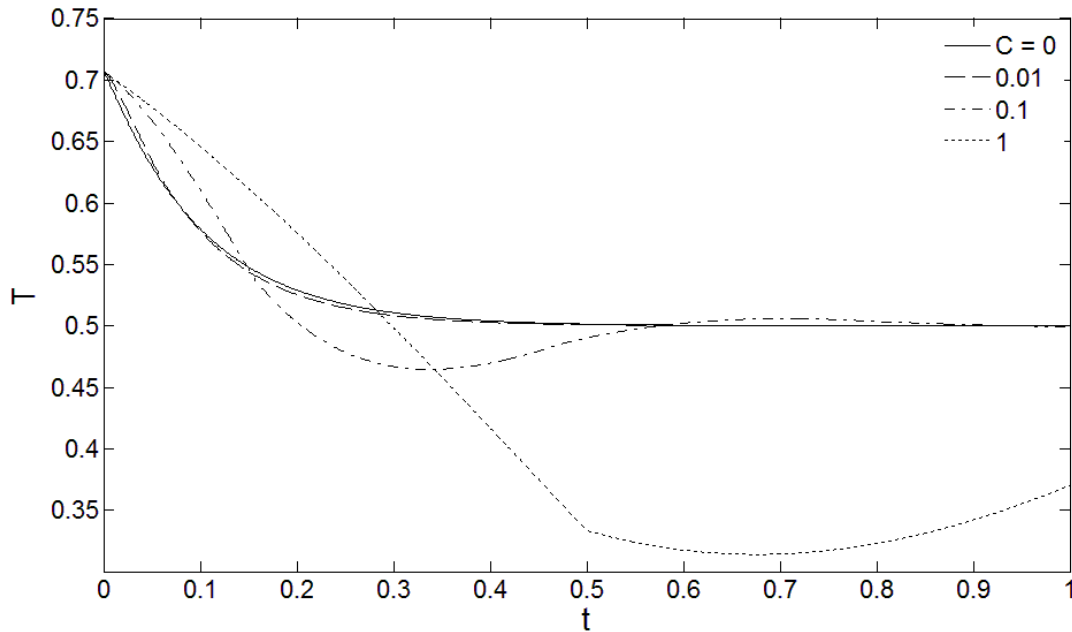


**Figure 1.4 - Temperature  $T$  vs time  $t$  for  $x = 0.5$  with varying  $C$ . As  $C$  increases, damped oscillations appear, eventually reaching the steady state,  $n = 1000$ .**

For Fourier heat conduction, the temperature profile monotonically decreases from  $T(x, 0) = \cos(\pi x/2)$  to the steady state solution  $T(x) = 1 - x$ . As the relaxation time increases, and consequently  $C$  increases, oscillations begin to emerge. These oscillations are dampened and the steady state is eventually reached.

These two examples show that non-Fourier heat conduction should be expected to introduce interesting new phenomena. When non-Fourier effects are relevant, Fourier's law will no longer accurately characterize the solution and a non-Fourier heat conduction model must be employed. This will be discussed in the next section.

## 1.5 Breakdown of Fourier's law and the generalized non-Fourier equation for fluids

For most practical problems, Fourier's law is an accurate representation of the system.

There are, however, systems where the finite thermal response time still matters and can lead to significant non-Fourier effects. Thermal waves in superfluid liquid Helium, known as second sound, are expected to lead to non-Fourier effects [13], [14].

Additionally, there exists acids and biological tissues that are known to possess relaxation times between 1-100 seconds [15]–[18]. Non-Fourier contributions have also been predicted in theories of granular flows [19], [20]. These effects may also be prevalent for cases such as laser pulse heating [21] where the frequency of temperature variation at the surface can be on the order of femtoseconds. Here, even though the relaxation time of many practical media can be as short as picoseconds [15], the relaxation time may need to be considered relative to the period of the laser pulse.

Another area of particular interest in non-Fourier effects has been with nanofluids.

Nanofluids consist of a base fluid such as water or organic fluids, and 1-5% volume fraction of nanoparticles. These particles are between 1-100 nm and can be made from copper, gold, diamonds, nanotubes or oxides of aluminum and silicon. Nanofluids have been given special interest recently due to their unexpected enhancement in conduction heat transfer. Despite the low volume fractions involved, thermal conductivity has been found to increase by as much as 40% [22]. This makes them useful in industrial cooling applications, nuclear reactors, extraction of geothermal power, vehicle radiators, fuel additives, cooling of microchips, nanocryosurgery and more [23].

The earliest attempts to model nanofluids used existing models to develop equations illustrating the overall change in the thermophysical properties as a whole [24]. These models ultimately failed due to their inability to properly predict the fluid viscosity as well as the single phase heat transfer coefficient. Buongiorno [24] analyzed potential mechanisms within nanofluids that could cause a relative slip between the nanoparticles and the base fluid, which may be responsible for the unaccounted heat transfer. He concluded that the effects of Brownian motion and thermophoresis should be accounted

for. This was further investigated by Tzou [25] and Nield [26], who showed through linear stability analysis, that the addition of nanoparticles resulted in a less stable conduction state, leading to an earlier onset of convection in a Rayleigh-Bénard cell. The major downfall of their formulation is the boundary conditions imposed on the nanoparticle concentration, which they assumed to be unrealistically fixed and different from one another. Although due to the effects of thermophoresis, a concentration gradient can exist, nanofluids are generally quite homogeneous solutions. Furthermore, if the concentration of nanoparticles at each boundary was set to be equal, no change in the stability picture could be observed. In this case, the nanofluid was predicted to behave as if it were just the base fluid due to their choice of reference density.

A different approach to model nanofluids was brought forth by Wang [27], showing the similarities between the Fourier heat transport in a two-phase medium and a single-phase medium with dual-phase-lagging non-Fourier effects. The dual-phase-lagging constitutive equation for heat conduction relates the temperature gradient at a material point  $\mathbf{x}$  and time  $t + \tau_T$  to the heat flux density at  $\mathbf{x}$  and time  $t + \tau_Q$  by

$$\mathbf{Q}(\mathbf{x}, t + \tau_Q) = -\mathbf{K}\nabla T(\mathbf{x}, t + \tau_T). \quad (1.5.1)$$

Here,  $\tau_Q$  is the relaxation time and  $\tau_T$  is the retardation time of the medium. By employing a first-order Taylor series expansion of Eq. (1.5.1) and combining it with the energy equation including energy generation terms, then if all thermophysical properties are assumed to be constant, one arrives at,

$$\frac{\partial T}{\partial t} + \tau_Q \frac{\partial^2 T}{\partial t^2} = \kappa \Delta T + \kappa \tau_T \frac{\partial}{\partial t} (\Delta T) + \frac{\kappa}{\mathbf{K}} \left[ S(\mathbf{x}, t) + \tau_Q \frac{\partial S(\mathbf{x}, t)}{\partial t} \right]. \quad (1.5.2)$$

Above,  $S$  is the volumetric internal heat source. Next, Wang used a volume averaging process to analyze Fourier heat conduction within a two-phase solid. After considerable mathematical manipulation, he was able to generate a single equation for the temperature field, which is of the same form as Eq. (1.5.2), except that the coefficients are written in terms of the physical properties of the medium. As a result, he was able to show that two-phase systems with Fourier heat transport can be analyzed as a single-phase medium with

non-Fourier effects, making results in these two fields mutually applicable. He specifically mentions studying nanofluids in this way. This result can be very advantageous since the analysis of two-phase media is significantly more mathematically involved than studying non-Fourier effects, producing a much simpler method of analysis to a difficult problem.

Eq. (1.4.5) is only sufficient to solve the problem of instantaneous heat propagation [28]–[30] for conduction. The Maxwell-Cattaneo equation is not frame-invariant and thus its application is restricted to non-deformable media. In order to remedy this situation, heat transport equations involving different objective derivatives have been introduced to replace the partial derivative, although many had significant shortfalls. The most promising modification of the Maxwell-Cattaneo equation appears to be that of Christov [31], which was later revisited by Khayat and Ostoja-Starzewski [32]. They were able to derive Eq. (1.5.3), which when coupled with the energy equation, yields a single equation for the temperature field, an advantage that other frame-invariant formulations do not possess [31].

$$\tau(\mathbf{Q}_t + \mathbf{V} \cdot \nabla \mathbf{Q} - \mathbf{Q} \cdot \nabla \mathbf{V}) = -\mathbf{Q} - K \nabla T \quad (1.5.3)$$

Eq. (1.5.3) is the Cattaneo Vernotte equation, which replaces Fourier's law whenever non-Fourier effects are relevant, collapses back to Fourier's law when they are not, and can be applied to both deformable and non-deformable media. Throughout this thesis, any media in which the effects of the relaxation time are non-negligible are referred to as non-Fourier, while those in which the effects of the relaxation time can be ignored are referred to as Fourier.

Non-Fourier effects are not only characterized by the magnitude of the relaxation time. Using non-dimensional arguments, non-Fourier effects become important when the ratio of the thermal relaxation time and time scale for thermal diffusion becomes significant. If  $D$  is a characteristic length scale and  $\kappa$  is the thermal diffusivity of the fluid, then  $D^2/\kappa$  is the thermal diffusion time. The Cattaneo number,  $C = \frac{\tau\kappa}{D^2}$ , thus determines when non-

Fourier effects are to be considered. As the length scale of any heat transfer problem

decreases,  $C$  increases relatively quickly and so non-Fourier effects are expected to be prevalent in small scale systems that involve heat transport such as in micro- and nanodevices [12], [33]–[43] as well as rarefied gases [44], [45]. The importance of small length scale effects are generally measured by the Knudsen number,  $Kn = \lambda / D$ , where  $\lambda$  is the mean free path of the fluid particles. When  $Kn$  is small, the familiar macroscopic equations such as Navier-Stokes and Fourier's law produce accurate models and are actually derived from low order expansions of Boltzmann's equation in kinetic theory.

Kinetic theory concerns itself with the solution of the particle distribution function  $f(\mathbf{x}, t, \mathbf{s})$  where  $\mathbf{s}$  is the microscopic velocities of the particles. This defines the number density of particles in a given position  $\mathbf{x}$ , and at given time  $t$ , with velocity  $\mathbf{s}$ . Macroscopic quantities for mass density, velocity and internal energy  $U$ , respectively, are obtained by the following integrations

$$\rho = m \int f d\mathbf{s}, \quad \rho \mathbf{V} = m \int \mathbf{s} f d\mathbf{s}, \quad \rho U = \frac{3}{2} \rho \theta = \frac{m}{2} \int S^2 f d\mathbf{s}, \quad (1.5.4)$$

where  $\theta = \frac{\sigma_R}{m} T$ ,  $m$  is the mass of the particle and  $\mathbf{S} = \mathbf{s} - \mathbf{V}$ . The pressure tensor is given by

$$p \delta + \bar{\sigma} = m \int \mathbf{S} \mathbf{S} f d\mathbf{s} \quad \text{where} \quad p = \frac{m}{3} \int S^2 f d\mathbf{s} \quad \text{and} \quad \bar{\sigma} = m \int \mathbf{S} \mathbf{S} f d\mathbf{s}. \quad (1.5.5)$$

The pressure obeys the ideal gas law,  $p = \rho \theta$ , due to Eq. (1.5.4) and  $\bar{\sigma}$  describes the stress where  $\sigma_{ii} = 0$  and  $\sigma_{ij} = \sigma_{ji}$ . Finally, the heat flux is given by

$$\mathbf{q} = \frac{m}{2} \int S^2 \mathbf{S} f d\mathbf{s}. \quad (1.5.6)$$

Governing the particle distribution function in space and time is the Boltzmann equation,

$$\frac{\partial f}{\partial t} + \mathbf{s} \cdot \nabla f = \Gamma, \quad (1.5.7)$$

where  $\Gamma$  is the collision term describing the change of  $f$  due to particle collisions. The collision term, shown by Eq. (1.5.8), is a complex equation that assumes all collisions are between only two particles:

$$\Gamma = m \iint I(\mathbf{S}_B - \mathbf{S}_A, \Omega) |\mathbf{S}_B - \mathbf{S}_A| [f(\mathbf{S}'_A, t) f(\mathbf{S}'_B, t) - f(\mathbf{S}_A, t) f(\mathbf{S}_B, t)] d\Omega d^3\mathbf{S}_A. \quad (1.5.8)$$

Here, the subscripts A and B denote any two colliding particles, the prime notation indicates the value before the collision, and  $I$  is the differential cross section of the collision in which the solid angle is denoted by  $\Omega$ . When considering deriving macroscale equations, the particles are assumed to move together with an average velocity with no collisions, and thus  $\Gamma$  is equal to zero for  $\text{Kn} \rightarrow 0$ . In this case, the solution to the Eq. (1.5.7) is the Maxwellian distribution. For larger  $\text{Kn}$ , the interaction between individual particles becomes more important and a correction to  $\Gamma = 0$  will need to be considered. In order to develop meaningful macroscopic equations from the particle distribution function, Eq. (1.5.7) is multiplied by  $m$ ,  $m\mathbf{s}_i$  and  $mS^2/2$  to get, respectively, the equations for conservation of mass, momentum and internal energy as follows:

$$\begin{aligned} \frac{\partial \rho}{\partial t} + \nabla \cdot (\rho \mathbf{V}) &= 0, \\ \rho \frac{\partial \mathbf{V}}{\partial t} + \rho \mathbf{V} \cdot \nabla \mathbf{V} + \nabla \mathbf{p} + \nabla \cdot \mathbf{\bar{\sigma}} &= 0, \\ \frac{3\rho}{2} \frac{\partial \theta}{\partial t} + \frac{3\rho}{2} \mathbf{V} \cdot \nabla \theta + \nabla \cdot \mathbf{q} &= -(\mathbf{p}\delta + \mathbf{\bar{\sigma}}) : \nabla \mathbf{V} \end{aligned} \quad (1.5.9)$$

In order to solve these equations completely, additional macroscopic equations must be obtained for  $\mathbf{\bar{\sigma}}$  and  $\mathbf{q}$  from the Boltzmann equation. The first well-known approach is the Chapman-Enskog [46] method which uses a correction to the Maxwellian distribution function by adding higher order terms in  $\text{Kn}$  as a correction to  $\Gamma = 0$ . For zeroth-order, the expansion gives zero stress and heat flux, known as the Euler equations which do not describe dissipative processes. For first-order solutions using this method, the Navier-Stokes and Fourier heat transfer equations are achieved, where the stress is proportional to the rate of strain. However for larger  $\text{Kn}$ , higher order extended transport equations are needed. Using the Chapman-Enskog method for higher orders leads to Burnett [47] and super-Burnett [48] equations, however they are inadequate for time-dependent problems,



are only applicable to  $Kn < 1$ , and lack of a complete set of boundary conditions making them difficult to solve [49].

Another approach to finding extended transport equations for  $Kn > 0$  is Grad's moment method [50]. Grad developed a set of 5 equations containing 13 moments in the variables  $\rho$ ,  $\mathbf{s}$ ,  $\theta$ ,  $\vec{\sigma}$  and  $\mathbf{q}$ . The resulting equations for the stress and heat flux are both non-Newtonian and non-Fourier in nature. Although these equations are stable, they lack proper guidelines for their use at different  $Kn$  and illegitimate subshocks can occur due to its hyperbolic nature.

The equations for the stress and heat flux from the Chapman-Enskog [46] method and Grad's 13 [50] moment method are highly non-linear and complex (the reader is referred to Eqs. (3.7)-(3.8) and Eq. (3.10)-(3.11) in [49]). Instead of using the complicated extended transport equation for the heat flux, we have adopted the frame invariant Cattaneo-Vernotte equation (Eq. (1.5.3)) and assumed Newtonian stresses. Not only is this equation well behaved, but it has been widely accepted and used previously in the exploration of viscoelastic fluids [51]–[53] where a non-Newtonian stress equation based on Oldroyd's upper-convected derivative is used in place of extended transport equations from kinetic theory for the stress. In viscoelasticity, the elasticity number  $E = \tau_{sv} / D^2$  represents the level of non-Newtonian character and closely resembles the Cattaneo number. Here,  $\tau_s$  represents the relaxation time of the stress to changes in strain rate, which is analogous to  $\tau$  in the Cattaneo-Vernotte equation, representing the relaxation of the heat flux to changes in the temperature gradient.

So far, investigation of non-Fourier heat transport has been sparse and pertains mostly to instability [28], [54]–[56].

## 1.6 Breakdown of the No-Slip Boundary Condition

Macroscopic fluid flow over solid surfaces is regularly modeled using the no-slip boundary condition. This boundary condition makes the assumption that both the fluid velocity and temperature are equal to that of the solid surface. The validity of the no-slip boundary condition is measured by the Knudsen number. To date, the most practical

engineering flows have been largely in the macroscopic regime (larger length scales), where  $\text{Kn} \ll 1$  and the no-slip boundary condition is a suitable assumption. However, at the macroscopic level, slip flows have been known to occur for polymer flows [57] and gases that have been rarefied due to an imposed low pressure [58], [59]. At the microscopic level, as with Fourier's law, the no-slip assumption may no longer be valid. With the introduction of micro-electromechanical systems (MEMS) and nanotechnology, the length scale can now approach the mean free path of ordinary fluids, yielding non-negligible values of the Knudsen number. Slip flows have been explored in micro-devices a great deal in the last two decades [60]–[67].

For  $0.01 < \text{Kn} < 0.1$ , known as the slip-flow regime [68], [69], no-slip is no longer a realistic boundary condition and also leads to a potential breakdown in Fourier's law, the Newtonian stress assumption and the Boussinesq approximation which have been previously investigated [53], [70]–[73]. When  $\text{Kn} \gg 1$ , even the continuum assumption must be abandoned [74]. In the slip-flow regime and beyond, partial-slip boundary conditions must be implemented. These represent that the velocity of the fluid immediately in contact with the solid surface is not equal to the velocity of the surface and that there exists a temperature jump at the boundary [58], [59], [74]–[76]. The most general form of hydrodynamic slip and temperature jump boundary conditions including second-order effects are given by

$$\mathbf{V} - \mathbf{V}_w = a_1 \lambda \left( \frac{\partial \mathbf{V}}{\partial \mathbf{n}} \right)_{\text{wall}} + a_2 \lambda^2 \left( \frac{\partial^2 \mathbf{V}}{\partial \mathbf{n}^2} \right)_{\text{wall}} + a_3 \lambda^2 \left( \frac{\partial \mathbf{T}}{\partial \mathbf{m}} \right) \quad (1.6.1)$$

$$T - T_w = b_1 \lambda \left( \frac{\partial T}{\partial \mathbf{n}} \right)_{\text{wall}} + b_2 \lambda^2 \left( \frac{\partial^2 T}{\partial \mathbf{n}^2} \right)_{\text{wall}} \quad (1.6.2)$$

Here,  $\mathbf{n}$  is the unit vector normal to the boundary facing into the fluid and  $\mathbf{m}$  is the unit vector in the tangential direction. As there is currently no globally accepted values of  $a_n$  and  $b_n$ , coefficients with different characteristics will be explored in the thesis. First order slip effects are sufficient for  $\text{Kn} < 0.1$  and have been considered by [74], however, in order to reach into the transition regime ( $0.1 < \text{Kn} < 10$ ), second-order slip effects must

be considered [62], [68], [69]. Second-order effects can increase or decrease the amount of slip compared to first-order depending on the sign of the coefficient.

In order to demonstrate the effects of slip, consider a 2D non-dimensional isothermal Poiseuille flow between two stationary plates such that  $\mathbf{V}_w$ , the last term in Eq. (1.6.1) and all of Eq. (1.6.2) are equal to zero. The solution is then

$$u(y) = \frac{1}{2} \frac{\partial P}{\partial x} y^2 - \frac{1}{2} \frac{\partial P}{\partial x} y - a_1 \text{Kn} \frac{1}{2} \frac{\partial P}{\partial x} + a_2 \text{Kn}^2 \frac{\partial P}{\partial x} \quad (1.6.3)$$

where  $u$  is the horizontal velocity and  $y$  is the vertical direction. For  $\text{Kn} = 0$ , the solution quickly collapses onto the familiar solution for stick boundaries. For a negative pressure gradient and where second-order slip effects increase the amount of slip, Fig. 1.5 shows the change in the velocity profile, comparing no-slip with first- and second-order effects.

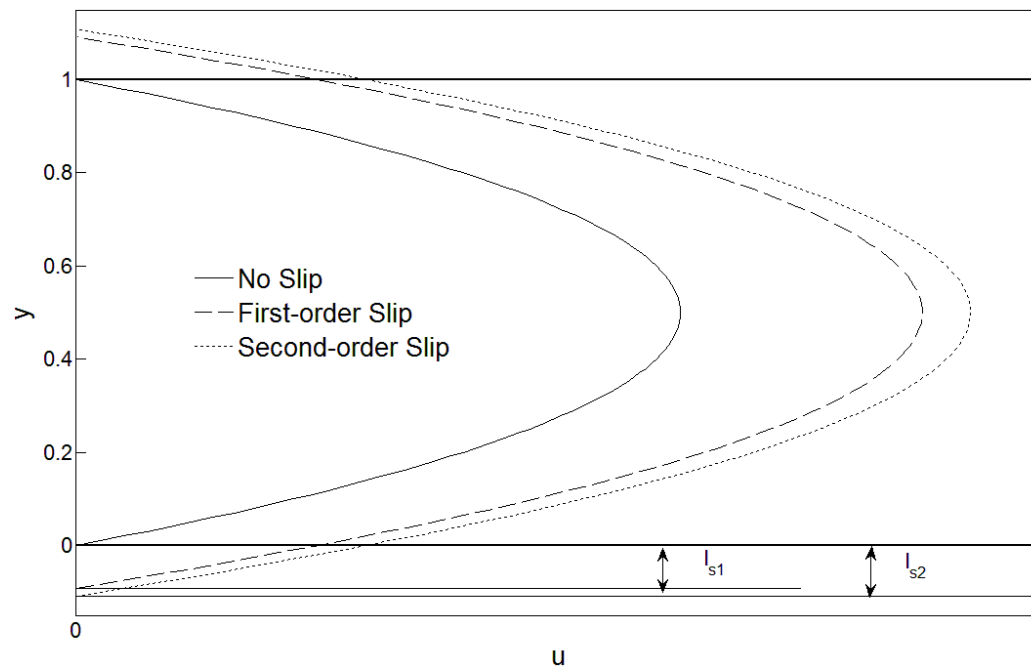


**Figure 1.5 - Comparison of first- and second-order slip effects with the no slip boundary condition. Bold lines denote the upper and lower surface.  $l_{s1}$  and  $l_{s2}$  denote the slip length for first- and second-order effects, respectively.**

In Fig. 1.5  $\text{Kn} = 0.1$ ,  $a_1 = 1$  for both slip cases and  $a_2 = -1$  for second-order slip effects.

As the effects of slip are considered, the velocity at the boundary, as well as the

maximum velocity, increases. When the velocity profile is extrapolated toward the outside of the boundaries at  $y = 0$  and  $1$ , it intersects with the  $u = 0$  axis. The distance  $y$  outside of the boundary where the velocity is extrapolated to zero is known as the slip length  $l_s$  which can be solved for analytically using the quadratic formula:

$$l_s = \frac{1}{2} - \sqrt{\frac{1}{4} + 2 \left[ a_1 \text{Kn} \frac{1}{2} - a_2 \text{Kn}^2 \right]}. \quad (1.6.4)$$

Again, depending on the sign of  $a_2$ , second-order slip can be greater than or less than that for first-order effects.

Although the validity of the Navier-Stokes equation comes into question in the transition regime, second-order boundary conditions are expected to push its realm of applicability [62]. Furthermore, higher-order continuum equations such as those predicted by the Chapman-Enskog method and Grad are expected to give better solutions than the Navier-Stokes equation with Fourier's law in the slip and transition regime [77]. Thus, it seems logical to explore both non-Fourier effects through the frame invariant Cattaneo-Vernotte equation, and second-order slip hydrodynamic slip and temperature jump as it applies to Rayleigh-Bénard convection. Although the combination of these effects will not be explored in this thesis, it is realistic to expect that good results could be obtained by such a continuum solution for  $\text{Kn}$  in the slip and transition regime [77], [78].

## 1.7 Linear Stability and Steady State Analysis

An important aspect of Rayleigh-Bénard convection is the stability of the steady conduction state. As stated previously, the fluid is initially at rest until critical conditions are reached, causing convection to set in. Determining the critical conditions requires that a perturbation be applied to the steady conduction state, where each quantity of interest  $\varepsilon$  is perturbed by

$$\varepsilon(\mathbf{x}, t) = E(z) e^{\sigma t + i k x}. \quad (1.7.1)$$

Here,  $k$  is the perturbation wave number in the  $x$  direction and the time evolution of the disturbance is described by  $\sigma$  which can have both real and imaginary parts. These

perturbations are assumed to be small, and thus non-linear quantities are neglected, which linearizes the set of equations. For example, substituting Eq. (1.7.1) into the Lorenz model Eq. (1.3.3) yields the following linearized set of equations after dividing through by the exponential term:

$$\begin{aligned}\sigma X &= -\text{Pr}(X + \text{Ra}Y) \\ \sigma Y &= -\frac{X}{\text{Ra}_{cF}} - Y \\ \sigma Z &= -bZ\end{aligned}\quad (1.7.2)$$

Through elimination of the variables  $X$ ,  $Y$  and  $Z$ , the dispersion relation is generated which relates the temporal response term  $\sigma$  and the Rayleigh number, shown by Eq. (1.7.3) as,

$$\text{Ra}_{cF}\sigma^2 + \text{Ra}_{cF}(\text{Pr}+1)\sigma + \text{Pr Ra} - \text{Pr Ra}_{cF} = 0. \quad (1.7.3)$$

When  $\sigma < 0$ , then the perturbation will die out and the original steady state is recovered. After reaching some critical limit in  $\text{Ra}$  which contains the temperature difference between the two plates,  $\sigma > 0$ , and the perturbations are expected to grow until a new state is established. The critical value can be deduced by setting  $\sigma = 0$  (no growth or decay of the perturbations) and solving for  $\text{Ra}$ . In the case of the Lorenz model,  $\sigma$  can only exist as a real number. However, as we will show in Chapter 2, the system of equations generated when including non-Fourier effects has 5 degrees of freedom (as opposed to 3 in the Lorenz model), which will yield a cubic term in the dispersion relation. Due to this fact, the solution for the dispersion relation must allow for the possibility of an imaginary portion to temporal response term such that  $\sigma = \sigma_r + i\omega$ . In this case, to solve for the critical Rayleigh number, only the real part of  $\sigma$  is set equal to zero. Under the correct conditions, the growth of the perturbations will be oscillatory in nature, a phenomena seen in nanofluids and in the case of viscoelastic fluids [52], [79].

Determining the critical conditions for which the steady conduction state loses its stability is of particular interest in this thesis. As well as the changes in these critical

conditions due to their relationship to properties of the fluid or gap size. This will be explored extensively in Chapter 2.

When Eqs. (1.2.1-1.2.2) and Eqs. (1.3.1-1.3.2) are used in conjunction with no-slip boundary conditions, the minimum criteria for the instability of the steady conduction state are  $Ra \approx 1708$  corresponding to  $k \approx 3.117$ . If stress-free boundary conditions are employed, then the critical conditions become  $Ra \approx 657$  at  $k \approx 2.22$ , and thus partial slip boundary conditions will significantly affect the stability criteria. The introduction of non-Fourier effects are also expected to change the conditions for critical stability as well as the behaviour of the growth of the perturbations.

Once the steady conduction state has lost stability, it can lead to either stationary or oscillatory convection. In order to analyze this non-linear behaviour, a system of ordinary differential equations is generated, such as in the Lorenz model [9]. This can be achieved by describing the spatial dependence of the solution to Eqs. (1.2.1-1.2.2) and Eqs. (1.3.1-1.3.2) as an infinite series such as Fourier series. Each mode has a separate weight in this expansion and the weight comes in the form of the time dependent coefficients. Since it is not realistic to find the solution with an infinite number of modes, this series must be truncated to a finite number of modes, which introduces an error. In an attempt to minimize this error, a Galerkin projection [5] can be employed by projecting these equations onto each of the chosen modes, taking advantage of their orthogonality. This is similar to projecting a vector onto orthogonal axes. Now, that the spatial dependence is eliminated, the system of partial differential equations is transformed into a system of ordinary differential equations. As the complexity of the flow increases, higher order modes will need to be taken into consideration.

In the case that the system achieves a stationary mode of convection, this can be analyzed mathematically by setting the time derivatives (such as in Eqs. (1.3.3)) equal to zero. The resulting non-linear system can be solved analytically as a function of the Rayleigh number in order to investigate its behaviour as the temperature difference between the plates increases. Eventually, the steady conduction state can also become unstable, and a

linear stability analysis can again be invoked to explore when this will occur, leading to a new mode of convection.

## 1.8 Motivation

With the advent of new technologies, such as fast processes, nanofluids, micro-and nano-technology and low temperature liquids, new heat transfer phenomena are being observed. These topics are complex and non-Fourier heat transfer has been experimentally observed, or at least suggested to play a significant role, in these phenomena [27], [34], [35], [38]. In particular, the existence of non-Fourier heat transfer in microscale and nanoscale applications is backed by kinetic theory [49], [80]. With advances in technology allowing us to create smaller devices, care must be taken to characterize the heat transfer from these small devices in order to safely and efficiently take advantage of them. Although non-Fourier heat transfer is expected in many applications, this thesis will focus particularly on small length scale systems. Another occurrence in flow in the microscale is the relevance of hydrodynamic slip and temperature jump at the fluid-solid interface [58], [59], [81], and thus, it makes sense to also investigate these phenomena.

Rayleigh-Bénard convection is a very commonly occurring natural process, driving ocean currents, the weather and the Earth's mantle. It is also a naturally occurring process in heating and cooling applications. Rayleigh-Bénard convection in macroscale systems has been well understood for quite some time and due to its physical relevance as well as theoretical and mathematical simplicity[4], [5], it is a well suited platform for analyzing the effects of non-Fourier heat transfer and partial slip boundary conditions.

## 1.9 Thesis Summary

Chapter 2 analyzes the linear stability of a non-Fourier fluid in a Rayleigh-Bénard configuration subject to stress-free boundary conditions. The changes in the stability boundary are discussed, outlining the introduction of a new oscillatory mode of instability with increased non-Fourier effect. The critical wave number, Rayleigh number and oscillation frequency are also explored as a function of the Prandtl number.

The third chapter investigates the stationary convection of a non-Fourier fluid in Rayleigh-Bénard convection. The bifurcation curves are studied in detail, highlighting the important qualitative behaviour expected of non-Fourier fluids. Non-dimensional heat transfer is analyzed via the Nusselt number and compared to experiment, showing agreement that increased heat transfer is expected. The linear stability of the steady convection state is also investigated showing that non-Fourier effects lead to a loss of stability for lower Ra than for a Fourier fluid.

The effect of second-order boundary conditions on the tangential velocity and the temperature will be considered exclusively in Chapter 4 in order to isolate their contribution to Rayleigh-Bénard convection from non-Fourier effects. Highlighted are the minimum critical Rayleigh number and corresponding critical wave number that are expected with different slip conditions. As the length scale of the problem decreases, both the critical Rayleigh number and wave number are predicted to decrease. Finally, the conclusion chapter will reiterate the key conclusions from the preceding chapters for a thorough understanding of the concepts at hand.

## 1.10 References

- [1] F. P. Incropera and D. P. DeWitt, *Fundamentals of Heat and Mass Transfer*, Fifth Edit. New York: John Wiley & Sons, 2002.
- [2] D. Joseph and L. Preziosi, “Heat waves,” *Rev. Mod. Phys.*, vol. 61, no. 1, pp. 41–73, 1989.
- [3] C. Israel-Cookey and V. Omubo-Pepple, “The Effects of Radiation on the Linear Stability of a horizontal layer in a Fluidsaturated Media heated from below,” *J. Appl. Sci. Environ. Manag.*, vol. 11, no. 3, pp. 59–62, 2007.
- [4] E. Bodenschatz, W. Pesch, and G. Ahlers, “Recent Developments in Rayleigh-Bénard Convection,” *Annu. Rev. Fluid Mech.*, vol. 32, pp. 709–778, 2000.
- [5] A. V. Getling, *Rayleigh-Benard Convection: Structures and Dynamics*. World Scientific, 1998.



- [6] P. Urban, "Helium Cryostat for Experimental Study of Natural Turbulent Convection." [Online]. Available: <http://www.isibrno.cz/cryogenics/convection.html>. [Accessed: 23-Jul-2014].
- [7] F. . White, *Fluid Mechanics*, Sixth Edit. New York: McGraw-Hill, 2008.
- [8] E. Spiegel and G. Veronis, "On the Boussinesq approximation for a compressible fluid.," *Astrophys. J.*, vol. 131, p. 442, 1960.
- [9] E. Lorenz, "Deterministic nonperiodic flow," *J. Atmos. Sci.*, vol. 20, p. 130, 1963.
- [10] A. Hood, "Solution of the heat equation: separation of variables," 2000. [Online]. Available: <https://mail.google.com/mail/u/0/#inbox/148e6ff3367627c8>. [Accessed: 08-Oct-2014].
- [11] D. E. Glass, M. N. Özişik, D. S. McRae, and B. Vick, "Hyperbolic heat conduction with temperature-dependent thermal conductivity," *J. Appl. Phys.*, vol. 59, no. 6, p. 1861, 1986.
- [12] D. Y. Tzou and J. Xu, "Nonequilibrium Transport: The Lagging," in *Advances in Transport Phenomena*, 2011, pp. 93–170.
- [13] H. Liepmann and G. Laguna, "Nonlinear interactions in the fluid mechanics of helium II," *Annu. Rev. Fluid Mech.*, p. 34, 1984.
- [14] R. Donnelly, "The two-fluid theory and second sound in liquid helium," *Phys. Today*, no. October, p. 34, 2009.
- [15] D. S. Chandrasekharaiah, "Hyperbolic thermoelasticity: a review of recent literature," *Appl. Mech. Rev.*, vol. 51, no. 12, pp. 705–729, 1998.
- [16] K. Mitra, S. Kumar, A. Vedevarz, and M. K. Moallemi, "Experimental Evidence of Hyperbolic Heat Conduction in Processed Meat," *J. Heat Transfer*, vol. 117, no. 3, pp. 568–573, 1995.

- [17] F. Xu, M. Lin, and T. J. Lu, "Modeling skin thermal pain sensation: Role of non-Fourier thermal behavior in transduction process of nociceptor," *Comput. Biol. Med.*, vol. 40, no. 5, pp. 478–486, May 2010.
- [18] H. Herwig and K. Beckert, "Experimental evidence about the controversy concerning Fourier or non-Fourier heat conduction in materials with a nonhomogeneous inner structure," *Heat Mass Transf.*, vol. 36, no. 5, pp. 387–392, Sep. 2000.
- [19] N. Sela and I. Goldhirsch, "Hydrodynamic equations for rapid flow of smooth inelastic spheres, to Burnett order," *J. Fluid Mech.*, vol. 361, pp. 41–74, 1998.
- [20] J. J. Brey, J. W. Dufty, C. S. Kim, and A. Santos, "Hydrodynamics for granular flow at low density," *Phys. Rev. E*, vol. 58, no. 4638, 1998.
- [21] R. R. Letfullin, T. F. George, G. C. Duree, and B. M. Bollinger, "Ultrashort Laser Pulse Heating of Nanoparticles: Comparison of Theoretical Approaches," *Adv. Opt. Technol.*, vol. 2008, pp. 1–8, 2008.
- [22] J. Eastman, "Anomalously Increased Effective Thermal Conductivities of Ethylene-Glycol-Based Nanofluids Containing Copper Nanoparticles," *Appl. Phys. Lett.*, vol. 78, no. 6, pp. 718–720, 2001.
- [23] K. V. Wong and O. De Leon, "Applications of Nanofluids: Current and Future," *Adv. Mech. Eng.*, vol. 2010, pp. 1–11, 2010.
- [24] J. Buongiorno, "Convective Transport in Nanofluids," *J. Heat Transfer*, vol. 128, no. 3, p. 240, 2006.
- [25] D. Y. Tzou, "Thermal instability of nanofluids in natural convection," *Int. J. Heat Mass Transf.*, vol. 51, no. 11–12, pp. 2967–2979, Jun. 2008.
- [26] D. A. Nield and A. V. Kuznetsov, "The onset of convection in a horizontal nanofluid layer of finite depth," *Eur. J. Mech. - B/Fluids*, vol. 29, no. 3, pp. 217–223, May 2010.

- [27] L. Wang and X. Wei, "Equivalence between dual-phase-lagging and two-phase-system heat conduction processes," *Int. J. Heat Mass Transf.*, vol. 51, no. 7–8, pp. 1751–1756, Apr. 2008.
- [28] G. Lebon and A. Clout, "Bénard-Marangoni instability in Maxwell–Cattaneo fluids," *Phys. Lett. A*, vol. 105, no. 7, pp. 361–364, 1984.
- [29] D. Y. Tzou and K. S. Chiu, "Temperature-dependent thermal lagging in ultrafast laser heating," *Int. J. Heat Mass Transf.*, vol. 44, no. 9, pp. 1725–1734, May 2001.
- [30] P. Haupt, *Continuum Mechanics and Theory of Materials*. New York: Springer Verlag, 2002.
- [31] C. I. Christov, "On frame indifferent formulation of the Maxwell–Cattaneo model of finite-speed heat conduction," *Mech. Res. Commun.*, vol. 36, no. 4, pp. 481–486, Jun. 2009.
- [32] R. Khayat and M. Ostoja-Starzewski, "On the objective rate of heat and stress fluxes. Connection with micro/nano-scale heat convection," *Discret. Contin. Dyn. Syst. - Ser. B*, vol. 15, no. 4, pp. 991–998, Mar. 2011.
- [33] B. Vermeersch and G. Mey, "Non-Fourier thermal conduction in nano-scaled electronic structures," *Analog Integr. Circuits Signal Process.*, vol. 55, no. 3, pp. 197–204, Apr. 2007.
- [34] H. A. Stone, A. D. Stroock, and A. Ajdari, "Engineering Flows in Small Devices," *Annu. Rev. Fluid Mech.*, vol. 36, no. 1, pp. 381–411, Jan. 2004.
- [35] X. B. Nie, S. Y. Chen, W. N. E, and M. O. Robbins, "A continuum and molecular dynamics hybrid method for micro- and nano-fluid flow," *J. Fluid Mech.*, vol. 500, pp. 55–64, Jan. 2004.
- [36] S. Bhattacharyya, Z. Zheng, and A. T. Conlisk, "Electro-osmotic flow in two-dimensional charged micro- and nanochannels," *J. Fluid Mech.*, vol. 540, p. 247, 2005.

- [37] M. Oliveira and L. Rodd, “Simulations of extensional flow in microrheometric devices,” *Microfluid. Nanofluidics*, vol. 5, no. 6, pp. 809–826, Apr. 2008.
- [38] Z. Y. Guo and Z. X. Li, “Size effect on microscale single-phase flow and heat transfer,” *Int. J. Heat Mass Transf.*, vol. 46, no. 1, pp. 149–159, Jan. 2003.
- [39] S. G. Kandlikar, S. Colin, Y. Peles, S. Garimella, R. F. Pease, J. J. Brandner, and D. B. Tuckerman, “Heat Transfer in Microchannels—2012 Status and Research Needs,” *J. Heat Transfer*, vol. 135, no. 9, Jul. 2013.
- [40] X. J. Hu, A. Jain, and K. E. Goodson, “Investigation of the natural convection boundary condition in microfabricated structures,” *Int. J. Therm. Sci.*, vol. 47, no. 7, pp. 820–824, Jul. 2008.
- [41] X. G. Liang and Z. Y. Guo, “The Scaling Effect on the Thermal Processes at Mini/Microscale,” *Heat Transf. Eng.*, vol. 27, no. 4, pp. 30–40, May 2006.
- [42] M. Krishnan, V. Ugaz, and M. Burns, “PCR in a Rayleigh-Bénard convection cell,” *Science (80-. )*, vol. 298, p. 793, 2002.
- [43] Z. Y. Guo and Z. X. Li, “Size effect on single-phase channel flow and heat transfer at microscale,” *Int. J. Heat Fluid Flow*, vol. 24, no. 3, pp. 284–298, Jun. 2003.
- [44] L. S. Pan, D. Xu, J. Lou, and Q. Yao, “A generalized heat conduction model in rarefied gas,” *Europhys. Lett.*, vol. 73, no. 6, pp. 846–850, Mar. 2006.
- [45] Z. Wang, L. Bao, and B. Tong, “Rarefaction criterion and non-Fourier heat transfer in hypersonic rarefied flows,” *Phys. Fluids*, vol. 22, no. 12, p. 126103, 2010.
- [46] S. Chapman and T. . Cowling, *The Mathematical Theory of Non-Uniform Gases*. Cambridge: Cambridge University Press, 1970.
- [47] D. Burnett, “The distribution of molecular velocities and the mean motion in a non-uniform gas,” *Lond. Math. Soc.*, vol. 40, pp. 382–435, 1936.

- [48] M. S. Shavaliyev, “Super-Burnett corrections to the stress tensor and the heat flux in a gas of Maxwellian molecules,” *J. Appl. Math. Mech.*, vol. 57, pp. 573–576, 1993.
- [49] H. Struchtrup and P. Taheri, “Macroscopic transport models for rarefied gas flows: a brief review,” *IMA J. Appl. Math.*, vol. 76, no. 5, pp. 672–697, Feb. 2011.
- [50] H. Grad, “On the kinetic theory of rarefied gases,” *Commun. Pure Appl. Math.*, vol. 2, no. 4, pp. 331–407, 1949.
- [51] R. Khayat, “Finite-amplitude Taylor-vortex flow of viscoelastic fluids,” *J. Fluid Mech.*, vol. 400, pp. 33–58, 1999.
- [52] R. E. Khayat, “Chaos and overstability in the thermal convection of viscoelastic fluids,” *J. Nonnewton. Fluid Mech.*, vol. 53, pp. 227–255, Jul. 1994.
- [53] R. Khayat, “Fluid elasticity and the transition to chaos in thermal convection,” *Phys. Rev. E*, 1995.
- [54] P. Dauby, M. Nélis, and G. Lebon, “Generalized Fourier equations and thermoconvective instabilities,” *Rev. Mex. física*, no. 4, pp. 57–62, 2002.
- [55] B. Straughan and F. Franchi, “Benard convection and the Cattaneo law for heat conduction,” *Proc. R. Soc. Edinburgh Sect. A Math.*, vol. 96, no. 1–2, p. 175, 1984.
- [56] B. Straughan, “Tipping points in Cattaneo-Christov thermohaline convection,” *Proc. R. Soc. A Math. Phys. Eng. Sci.*, vol. 467, no. 2125, pp. 7–18, May 2010.
- [57] W. B. Black and M. D. Graham, “Wall-Slip and Polymer-Melt Flow Instability,” 1996.
- [58] E. Arkilic, “Slip in microchannels,” in *Proceedings of Rarefied Gas Dynamics Symposium*, 1994.
- [59] E. Arkilic, “Mass flow and tangential momentum accommodation in silicon micromachined channels,” *J. Fluid ...*, vol. 437, pp. 29–43, 2001.

- [60] B.-Y. Cao, M. Chen, and Z.-Y. Guo, "Temperature dependence of the tangential momentum accommodation coefficient for gases," *Appl. Phys. Lett.*, vol. 86, no. 9, p. 091905, 2005.
- [61] L. Bocquet and E. Charlaix, "Nanofluidics, from bulk to interfaces," *Chem. Soc. Rev.*, vol. 39, no. 3, pp. 1073–95, Mar. 2010.
- [62] S. Colin, P. Lalonde, and R. Caen, "Validation of a Second-Order Slip Flow Model in Rectangular Microchannels," *Heat Transf. Eng.*, vol. 25, no. 3, pp. 23–30, Apr. 2004.
- [63] L. O'Hare, D. a. Lockerby, J. M. Reese, and D. R. Emerson, "Near-wall effects in rarefied gas micro-flows: some modern hydrodynamic approaches," *Int. J. Heat Fluid Flow*, vol. 28, no. 1, pp. 37–43, Feb. 2007.
- [64] P. Y. Tzeng, C. Y. Soong, M. H. Liu, and T. H. Yen, "Atomistic simulation of rarefied gas natural convection in a finite enclosure using a novel wall-fluid molecular collision rule for adiabatic solid walls," *Int. J. Heat Mass Transf.*, vol. 51, no. 3–4, pp. 445–456, Feb. 2008.
- [65] O. I. Vinogradova, "Slippage of water over hydrophobic surfaces," *Int. J. Miner. Process.*, vol. 56, no. 1–4, pp. 31–60, Apr. 1999.
- [66] C. Neto, D. R. Evans, E. Bonaccorso, H.-J. Butt, and V. S. J. Craig, "Boundary slip in Newtonian liquids: a review of experimental studies," *Reports Prog. Phys.*, vol. 68, no. 12, pp. 2859–2897, Dec. 2005.
- [67] V. Craig, C. Neto, and D. Williams, "Shear-Dependent Boundary Slip in an Aqueous Newtonian Liquid," *Phys. Rev. Lett.*, vol. 87, no. 5, p. 054504, Jul. 2001.
- [68] N. G. Hadjiconstantinou, "Comment on Cercignani's second-order slip coefficient," *Phys. Fluids*, vol. 15, no. 8, p. 2352, 2003.
- [69] B. Cetin and O. Bayer, "Evaluation of Nusselt Number for a flow in a Microtube using Second-Order Slip Model," vol. 15, pp. 103–109, 2011.

- [70] D. F. Stranges, R. E. Khayat, and B. Albaalbaki, "Thermal convection of non-Fourier fluids. Linear stability," *Int. J. Therm. Sci.*, vol. 74, pp. 14–23, Dec. 2013.
- [71] M. Niknami and R. E. Khayat, "Energy growth of disturbances in a non-Fourier fluid," *Int. J. Heat Mass Transf.*, vol. 67, pp. 613–626, Dec. 2013.
- [72] Z. Li and R. E. Khayat, "Finite-amplitude Rayleigh–Bénard convection and pattern selection for viscoelastic fluids," *J. Fluid Mech.*, vol. 529, pp. 221–251, Apr. 2005.
- [73] A. Manela and I. Frankel, "On the Rayleigh–Bénard problem: dominant compressibility effects," *J. Fluid Mech.*, vol. 565, p. 461, Sep. 2006.
- [74] L. S. Kuo and P. H. Chen, "Effects of Slip Boundary Conditions on Rayleigh–Bénard Convection," *J. Mech.*, vol. 25, no. 02, pp. 205–212, May 2011.
- [75] R. G. Deissler, "An Analysis of Second-Order Slip Flow and Temperature-Jump Boundary Conditions for Rarefied Gases," *Int. J. Heat Mass Transf.*, vol. 7, no. 6, pp. 681–694, 1964.
- [76] G. E. Karniadakis, A. Beskok, and N. Aluru, *Microflows and Nanoflows: Fundamentals and Simulation*. New York: Springer-Verlag, 2002.
- [77] N. Singh and A. Agrawal, "The Burnett equations in cylindrical coordinates and their solution for flow in a microtube," *J. Fluid Mech.*, vol. 751, pp. 121–141, Jun. 2014.
- [78] I. Zahmatkesh, M. M. Alishahi, and H. Emdad, "New velocity-slip and temperature-jump boundary conditions for Navier–Stokes computation of gas mixture flows in microgeometries," *Mech. Res. Commun.*, vol. 38, no. 6, pp. 417–424, Sep. 2011.
- [79] G. Donzelli, R. Cerbino, and A. Vailati, "Bistable Heat Transfer in a Nanofluid," *Phys. Rev. Lett.*, vol. 102, no. 10, p. 104503, Mar. 2009.

- [80] H. Struchtrup and M. Torrilhon, “Regularized 13 moment equations for hard spheres,” vol. 206, pp. 199–206, 2012.
- [81] T. Squires and S. Quake, “Microfluidics: Fluid physics at the nanoliter scale,” *Rev. Mod. Phys.*, vol. 77, no. July, 2005.



## Chapter 2

### 2 Thermal convection of non-Fourier fluids. Linear stability

#### 2.1 Introduction

Heat transfer is commonly governed by the classical Fourier's constitutive law. When used in combination with the First Law of Thermodynamics, Fourier's law assumes an infinite speed of heat propagation, and a parabolic temperature field. In reality, a disturbance wave in the temperature will travel at a finite speed since it is transferred by molecular interaction [1]. This behaviour is characterized by the Maxwell-Cattaneo equation, which adds a transient term multiplied by the thermal relaxation time of the medium. This is the time required for the heat flux to reach a new steady state following a perturbation to the temperature gradient, establishing a hyperbolic heat (wave) response. Non-Fourier effects have long been recognized to emerge in the form of *second-sound* thermal waves in low-temperature liquids [2], [3], but are increasingly observed in a variety of phenomena involving ultrafast heating, heat transfer in biological tissues, convection in nano-devices and complex fluids [4]–[8]. Most common practical problems involve materials with relaxation times on the order of  $10^{-12}$  seconds [9], and thus, the Maxwell-Cattaneo equation collapses onto the classical Fourier model. However, physical media exist in which the relaxation time may not be considered negligible. Noteworthy examples include some acids and biological tissues, which may possess relaxation times between 1-100 seconds [9]. It is important to realize that 'large' relaxation times should also be identified relative to the rate of heating. Processes such as laser pulse heating introduce a large quantity of energy over a small period of time, which are comparable to the relaxation time of the medium. Letfullin, George, Duree & Bollinger [4] point out that, in some applications, the duration of the laser pulse can be measured on the scale of  $10^{-15}$  seconds, of the order of the relaxation time of electrons [10]. Thus, when the rate of heating is of the same order of magnitude as the relaxation time, non-Fourier effects must be accounted for. The fact that the importance of non-Fourier effects is not solely embedded in the absolute value of the relaxation time is,

perhaps, best illustrated using generalized non-dimensional arguments. More specifically, non-Fourier effects become significant whenever the relaxation time is of the same order as the thermal diffusion time. Thus, if  $D$  is the length scale, or typical gap width as in the present problem, and  $\tau$  and  $\kappa$  are, respectively, the relaxation time and thermal diffusivity of the fluid, then the dimensionless relaxation time is given by the Cattaneo number,  $C = \frac{\tau\kappa}{D^2}$ . Consequently,  $C$  increases relatively rapidly as  $D$  decreases, and non-Fourier (NF) effects are expected to be significant for a very small gap, as in the convection and flow in micro- and nano-devices [11]–[14].

It has long been realized that adding the partial time derivative does not completely solve the problem of instantaneous thermal relaxation [15]–[17]. The Maxwell-Cattaneo equation is not a frame-invariant constitutive relation and, as such, is restricted to non-deformable media. Several objective derivatives have been applied to remedy this situation. However, they each have their own shortcomings. The most promising modification is that of Christov [18], which was recently revisited by Khayat & Ostoja-Starzewski [19], whose use of the Oldroyds' upper-convected derivative leads to the frame indifferent Maxwell-Cattaneo equation. Coupled with the energy equation, this constitutive equation can also yield a single equation for the temperature field, an advantage that other invariant formulations do not possess [18]. This equation replaces Fourier's law for fluid flow whenever the relaxation time is relevant, and collapses back to Fourier's law whenever it is not.

Currently, there is limited literature available on NF convection, and much of it pertains only to thermal instability [15], [20]–[22]. However, this is rapidly changing with the advent of fast processes and the emergence of nanofluids, which are solutions consisting of a base fluid solvent, containing a small volume fraction (1-5%) of nanoparticles of size of  $O(1-100\text{nm})$ . Nanofluids allow a substantial enhancement in conductive heat transfer, as much as 40 percent increase in thermal conductivity, despite the low volume fraction of the nanoparticles [23]–[25]. The presence of flow is expected to lead to complex and rich physical behavior [26]. Given the small spatio-temporal scales involved in heat transfer enhancement in nanofluids, resulting from the addition of nanoparticles to the

base fluid, it is not surprising that NF effects are envisaged as being behind this enhancement. That this may be the case is suggested at both the theoretical [8], [24], [27] and the experimental [28] levels. The NF effects resulting from the addition of nanoparticles are reminiscent of the non-Newtonian effects for viscoelastic fluids with colloidal and particle suspensions. The addition of the polymer to a base solvent leads to a finite relaxation time of the stress [29].

The NF constitutive equation for heat will be revisited in Section 2.2. The formulation is then applied to thermal convection (Section 2.3) and its linear stability (Section 2.4). Discussion and results will be covered in Section 2.5. Finally, concluding remarks are given in Section 2.6.

## 2.2 Constitutive equation for heat

The most commonly used NF constitutive equation for the heat flux,  $\mathbf{Q}$ , is the Maxwell-Cattaneo equation for heat conduction [1]. For a moving fluid, however, this equation needs to be reformulated and rendered objective (frame indifferent). This was achieved by Christov [18]. The resulting equation is simply reproduced here as

$$\tau \frac{\delta \mathbf{Q}}{\delta t} + \mathbf{Q} = -k \nabla T, \quad (2.2.1)$$

where  $\tau$  is the relaxation time, and the Oldroyd upper-convected derivative [30] is given by

$$\frac{\delta(\ )}{\delta t} \equiv \frac{\partial(\ )}{\partial t} + \mathbf{V} \cdot \nabla(\ ) - (\ ) \cdot \nabla \mathbf{V} - (\ ) \nabla \cdot \mathbf{V}. \quad (2.2.2)$$

For pure heat conduction, Eq. (2.2.2) reduces to

$$\tau \frac{\partial \mathbf{Q}}{\partial t} + \mathbf{Q} = -k \nabla T. \quad (2.2.3)$$

It is not difficult to see that this equation relates the temperature gradient at a material point  $\mathbf{x}$  and time  $t$  to the heat flux vector at the same point at time  $t + \tau$  for a medium of thermal conductivity  $k$ . The relation reads:

$$\mathbf{Q}(\mathbf{x}, t + \tau) = -k\nabla T(\mathbf{x}, t), \quad (2.2.4)$$

and Eq. (2.2.3) is recovered by Taylor expansion of Eq. (2.2.4) for small relaxation time. Note that Eq. (2.2.3) is hyperbolic. It is worth noting that other two-phase systems do reflect the phase-lagging character exhibited in Eq. (2.2.3). One such connection is the case of a hot jet penetrating a porous medium [31] or the flow through porous layers [32]. In this regard, Eqs. (2.1a and b) of Rees *et al.* [31] are comparable to Eqs. (4) and (5) of Wang & Wei [8]. Also, in this case, the former equations switch from parabolic to hyperbolic for high jet penetration velocity.

### 2.3 Governing equations and boundary conditions

Consider a thin layer of a Newtonian non-Fourier liquid confined between the planes  $Z = 0$  and  $Z = D$ , maintained at fixed temperatures  $T_0 + \delta T$  and  $T_0$ , respectively. The fluid layer is assumed to be of infinite horizontal extent. Convection emerges when the buoyancy effect exceeds a critical threshold relative to the viscous effect. The gravity acceleration vector is given by  $\mathbf{g} = -g\hat{\mathbf{z}}$ , where  $\hat{\mathbf{z}}$  is the unit vector in the  $Z$  direction. The fluid density,  $\rho$ , is assumed to depend on the temperature,  $T$ , following

$$\rho = \rho_0 [1 - \alpha_T (T - T_0)], \quad (2.3.1)$$

where  $\alpha_T$  is the coefficient of volume expansion and  $\rho_0$  is the mass density of the fluid at  $T_0$ . The fluid is assumed to be incompressible, of specific heat at constant pressure  $C_p$ , thermal conductivity  $k$  and viscosity  $\mu$ . In this case, the general governing equations for a non-Fourier fluid comprises the conservation of mass, linear momentum and energy, as well as the constitutive equation for the heat flux. In this case, the conservation equations are given by

$$\nabla \cdot \mathbf{V} = 0, \quad (2.3.2)$$

$$\rho_0(\mathbf{V}_t + \mathbf{V} \cdot \nabla \mathbf{V}) = -\nabla P - \rho g \hat{\mathbf{z}} + \mu \Delta \mathbf{V}, \quad (2.3.3)$$

$$\rho_0 c_p (\mathbf{T}_t + \mathbf{V} \cdot \nabla T) = -\nabla \cdot \mathbf{Q}, \quad (2.3.4)$$

where  $\nabla$  and  $\Delta$  are the gradient and Laplacian operators, respectively, and a subscript  $t$  denotes partial differentiation with respect to time. Here  $\mathbf{V}$  is the velocity vector,  $P$  is the pressure,  $T$  is the temperature and  $\mathbf{Q}$  is the heat flux vector. Note that the Boussinesq approximation, is assumed to hold as it is valid when “a) the vertical dimension of the fluid is much less than any scale height, and b) the motion-induced fluctuations in the density and pressure do not exceed, in order of magnitude, the total static variations of these quantities” [33]. Consequently, the Boussinesq approximation should hold for an ordinary fluid and a small gap, where the temperature gradient is typically small. For a non-Fourier fluid, however, the temperature gradient may not be sufficiently small, and the Boussinesq approximation may break down. Given the complexity of non-Fourier convection, it is reasonable to adopt the approximation at this exploratory stage.

Furthermore, the Boussinesq approximation is only used here as far as linear stability analysis is concerned. If the approximation were to break down, it would likely happen further from criticality where flow and thermal fluctuations are larger.

In this work, the heat flux is assumed to be governed by the Cattaneo-Vernotte phase-lagging Eq. (2.2.1), explicitly re-written here as

$$\tau(\mathbf{Q}_t + \mathbf{V} \cdot \nabla \mathbf{Q} - \mathbf{Q} \cdot \nabla \mathbf{V}) = -\mathbf{Q} - \kappa \nabla T, \quad (2.3.5)$$

where  $\tau$  is the relaxation time. With this equation, it is possible to generate a generalized energy equation. Indeed, upon taking the divergence of Eq. (2.3.4), noting the identity  $\nabla \cdot (\mathbf{a} \cdot \nabla \mathbf{b}) = \nabla \mathbf{a} : \nabla \mathbf{b} + \mathbf{a} \cdot \nabla (\nabla \cdot \mathbf{b})$ ,  $\mathbf{a}$  and  $\mathbf{b}$  being two general vectors, and using Eq. (2.3.5), one obtains

$$\tau[\mathbf{T}_{tt} + 2\mathbf{V} \cdot \nabla \mathbf{T}_t + \mathbf{V}_t \cdot \nabla T + \mathbf{V} \cdot \nabla (\mathbf{V} \cdot \nabla T)] + \mathbf{T}_t + \mathbf{V} \cdot \nabla T = \kappa \nabla^2 T, \quad (2.3.6)$$

where  $\kappa = \frac{K}{\rho_0 c_p}$  is the thermal diffusivity. The boundary conditions at the lower and upper surfaces are taken to correspond to free-free conditions. In this case

$$\begin{aligned} \mathbf{V}(x, Z=0, t) \cdot \hat{\mathbf{z}} &= \mathbf{V}(x, Z=D, t) \cdot \hat{\mathbf{z}} = 0, \\ \mathbf{V}_{ZZ}(x, Z=0, t) \cdot \hat{\mathbf{z}} &= \mathbf{V}_{ZZ}(x, Z=D, t) \cdot \hat{\mathbf{z}} = 0, \end{aligned} \quad (2.3.7)$$

$$T(x, Z=0, t) = T_0 + \delta T, \quad T(x, Z=D, t) = T_0.$$

Other boundary conditions could be adopted, such as the rigid-rigid or rigid-free conditions [34]. However, the free-free conditions are convenient and most commonly used in the literature. Moreover, no qualitative change in behaviour is expected if one set of boundary conditions is used over another [35]. In fact, Khayat [36] confirmed this consistency in behaviour for rotating flow as well.

The base state corresponds to stationary heat conduction, which remains the same as that for a Fourier fluid since both transient and upper convective terms in Eq. (2.3.5) vanish in this case. Consequently, the temperature, pressure gradient and heat flux for the conductive state are given by

$$\begin{aligned} T_B &= -(Z/D)\delta T + T_0 + \delta T, \\ dP_B / dZ &= -\rho_0 [1 - \alpha_T \delta T (1 - Z/D)] g, \end{aligned} \quad (2.3.8)$$

$$\mathbf{Q}_B = \left( 0, K \frac{\delta T}{D} \right),$$

respectively. The problem is conveniently cast in dimensionless form by taking the

length, time and velocity scales as  $D$ ,  $\frac{D^2}{\kappa}$  and  $\frac{\kappa}{D}$ , respectively. Let  $p = \frac{D^2}{\kappa \mu} (P - P_B)$  and

$\theta = \frac{T - T_B}{\delta T}$  be the dimensionless pressure and temperature deviations from the base (conductive) state. In this case, the dimensionless perturbation equations are given by

$$\nabla \cdot \mathbf{V} = 0, \quad (2.3.9)$$

$$\text{Pr}^{-1} (\mathbf{V}_t + \mathbf{V} \cdot \nabla \mathbf{V}) = -\nabla p + \text{Ra} \theta \hat{\mathbf{z}} + \Delta \mathbf{V}, \quad (2.3.10)$$

$$\theta_t + \mathbf{V} \cdot \nabla \theta = -j + w, \quad (2.3.11)$$

$$C(\mathbf{q}_t - \mathbf{V}_z + \mathbf{V} \cdot \nabla \mathbf{q} - \mathbf{q} \cdot \nabla \mathbf{V}) = -\mathbf{q} - \nabla \theta, \quad (2.3.12)$$

where  $\mathbf{V}(u, w)$  and  $\mathbf{q}$  are the dimensionless velocity and heat flux vectors, respectively. Here  $j = \nabla \cdot \mathbf{q}$ . It is interesting to note the presence of two linear terms of non-Fourier origin in Eq. (2.3.12), namely the transient term and the velocity gradient in the  $z$  direction. This contrasts with the convection of viscoelastic fluids where the transient terms are the only linear terms that survive in the stress equations (see [37]). This is an important point that will be explored further in Section 2.4. Eq. (2.3.6) takes the form:

$$C[\theta_{tt} + 2\mathbf{V} \cdot \nabla \theta_t + \mathbf{V}_t \cdot \nabla \theta - w_t + \mathbf{V} \cdot \nabla (\mathbf{V} \cdot \nabla \theta)] + \theta_t + \mathbf{V} \cdot \nabla \theta - w = \nabla^2 \theta. \quad (2.3.13)$$

The following non-dimensional groups have been introduced, namely, the Prandtl number, the Cattaneo number and the Rayleigh number, respectively, given by

$$\text{Pr} = \frac{\nu}{\kappa}, \quad C = \frac{\tau \kappa}{D^2}, \quad \text{Ra} = \frac{\delta T \alpha_T g D^3}{\nu \kappa}. \quad (2.3.14)$$

The problem can be simplified by casting the constitutive equation for heat flux in terms of the scalar variable  $j$ . Thus, upon taking the divergence of Eq. (2.3.12), and recalling again the identity  $\nabla \cdot (\mathbf{a} \cdot \nabla \mathbf{b}) = \nabla \mathbf{a} : \nabla \mathbf{b} + \mathbf{a} \cdot \nabla (\nabla \cdot \mathbf{b})$ , one obtains the following constitutive equation for  $j$ :

$$C(j_t + \mathbf{V} \cdot \nabla j) + j = -\Delta \theta, \quad (2.3.16)$$

where the continuity Eq. (2.3.9) is used. The boundary conditions Eq. (2.3.7) reduce to

$$\begin{aligned} w(x, z = 0, t) &= w(x, z = 1, t) \\ &= u_z(x, z = 0, t) = u_z(x, z = 1, t) \\ &= \theta(x, z = 0, t) = \theta(x, z = 1, t) = 0, \end{aligned} \quad (2.3.17)$$

which must be used to solve Eqs. (2.3.9), (2.3.10), (2.3.11) and (2.3.16). Finally, the Fourier model is recovered upon setting  $C = 0$  (zero relaxation time) in Eqs. (2.3.12), (2.3.13) or (2.3.16). In this case,  $\mathbf{q} = -\nabla\theta$  and  $\mathbf{j} = -\Delta\theta$  satisfy Eqs. (2.3.12) and (2.3.16), respectively.

At this stage, it is helpful to examine the order of magnitude of the Cattaneo number for practical fluids and thermal processes. For most fluids under normal conditions, the relaxation time is typically small. In particular, the Cattaneo number can be sufficiently large for some real fluids. Helium II, a low temperature liquid, possesses a relaxation time of  $O(10^{-2})$  [38]–[40] which corresponds to a Cattaneo number of  $O(10)$  for a 5cm gap. Furthermore, using Wang's formula for the relaxation time of a nanofluid [8], a 5% v/v mixture of water and TiO<sub>2</sub> has a relaxation time of  $O(10^{-4})$  with Cattaneo number of  $O(10^{-2})$  for a 50 $\mu\text{m}$  gap.

## 2.4 Linear stability analysis

Comparable to a Fourier fluid, the conduction of a non-Fourier fluid is lost to convection once a critical value of the Rayleigh number,  $Ra_c(k)$ , is exceeded, where  $k$  is the wave number of the disturbance. However, in contrast to a Fourier fluid, and similar to a viscoelastic fluid [37], non-Fourier conduction can be lost to steady or oscillatory convection, depending on the flow parameters. The linear stability analysis of the conduction state is similar to the case of a viscoelastic fluid, except that, unlike a viscoelastic fluid, a non-Fourier fluid at rest does recognize the non-Fourier character, which is reflected by the presence of the additional linear velocity gradient on the left hand side of Eq. (2.3.12), in addition to the transient term. The stability of the conduction state is examined by applying a small (infinitesimal) perturbation of the form



$$\begin{aligned} \mathbf{V}(x, z, t) &= \mathbf{v}(z)e^{\sigma t + ikx}, & \theta(x, z, t) &= \Theta(z)e^{\sigma t + ikx}, \\ p(x, z, t) &= P(z)e^{\sigma t + ikx}, & j(x, z, t) &= J(z)e^{\sigma t + ikx}, \end{aligned} \quad (2.4.1)$$

where  $k$  is the perturbation wave number in the  $x$  direction, and  $\sigma$  dictates the time evolution of the disturbance. Thus, the conduction/base state is stable (unstable) if the real part of  $\sigma$  is negative (positive). In this case, the dispersion relation is given as

$$\sigma^3 + \left( \text{Pr} \beta_n + \frac{1}{C} \right) \sigma^2 + \left( \beta_n \frac{\text{Pr} + 1}{C} - \frac{k^2 \text{Ra} \text{Pr}}{\beta_n} \right) \sigma + \frac{\text{Pr}}{C \beta_n} (\beta_n^3 - k^2 \text{Ra}) = 0. \quad (2.4.2)$$

Where  $\beta_n = n^2 \pi^2 + k^2$ , and  $n$  is the mode number. In contrast to a Fourier fluid, the presence of the cubic term in Eq. (2.4.2) hints to the possibility of stationary or oscillatory convection. In this regard, it is well established that the  $n = 1$  mode is the most prominent mode for a Fourier fluid. This is not easily established analytically for a NF fluid by examining Eq. (2.4.2). However, the  $n = 1$  mode turns out to be the most prominent mode, for both stationary and oscillatory convection. Consequently, only the  $n = 1$  mode will be examined in this work.

For steady convection, one recovers the same critical Rayleigh number,  $\text{Ra}_c$ , as a Fourier fluid, namely

$$\text{Ra}_c = \text{Ra}_{cF} = \frac{\beta^3}{k^2}, \quad (2.4.3)$$

where  $\beta = n^2 \pi^2 + k^2$ . In this case,  $\text{Ra}_c$  displays a minimum,  $\text{Ra}_m = \frac{27\pi^4}{4}$  at  $k_m = \frac{\pi}{\sqrt{2}}$ .

For oscillatory convection, the corresponding neutral curves are obtained upon setting  $\sigma = i\omega_c$  in Eq. (2.4.2),  $\omega_c$  being the frequency, and separating real and imaginary parts to give

$$\text{Ra}_c = \frac{\text{Pr}^2 C \beta + \text{Pr} + 1}{\beta^2 C^2 \text{Pr}^2} \text{Ra}_{cF}, \quad \omega_c = \frac{1}{C} \sqrt{\frac{C \text{Pr} \beta - \text{Pr} - 1}{\text{Pr}}}. \quad (2.4.4)$$

Clearly, oscillatory convection is possible only if

$$\beta > \frac{1 + \text{Pr}}{\text{Pr} C} \quad \text{or} \quad k > \sqrt{\frac{1 + \text{Pr}}{\text{Pr} C} - \pi^2}. \quad (2.4.5)$$

This criterion constrains the range of wave number for oscillatory convection. Thus, it is anticipated that each marginal stability curve in the Ra-k plane comprises two distinct branches: a Fourier branch, corresponding to steady convection, for  $k < k_i$ , and a non-Fourier branch, corresponding to oscillatory convection, for  $k > k_i$ , where  $k_i$  is the wave number at which the two branches intersect, and satisfies the relation,

$$k_i = \sqrt{\frac{1 + \text{Pr}}{\text{Pr} C} - \pi^2}, \quad (2.4.6)$$

since, at intersection, the frequency vanishes. It is not difficult to verify that substituting Eq. (2.4.5) into Eq. (2.4.4) leads to  $\text{Ra}_c(k = k_i) \equiv \text{Ra}_i = \text{Ra}_{cF}(k = k_i)$ . Eq. (2.4.6)

suggests that a limit,  $C_\infty$ , of  $C$  exists for which  $k_i = 0$ , and thus only oscillatory convection should be expected.

Two limits are worth examining here. Consider first the limit of large Cattaneo number. This case could reflect the situation where the thermal process time ( $D^2/\kappa$ ) is at least of the same order as that of the relaxation time of the liquid. In particular, if the gap is small (for instance, in the thermal convection in a nano-device), then the molecular mean-free path becomes of the same order as the gap. In this case, it is well established that both Newton's Law of viscosity and Fourier's law of heat are no longer valid. In other words, the liquid behaves more like a rarified gas, of non-Newtonian and non-Fourier character [41], [42]. For large  $C$ , Eq. (2.4.4) suggests that

$$\text{Ra}_c \sim \frac{1}{C}, \quad \omega_c \sim \frac{1}{\sqrt{C}}. \quad (2.4.7)$$

A couple of interesting observations can be made. First, the oscillation frequency behaves like  $\omega_c \sim 1/\sqrt{C}$ , suggesting that oscillatory rolls may not be detected in reality for large  $C$ . Second, the critical Rayleigh number decreases even faster with  $C$ . Whether this behaviour holds for any  $C$  will be examined below. Another limit of interest is the large  $\text{Pr}$  limit. In this limit, Eq. (2.4.4) reduces to

$$\lim_{\text{Pr} \rightarrow \infty} \text{Ra}_c = \frac{1}{\beta C} \text{Ra}_{cF} = \frac{\beta^2}{Ck^2}, \quad \lim_{\text{Pr} \rightarrow \infty} \omega_c = \frac{1}{C} \sqrt{C\beta - 1}. \quad (2.4.8)$$

In this case, the intersection wave number becomes

$$\lim_{\text{Pr} \rightarrow \infty} k_i = \sqrt{\frac{1}{C} - \pi^2}. \quad (2.4.9)$$

In the double limit of large  $C$  and  $\text{Pr}$ , Eq. (2.4.8) suggests that oscillatory convection sets in at any Rayleigh number. Further physical insight of these limits will be gained below when numerical results are reported.

Finally, it is helpful to list the eigenvector components, which will be used later, and take the form:

$$\begin{aligned} U(z) &= -\frac{i\pi}{k} \cos(\pi z), & W(z) &= \sin(\pi z), \\ P(z) &= \left[ \frac{\text{Ra}}{\beta} \left( \frac{C\sigma + 1}{C\sigma^2 + \sigma + \beta} \right) - 2 \right] n\pi \cos(\pi z), \end{aligned} \quad (2.4.10)$$

$$\Theta(z) = \left( \frac{C\sigma + 1}{C\sigma^2 + \sigma + \beta} \right) \sin(\pi z), \quad J(z) = \left( \frac{1}{C\sigma^2 + \sigma + \beta} \right) \beta \sin(\pi z).$$

Of particular interest here is the non-Fourier character reflected in the flow and heat transfer. In fact, Eq. (2.4.10) clearly reflects the absence of non-Fourier effects at criticality for *stationary* convection. This is easily verified upon setting  $\sigma = 0$ , as one recovers the Fourier limit. This is, of course, not the case for oscillatory convection.

Consequently, stationary convection of a non-Fourier fluid is expected to be Fourier in character, near criticality. It is observed that other modes will be present near criticality, which do exhibit a non-Fourier character, but they will be dominated by the critical mode. Of course, as the Rayleigh number increases beyond the critical value, non-Fourier effects become increasingly significant. Similarly, in the case of a viscoelastic or a non-Newtonian fluid, in general, any convective *steady* state emerging near criticality will not have a significant non-Newtonian character to it given the absence of shearing and elongation rates of the base (conductive) state [37]. Despite the apparent similarity, there is a significant difference between the current non-Fourier and non-Newtonian loss of conduction to steady convection. For non-Newtonian convection near criticality, the elastic component of the stress remains small given the absence of flow in the pre-critical range of Rayleigh number. More generally, for a non-Newtonian flow, the destabilization of the base state to a steady state leads to a Newtonian state at criticality. However, if the base state involves shearing and elongation, as in the case of Taylor-Couette flow, the steady vortex flow does exhibit non-Newtonian character near criticality [36].

The lack of Fourier character in the stationary convection mentioned above is only apparent, as Eq. (2.4.10) does not reflect the whole situation. At the center of the argument is the relation between the heat flux vector components and the temperature (gradient), which has not been invoked so far in the discussion since  $j$ , and not  $\mathbf{q}$ , is needed for the solution of the problem. The replacement of the heat equation, Eq. (2.3.12), by Eq. (2.3.16) leads to significant simplification in the current linear stability (and, eventually, any nonlinear) analysis as the formulation includes the scalar variable,  $j$  instead of the vector  $\mathbf{q}$ , reducing the number of degrees of freedom. Moreover, the upper-convective terms are replaced by a convective term,  $\mathbf{v} \cdot \nabla j$ . This term does not survive in the linear analysis given the stationary character of the base conductive state. Even the generalized energy equation, Eq. (2.3.13), illustrates the absence of non-Fourier character upon the onset of stationary convection. However, the heat flux vector does exhibit a non-Fourier contribution at criticality, emerging from the upper-convective terms. Indeed, near criticality, the heat flux in Eq. (2.3.12) reduces to

$$\mathbf{q} = -\nabla\theta + C\mathbf{v}_z. \quad (2.4.11)$$

Although, as deduced upon setting  $\sigma = 0$  in Eq. (2.4.10), the temperature, velocity and pressure do not display any non-Fourier character at criticality, the heat flux does, as Eq. (2.4.11) suggests. This is verified further by substituting the temperature and velocity from Eq. (2.4.10) into Eq. (2.4.11), to give

$$Q_x = -i \left( \frac{C}{C\sigma+1} \frac{\pi^2}{k} + \frac{k}{C\sigma^2 + \sigma + \beta} \right) \sin(\pi z), \quad (2.4.12)$$

$$Q_z = n\pi \left( \frac{1}{C\sigma+1} C - \frac{1}{C\sigma^2 + \sigma + \beta_n} \right) \cos(n\pi z). \quad (2.4.13)$$

Clearly, the non-Fourier character survives when  $\sigma = 0$ . However, given the decoupling from  $\mathbf{q}$ , as Eqs. (2.3.9)-(2.3.11) and Eq. (2.3.16) suggest, the flow and temperature fields are not expected to reflect a significant non-Fourier character upon the onset of stationary convection. Of course, this is not the case for the onset of oscillatory convection.

## 2.5 Results and discussion

In this section, results based on the formulation above are discussed. Conditions for both stationary and oscillatory convection are emphasized. It is helpful to schematically summarize the stability picture and notations used, in anticipation of the ensuing discussion and details. The neutral curves are illustrated in the  $(Ra_c-k)$  plane in Fig. 2.1 for different non-Fourier levels. The Fourier limit is reflected by the  $C = 0$  curve. For a weakly non-Fourier fluid ( $C \ll C_H$ ), the neutral curve comprises a Fourier branch and an oscillatory branch, intersecting at  $(Ra_i, k_i)$ . In this case, the minimum critical Rayleigh number is that of the Fourier branch  $\left( Ra_{mF} = \frac{27\pi^4}{4}, k_{mF} = \frac{\pi}{\sqrt{2}} \right)$ . As  $C$  increases, a minimum develops in the oscillatory branch. At  $C = C_H$ , the minima of the stationary and oscillatory branches coincide at the same Rayleigh number but different wave numbers.

For a moderately strong non-Fourier fluid ( $C > C_H$ ), there is only one minimum ( $Ra_m < Ra_{mF}, k_m > k_{mF}$ ).

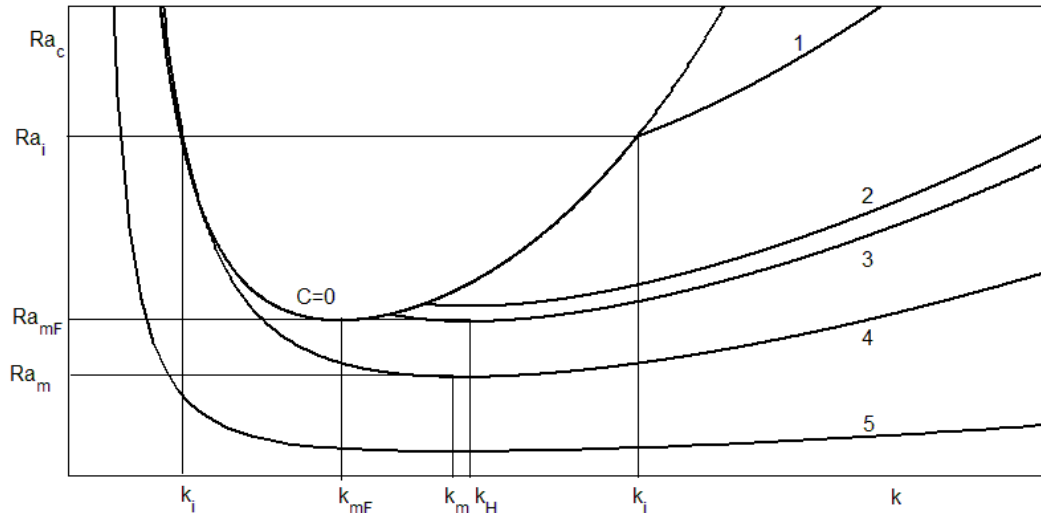


**Figure 2.1 - Schematic illustrating notations used in the (Ra-k) plane, qualitatively showing various marginal stability curves and corresponding regimes with respect to the critical Cattaneo number,  $C_H$ . The curves 1, 2, 3, 4 and 5 correspond to  $C \ll C_H$ ,  $C < C_H$ ,  $C = C_H$ ,  $C > C_H$ ,  $C \gg C_H$ .**

### 2.5.1 Stability of the conduction state

The influence of the Cattaneo number on the overall marginal stability picture is typically illustrated in Fig. 2.2, where the marginal stability curves (Fig. 2.2a) and corresponding frequency (Fig. 2.2b) are plotted against the wave number for  $Pr = 10$ . At the center, is the marginal stability curve for a Fourier fluid, which is recalled to be independent of  $Pr$ . For a Fourier fluid, there is an exchange of stability between the pure conduction state and stationary convection for any wave number. For relatively small  $C$ , each non-Fourier curve comprises a stationary branch, also part of the Fourier curve, for  $k < k_i$ , and an oscillatory convective branch (overstability) for  $k > k_i$ . The critical Rayleigh number and frequency for the oscillatory branch are given by Eq. (2.4.4). Clearly, oscillatory convection is possible only if  $k > k_i$ . In this case, it is not difficult to show that the

oscillatory branch always lies below the Fourier curve. This is also evident from Fig. 2.3a. Thus,

$$\frac{\text{Pr}^2 \beta C + \text{Pr} + 1}{\beta^2 C^2 \text{Pr}^2} < 1, \quad \text{or} \quad \text{Ra}_c < \text{Ra}_{cF}. \quad (2.5.1)$$

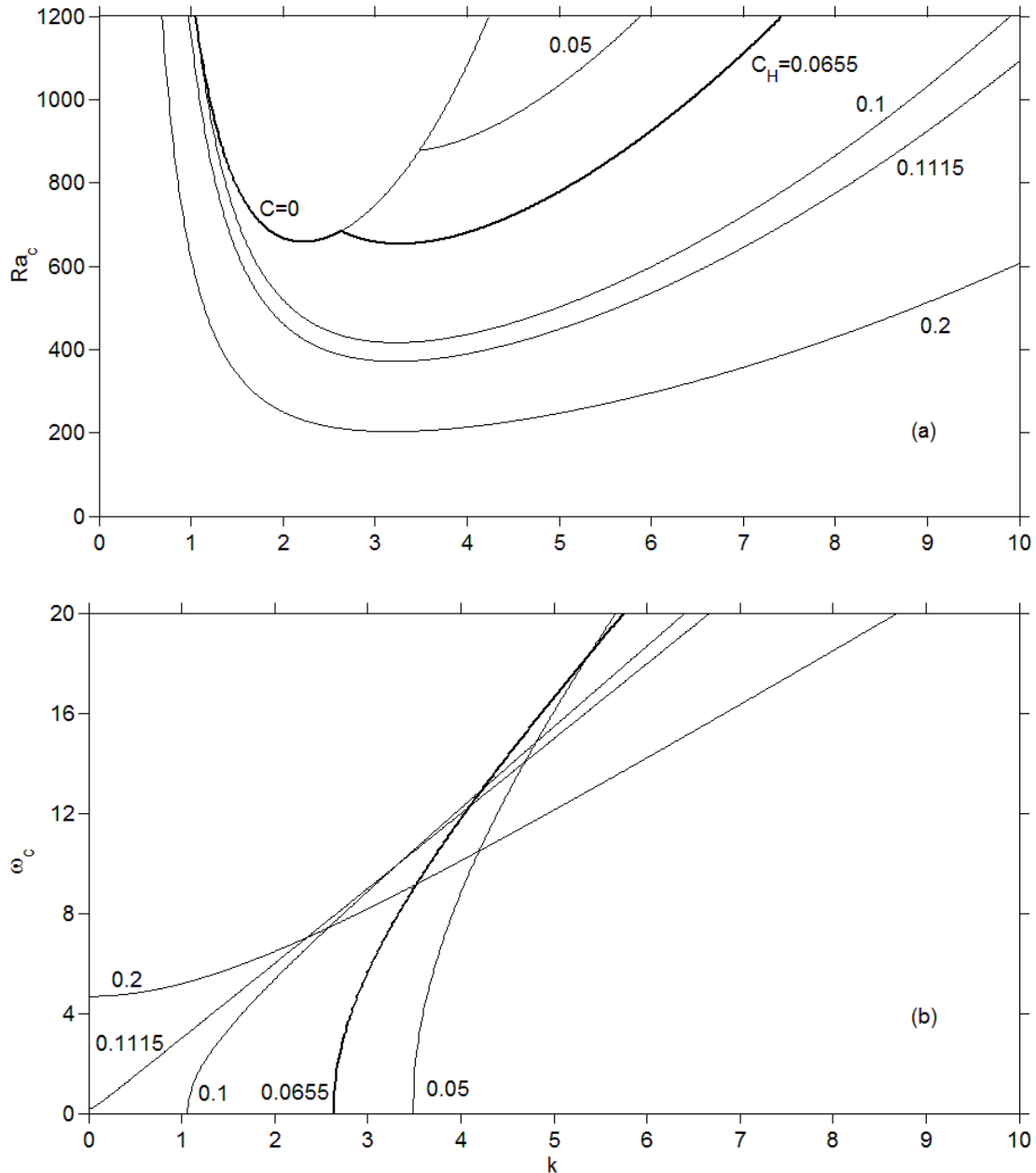


**Figure 2.2 - Influence of the Cattaneo number on (a) the marginal stability curves in the  $\text{Ra}$ - $k$  plane and (b) corresponding oscillation frequency for a  $\text{Pr} = 10$ .**

The inequality  $k > k_i$  constrains the range of wave numbers for oscillatory convection. As  $C$  increases,  $k_i$  moves to the left of the  $Ra$ - $k$  plane, reducing the range for stationary convection, and, simultaneously, lowering the oscillatory branch until the minimum

Rayleigh number of this branch becomes equal to  $Ra_{mF} = \frac{27\pi^4}{4}$ , at  $C = C_H$ .

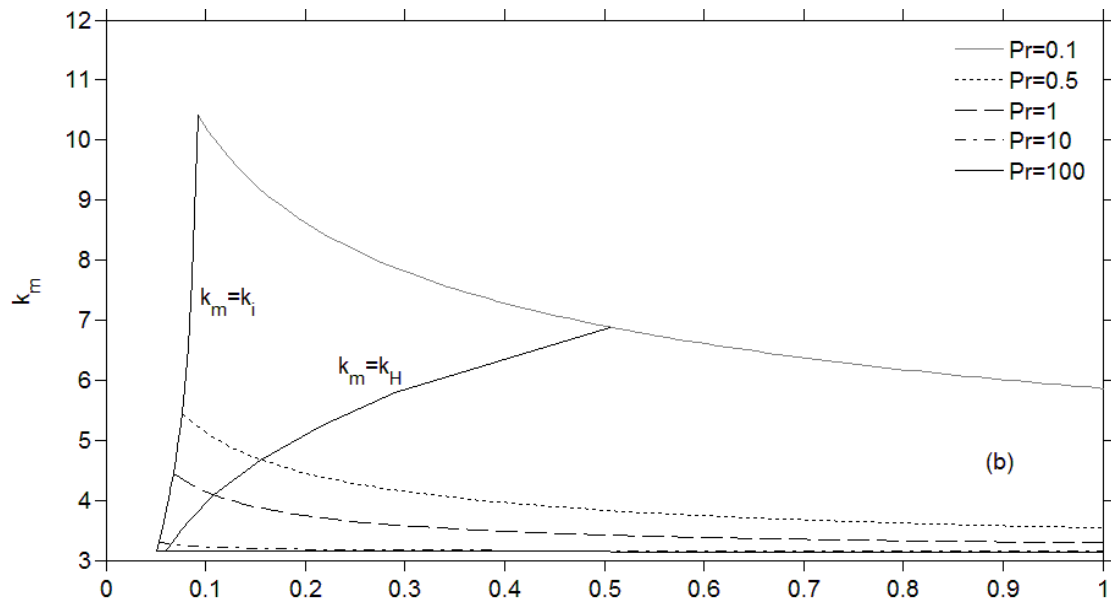
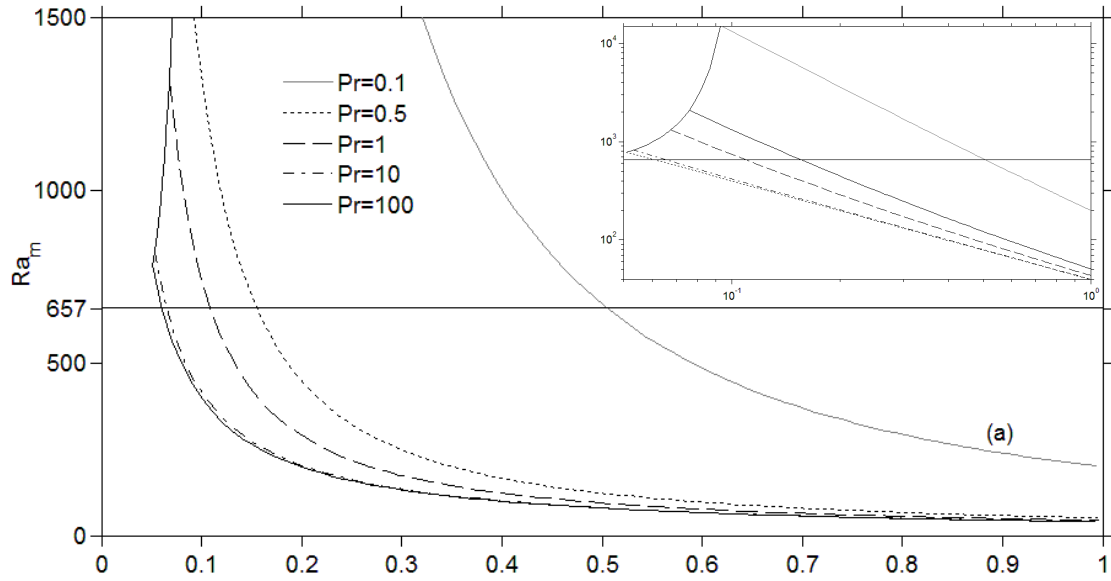
Consequently, two non-Fourier regimes are clearly distinguishable from Fig. 2.2 (see also Fig. 2.1). The weakly non-Fourier regime is taken to correspond to  $C < C_H$ . Here,  $C_H$  is the level of non-Fourier threshold below which stationary convection is predicted to be observed in reality since the minimum of the marginal stability curve lies above that of the Fourier curve, that is  $Ra_m > Ra_{mF}$ ,  $k_m > k_i$ . Note, however, that the oscillatory branch remains present for  $k > k_i$ . The oscillatory branch is expected to play an increasingly dominant role as  $C$  increases from zero in the post-critical range of Rayleigh number as a result of nonlinear modal interaction from different wave numbers. Here  $C_H$  signals the onset of oscillatory convection via a Hopf bifurcation at criticality. The values of  $C_H$  and corresponding wave number,  $k_H$ , must be determined numerically (see later). However,

some insight is gained for large  $Pr$ . In this case,  $Ra_c = \frac{\beta^2}{k^2 C}$ , which has a minimum at  $k =$

$$\pi, C_H = \frac{16}{27\pi^2} \approx 0.06 \text{ and } \omega_H = \frac{9}{16} \sqrt{\frac{5}{3}} \pi^2. \text{ This } C_H \text{ value should be compared to the}$$

0.0655 value for  $Pr = 10$  estimated from Fig. 2.3.





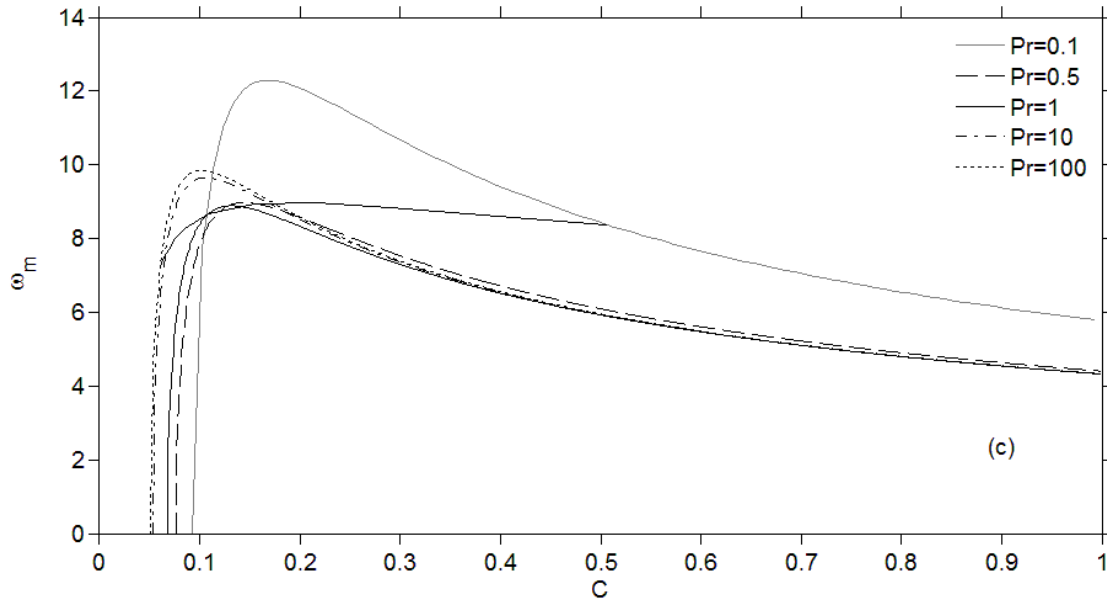


**Figure 2.3 - Influence of Pr and C on (a) the minimum critical Rayleigh number,  $Ra_m$ , (b) corresponding wave number,  $k_m$ , and (c) frequency,  $\omega_m$ .**

For a strongly non-Fourier fluid ( $C > C_H$ ), oscillatory convection is predicted to occur at  $Ra_c = Ra_m$ , with the steady convection range ( $k < k_i$ ) diminishing as  $C$  increases, to eventually disappear for  $C > C_\infty = \frac{11}{10\pi^2} = 0.111$ . In this domain, oscillatory convection is predicted to be observed first for any wave number. The conductive state loses its stability to oscillatory convection at a Rayleigh number that is increasingly smaller than  $Ra_{mF}$  as  $C$  increases. Eq. (2.4.4) suggests that the critical Rayleigh number vanishes at large  $C$ , indicating that strongly non-Fourier fluids exhibit spontaneous convection with no prior conduction. Note that the wave number,  $k_m$ , corresponding to the onset of oscillatory convection is always larger than  $k_{mF}$ . Thus, the decrease in roll size makes it more difficult to detect the convective roll pattern for more non-Fourier fluids.

The corresponding frequency values are shown in Fig. 2.2b. Obviously, the frequency vanishes for  $k < k_i$ . Typically, the frequency increases monotonically with  $k$ . Consequently, smaller rolls tend to oscillate faster. The rate of increase is large near  $k = k_i$ , but decreases with  $C$ . For  $C = 0.111$ ,  $\omega$  increases linearly with  $k$ . This linear behaviour

is not difficult to establish. In fact, for  $k_i = 0$ , Eq. (2.4.6) yields  $C = \frac{\text{Pr}+1}{\pi^2 \text{Pr}}$ . In this case,

the critical Rayleigh number and corresponding frequency are given by

$$\text{Ra}_c = \frac{\beta \pi^2 \text{Pr}+1}{\beta^2 (\text{Pr}+1)} \text{Ra}_{cF}, \quad \omega_c = \pi \sqrt{\frac{\text{Pr}}{\text{Pr}+1}} k. \quad (2.5.2)$$

Only oscillatory convection is possible for this and higher  $C$  values, with an increasing jump in  $\omega$  at  $k = 0$  as  $C$  increases. Interestingly, Fig. 2.2b reflects a slow increase in  $\omega_c$  with  $k$  for small wave number. Indeed, Eq. (2.4.4) suggests that the frequency behaves

like  $\omega_c \sim \sqrt{\frac{\beta}{C}}$  for large  $C$ , indicating that oscillation occurs at a small frequency,

independent of the Prandtl number. In this regard, the marginal stability curves for

$C > \frac{\text{Pr}+1}{\pi^2 \text{Pr}}$  reflect a weaker minimum with increasing  $C$  (Fig. 2.2a), suggesting that a

range of roll sizes are equally likely to be observed in experiment. The neutral curves in Fig. 2.2a are similar to the ones obtained by Tzou [43] for a nanofluid using a two-phase approach (see Tzou's Fig. 4b), and also behaves similar to the linear stability prediction of Nield [44]. This trend is also encountered when the level of elasticity increases for a viscoelastic fluid, for both Rayleigh-Benard convection [37] and rotating flows, such as Taylor-Couette flow [36], Taylor-Dean flow [45], the flows between two co-rotating disks [46] and cone-and-plate rheometer [47].

An important quantity in this analysis is the minimum critical Rayleigh number,  $\text{Ra}_m$ , as it reflects the Rayleigh number (temperature differential) for the observation of convection in experiment. Fig. 2.3 displays the influence of the Cattaneo and Prandtl numbers on  $\text{Ra}_m$  (Fig. 2.3a), corresponding wave number,  $k_m$  (Fig. 2.3b), and frequency,  $\omega_m$  (Fig. 2.3c). All curves in Fig. 3a show that  $\text{Ra}_m$  decreases monotonically with  $C$ , suggesting that rolls emerge more readily for strongly NF fluids, for any Prandtl number.

The figure also depicts the  $\text{Ra}_{mF} = \frac{27\pi^4}{4}$  line, the Fourier line that divides the weakly

from the strongly NF fluids, with corresponding  $Ra_m$  value located above and below the line, signaling the onset of stationary and oscillatory convection, respectively. Note that the intersection of a curve with the Fourier line occurs at  $C = C_H$ . Note also that each curve begins at a non-zero  $C$  value, below which no minimum exists in the oscillatory branch of the Rayleigh number (see also Fig. 2.2a). The starting point corresponds to the coincidence of the minimum with the intersection Rayleigh number,  $Ra_i$ . The log-log plots in the inset in Fig. 2.3a suggest that the minimum critical Rayleigh number decreases with  $C$ , essentially like  $Ra_m \sim C^{-a}$ , where  $a$  is a constant that depends on the Prandtl number.

The influence of the Prandtl number is significant, particularly for small  $Pr$ . This is of particular relevance to liquids at low temperature (see, for instance, [3], [48]). Conduction appears to be more stable for fluids with lower Prandtl number. For fluids with  $Pr > 10$ , the stability picture is essentially unaffected by the Prandtl number. This is also evident from the wave number and frequency curves in Fig. 2.3b and 2.3c, respectively. The wave number decreases with  $C$ , suggesting that the size of stationary and oscillatory rolls increases with  $C$ , but decreases with Prandtl number. The expression for the wave number is not difficult to establish from Eq. (2.5.1) to be

$$k_m = \pi \left( 1 + \frac{Pr+1}{\pi^2 C Pr^2} \right)^{1/4}. \text{ Clearly, at small Prandtl number, } k_m \sim C^{-1/4} Pr^{-1/2}, \text{ reflecting}$$

small roll size for low-temperature liquids. Finally, the frequency in Fig. 2.3c exhibits a non-monotonic response with  $C$ . In fact, there seems to be an optimal  $C$  value for the oscillation frequency. Interestingly, both the frequency maximum and corresponding  $C$  value do not depend strongly on the Prandtl number.

The interdependence on  $C$  and  $Pr$  is reminiscent of that predicted for a viscoelastic fluid, with  $C$  playing the role of the elasticity number,  $E$ . This becomes particularly evident at large Prandtl number. The large  $Pr$  oscillatory behaviour is captured from Eq. (2.4.8). In particular, the saturation in the minimum critical Rayleigh number, corresponding wave number and frequency shown in Fig. 2.3 is recovered as

$$\lim_{Pr \rightarrow \infty} Ra_m = \frac{4\pi^2}{C}, \quad \lim_{Pr \rightarrow \infty} k_m = \pi, \quad \lim_{Pr \rightarrow \infty} \omega_m = \frac{1}{C} \sqrt{2\pi^2 C - 1}. \quad (2.5.3)$$

These limit expressions are exactly the same as those for a viscoelastic fluid if  $C$  is replaced by  $E$  (see [36]). Similar to non-Fourier fluids, the region for elastic overstability grows as  $Pr$  increases. This observation is in agreement with the results of Brand & Zielinska and Eltayeb [49], [50] in the case of a Maxwell fluid. At large  $Pr$  values ( $Pr > 10$ ), which is typically the case of polymeric solutions, the region of overstability remains essentially unchanged, as indicated by the saturation of the curves, especially those corresponding to the critical Rayleigh number and wave number.

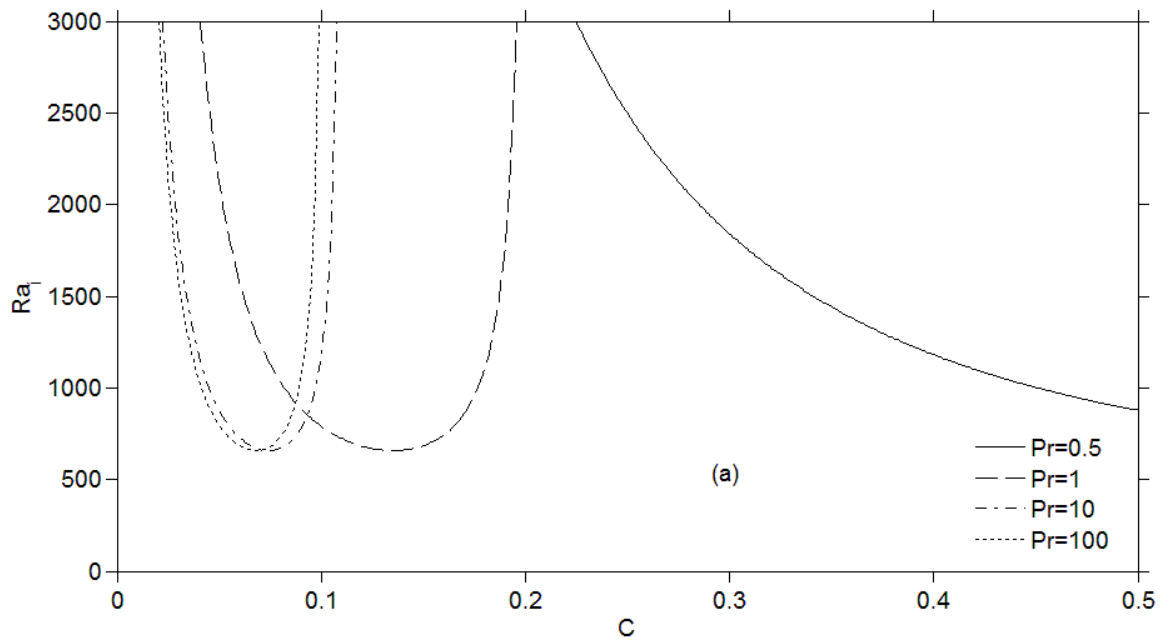
Although the parallels between non-Fourier and non-Newtonian effects are striking, there is, however, one significant difference in the behaviour of the frequency. The trends are simply opposite with respect to the Prandtl number, for small  $Pr$  (compare the current Fig. 2.3c to Fig. 4 in [37]). More particularly, while the frequency approaches infinity at large Prandtl number for a viscoelastic fluid, it reaches a finite value as in Eq. (2.4.8) for a NF fluid. However, the trend in frequency is not consistent with  $Pr$  as Fig. 2.3c suggests. Although there is an overall decrease in the frequency with  $Pr$  over most of the  $C$  range, this trend is markedly reversed for  $C$  near the critical threshold  $C_H$ . This is the trend that is most likely to correspond to reality.

## 2.5.2 Further influence of the Prandtl number

The influence of Prandtl number is assessed upon examining the behaviour of the Rayleigh number,  $Ra_i$ , and corresponding wave number,  $k_i$ , at the intersection of the oscillatory and stationary branches (see Fig. 2.2a and 2.3a). Fig. 2.4 displays the dependence of  $Ra_i$  (Fig. 2.4a) and  $k_i$  (Fig. 2.4b) on  $C$  for  $Pr \in [0.1, 100]$ . The curves in Fig. 2.4 are more easily interpreted in conjunction with the marginal stability curves as in Fig. 2.2a. Recall from those curves that two intersection points are possible for the same critical Rayleigh number, one for a weakly and another for a strongly NF fluid, on the right and left branch of the Fourier curve, respectively. The intersection wave number is

given by Eq. (2.4.6). The double-valuedness is reflected in Fig. 2.4a as well as in the expression of the Rayleigh number at intersection, namely

$$Ra_i = \frac{(1 + Pr)^3}{Pr^2 C^2 (1 + Pr - \pi^2 Pr C)}. \quad (2.5.4)$$



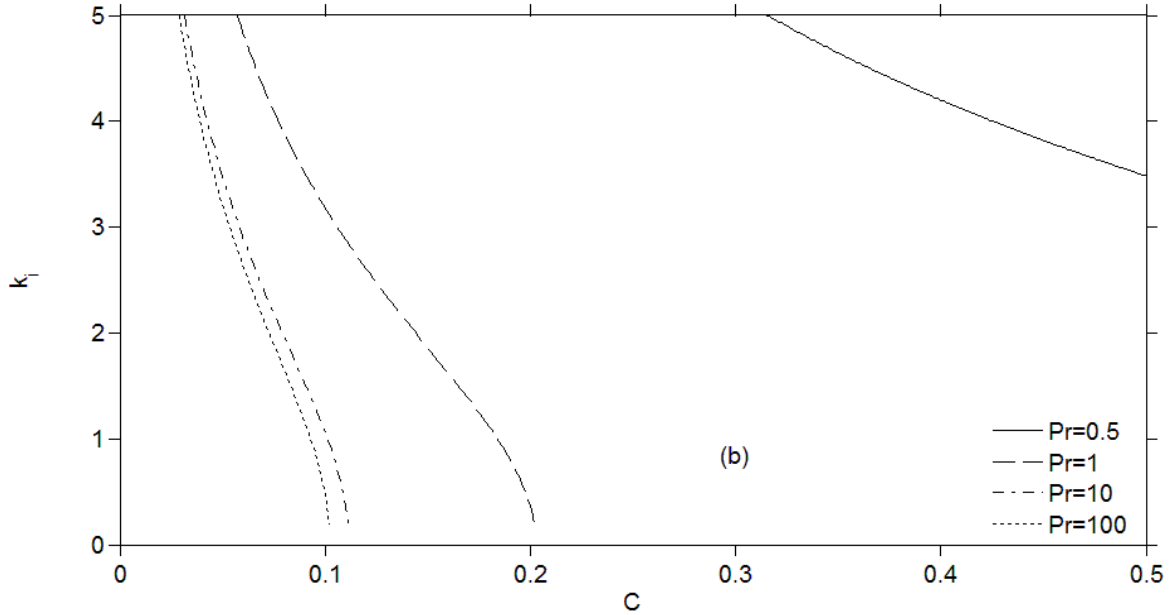


**Figure 2.4 - Influence of the Cattaneo and Prandtl numbers on (a) the Rayleigh number,  $Ra_i$ , and (b) wave number,  $k_i$ , at the intersection between the steady and oscillatory marginal stability branches.**

The minimum of  $Ra_i$  is the same regardless of the Prandtl number, but occurs at different

$C$  values corresponding to  $k_i = \frac{\pi}{\sqrt{2}}$ , given by  $C = \frac{2(\text{Pr} + 1)}{3\pi^2 \text{Pr}}$ . These  $C$  values coincide

with the intersection of the  $k_i$  curves and the  $\frac{\pi}{\sqrt{2}}$  line in Fig. 2.4b. Fig. 2.4a shows a

widening of the  $C$  range as  $\text{Pr}$  decreases. The intersection wave number in Fig. 2.4b decreases monotonically with  $C$  (or relaxation time), signaling a wider oscillatory range for more strongly NF fluids. The decrease is more rapid for larger  $\text{Pr}$ , leading to oscillatory convection over the whole  $k$  range at some critical  $C$  value. At small  $\text{Pr}$ , realistically, there is always a range of small wave number for stationary convection.

### 2.5.3 Overstability threshold

The emergence of oscillatory convection is an important phenomenon for non-Fourier fluids. When  $C$  approaches  $C_H$ , the critical Rayleigh number experiences a second

minimum, as apparent from Fig. 2.2a. Consequently, the quantity of prime interest is  $C_H$ , the value of  $C$  at which the minimum Rayleigh number for oscillatory convection coincides with the minimum of the Fourier curve for stationary convection. At  $C = C_H$ , the minimum Rayleigh number,  $Ra_m$ , coincides with the Fourier value  $Ra_{mF} = \frac{27\pi^4}{4}$ . It is helpful to refer to the curve corresponding to  $C = C_H = 0.0655$  in Fig. 2.2a. At  $C = C_H$ , the neutral curve possesses two minima in  $Ra_c$ , which suggests the existence of a bistable mode. Thus, depending on the initial conditions or even possibly the imposed cell size, as the curve in Fig. 2.2a suggests, conduction can be lost to stationary or oscillatory convection.

For  $C > C_H$ , linear stability predicts that oscillatory, and not stationary, convection is bound to be observed, with a Hopf bifurcation expected to emerge at  $Ra_m$ . Fig. 2.5 displays the dependence of the critical Cattaneo number,  $C_H$ , corresponding wave number,  $k_H$  and oscillation frequency,  $\omega_H$ , on the Prandtl number. Both the low and high ranges of  $Pr$  values are examined to cover a wide range of NF fluids. In this regard, low-temperature liquids ( $Pr < 1$ ) display a strong NF character (see [51] and references therein) despite their low  $Pr$ . For fluids at room temperature, the Prandtl number is typically much larger than one (on the order of 10 to 1000). In this case, Fig. 2.5 suggests that the conditions for onset of oscillatory convection are independent of the Prandtl number. Consequently, it is helpful to examine the critical conditions for large  $Pr$ . In this case, recalling the critical minimum Rayleigh number from Eq. (2.5.3) and setting it to  $Ra_{mF}$  leads to

$$\begin{aligned} \lim_{Pr \rightarrow \infty} Ra_c = \frac{4\pi^2}{C_H} = Ra_{mF} = \frac{27\pi^4}{4}, \quad C_H \rightarrow \frac{16}{27\pi^2}, \\ \lim_{Pr \rightarrow \infty} k_H = \pi, \quad \lim_{Pr \rightarrow \infty} \omega_H = \frac{1}{C_H} \sqrt{2\pi^2 C_H - 1} = \frac{3\pi^2}{16} \sqrt{15}. \end{aligned} \quad (2.5.5)$$



Fig. 2.5 indicates that NF fluids with higher thermometric conductivity (smaller  $Pr$ ) are less likely to exhibit oscillatory convection, and is difficult to detect in practice given the low oscillation frequency. However, for  $Pr \gg 1$ , the influence of fluid conductivity is less significant as indicated by the flattening of the curves at larger value of  $Pr$ . The critical  $C$  decreases monotonically with  $Pr$ , at a steeper rate in the small  $Pr$  range. Thus, a more viscous NF fluid tends to exhibit oscillatory convection more easily. However, there is a limit to the influence of the Prandtl number. Indeed,  $C_H$  remains essentially unchanged for  $Pr > 3$ .

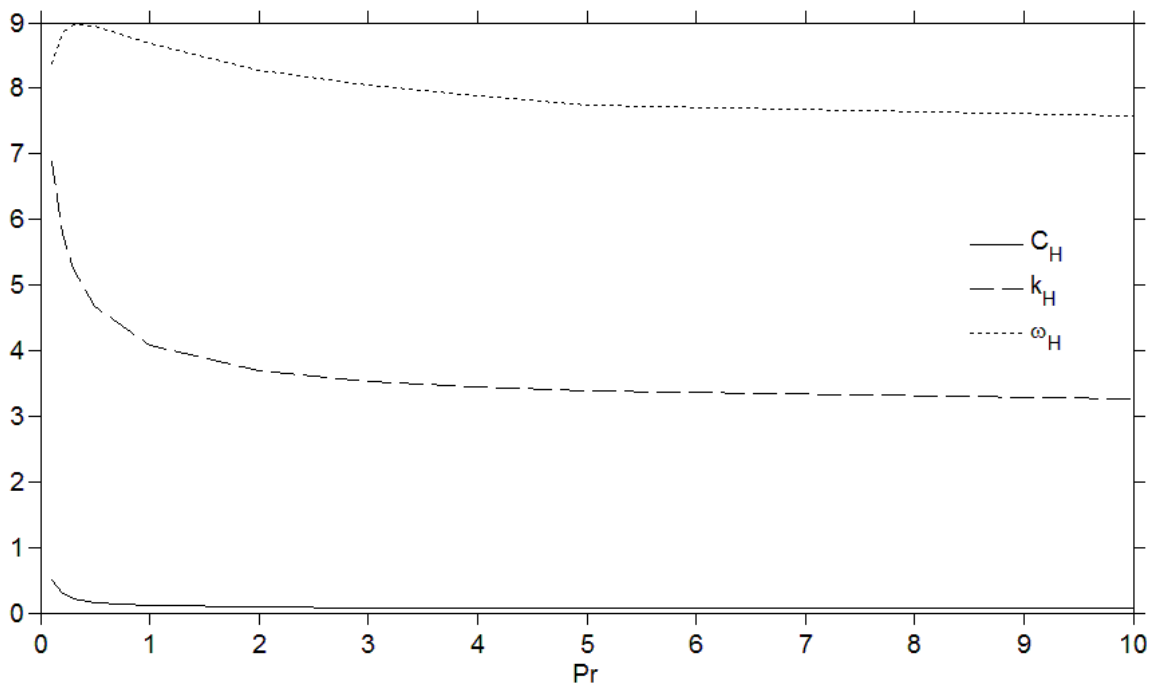


**Figure 2.5 - Influence of the Prandtl number on (a) the critical Cattaneo number,  $C_H$ , (b) the corresponding wave number,  $k_H$ , and (c) the oscillation frequency,  $\omega_H$ .**

In contrast to the threshold in Cattaneo and wave numbers, the frequency exhibits a nonmonotonic response against the Prandtl number. The frequency generally decreases with Prandtl number, but exhibits a weak maximum at small  $Pr$ .

The onset of overstability coincides with the emergence of a pair of imaginary eigenvalues in the characteristic Eq. (2.4.2). Oscillatory convection (overstability) always emerges for strongly non-Fourier fluids ( $C > C_H$ ) at a critical Rayleigh number  $Ra_m <$

$Ra_{mF}$ . The conductive state remains unconditionally stable for  $Ra < Ra_m$ , and becomes overstable for  $Ra > Ra_m$ . Both  $Ra_m$  and  $k_m$  generally decrease with  $C$ . The jump in wave number coincides with the sudden shift from  $k_{mF} = \frac{\pi}{\sqrt{2}}$  to  $k_m > k_{mF}$  when  $C$  exceeds  $C_H$ . The corresponding frequency,  $\omega_m$  generally displays a maximum. The frequency increases sharply (from zero) at  $C = C_H$ , reaching a maximum. The minimum Rayleigh number and corresponding frequency reduce to

$$\lim_{C \rightarrow \infty} Ra_m = \lim_{C \rightarrow \infty} \omega_m = 0. \quad (2.5.6)$$

There is a discontinuity for the wave number, which is easily established for large  $C$ .

Indeed,  $\lim_{C \rightarrow \infty} k_m = \pi$ .

Finally, the parallels between non-Fourier and non-Newtonian effects, at both the theoretical and experimental levels, cannot be overemphasized. Donzelli studied Rayleigh-Benard convection of nanofluids and found that when a uniform suspension was heated suddenly from below, transient oscillatory convection was observed [52]. In contrast to the current formulation, this behaviour is not within the capability of the models developed by Tzou [43] and Nield [44] who predict only stationary instability when equal concentrations of nanoparticles are imposed at the boundaries. In analogy with the current findings, the existence of an overstable mode for strongly elastic fluids was also predicted by linear stability analysis, and was confirmed experimentally. Kolodner [53] examined the thermal convection of DNA suspensions in a narrow annular configuration. Travelling short rolls (indicating oscillatory thermal convection) were observed at a Rayleigh number smaller than the Newtonian critical Rayleigh number (of the base solvent) for DNA suspensions, with sufficiently large elasticity number. Comparison between theory and experiment was carried out by Li & Khayat [37]. The threshold Rayleigh number for the onset of oscillation was found to be a decreasing function of  $E$ , dropping below the threshold for the onset of stationary convection, which parallels the behaviour in Fig. 2.4a with respect to  $C$  for a NF fluid. The theoretical

predictions of Li & Khayat [37] tend to overestimate the critical Rayleigh number, especially in the higher elasticity range.

#### 2.5.4 Mechanism behind oscillatory convection in non-Fourier fluids

The oscillation induced in NF heat conduction is not difficult to understand given the hyperbolic character of energy/heat equations [1]. Physical insight is gained for NF fluid convection by examining heat accumulation and invoking the divergence of the heat flux vector rather than the heat flux vector itself. Fig. 2.6 shows the distribution of  $j$  versus  $x$  at  $z = 0.5$  for a Fourier fluid ( $C = 0$ ) and a NF fluid ( $C = 0.5$ ), for a relatively large Prandtl number ( $Pr = 1000$ ). Note that if  $j$  is negative (positive), heat is accumulated

(removed) by conduction. Now, consider the centre of the roll  $\left(x = \frac{\pi}{k}, z = \frac{1}{2}\right)$  where there is no flow for a stationary roll (stagnation point), and thus, the only mode of heat transfer is conduction. For a Fourier fluid  $j\left(x = \frac{\pi}{k}, z = \frac{1}{2}\right) = 0$ , and, therefore, the temperature at

the centre of the roll remains constant. On the other hand, for a NF fluid,

$j\left(x = \frac{\pi}{k}, z = \frac{1}{2}\right) < 0$ . Consequently, the temperature at the centre rises, and, due to

buoyancy, an upward flow is generated. By considering a similar argument for other locations over the roll, one can explain the movement of the roll perpendicular to its axis in the horizontal plane, in the form of a travelling wave.

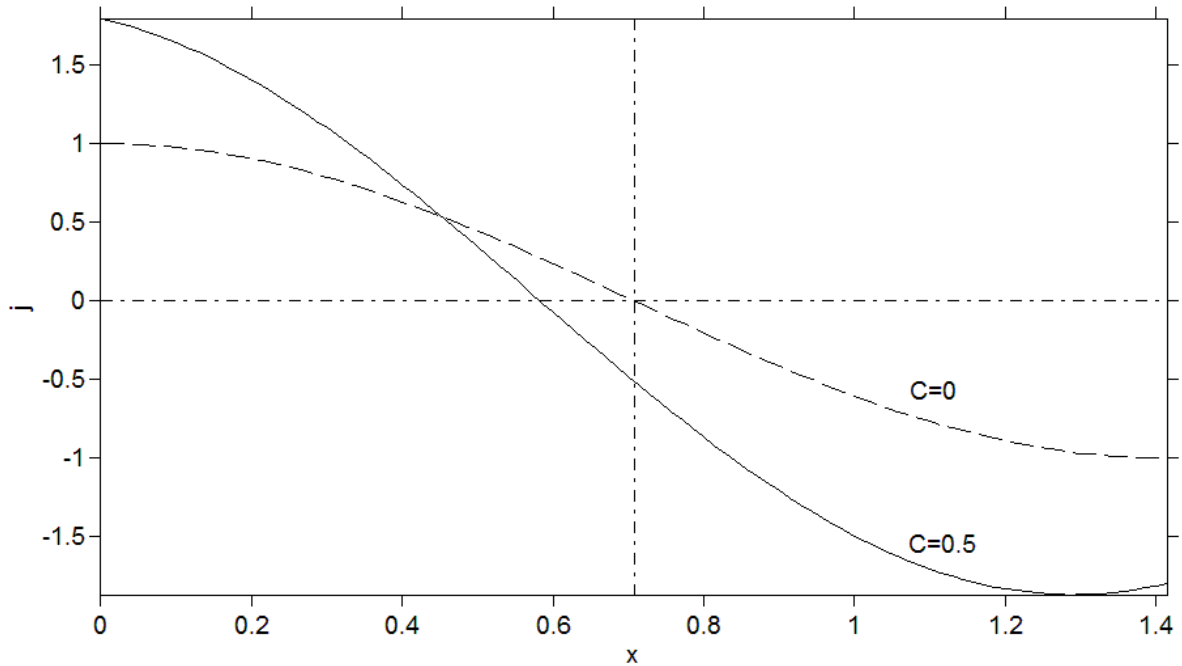


**Figure 2.6 - Distribution of  $j$  at  $z = 0.5$  for a Fourier ( $C = 0$ ) and a non-Fourier fluid ( $C = 0.5$ ).**

The increase in the oscillation frequency with increasing wave number, depicted in Fig. 2.2b, is physically rationalized by first invoking the argument of Manneville [54]. “The emergence of wide convection cells is hindered by horizontal shear viscous damping whereas narrow cells have to fight against both thermal diffusion and the vertical shear viscous damping.” For narrow rolls, thermal diffusion opposes the flow by transferring heat from hot regions (upward moving fluid) to the cold regions (downward moving fluid). As rolls become narrower due to thermal diffusion, the temperature difference between upward and downward flows decreases, and, consequently, fluid velocity decreases [54], [55]. However, for NF fluids the horizontal heat flux crosses the roll boundary and shifts the location of rolls perpendicular to the roll axis, as previously explained. As rolls become narrower, the effect of thermal diffusion becomes more dominant and thus rolls seem to move faster.

## 2.6 Concluding remarks

This study examines the natural convection of non-Fourier fluids of the single phase-lagging type. These fluids possess a relaxation time, reflecting the delay in the response of the heat flux and the temperature gradient. The study is particularly relevant to low-temperature liquids, small length scales and fast heat transfer processes. The relevance of NF effects to nanofluids has also been recently recognized in the literature. The parallels between NF and polymeric fluids are highlighted. Similar to viscoelastic fluids, the constitutive equation for heat flux used in the present analysis is frame invariant.

Linear stability analysis indicates that, in contrast to ordinary fluids, a NF fluid can lose its conductive mode to stationary or oscillatory convection. For small relaxation time (small Cattaneo number,  $C$ ), the neutral stability curve comprises a Fourier branch ( $k < k_i$ ) and an oscillatory branch ( $k > k_i$ ). As  $C$  increases and reaches a critical value,  $C_H$ , both stationary and oscillatory convection become equally probable, confirming the existence of the bistable mode observed in experiment [52]. For  $C > C_H$ , only oscillatory convection is predicted, at a Rayleigh number decreasing with  $C$  (see Fig. 2.3a). Thus, oscillatory convection becomes increasingly the mode of preference, compared to both conduction and stationary convection. In fact, for strongly non-Fourier fluids, oscillatory convection may practically become spontaneously observed, with no prior conduction. It is found that the oscillatory roll size grows with relaxation time. Although the oscillation frequency decreases monotonically with roll size (Fig. 2.3b), it exhibits a non-monotonic response with respect to relaxation time (emergence of a maximum with respect to  $C$ ). Finally, the effect of  $Pr$  on linear stability appears to be negligible for  $Pr > 10$ . The figures show a flattening of the curves well before  $Pr = 100$  and thus as far as linear stability is concerned, a fluid with  $Pr = 10^5$  should behave similar to a fluid with  $Pr = 10$ .

## 2.7 Acknowledgements

The financial support of the Natural Sciences and Engineering Council of Canada is gratefully acknowledged.

## 2.8 References

- [1] D. Joseph and L. Preziosi, “Heat waves,” *Rev. Mod. Phys.*, vol. 61, no. 1, pp. 41–73, 1989.
- [2] H. Liepmann and G. Laguna, “Nonlinear interactions in the fluid mechanics of helium II,” *Annu. Rev. Fluid Mech.*, p. 34, 1984.
- [3] R. Donnelly, “The two-fluid theory and second sound in liquid helium,” *Phys. Today*, no. October, p. 34, 2009.
- [4] R. R. Letfullin, T. F. George, G. C. Duree, and B. M. Bollinger, “Ultrashort Laser Pulse Heating of Nanoparticles: Comparison of Theoretical Approaches,” *Adv. Opt. Technol.*, vol. 2008, pp. 1–8, 2008.
- [5] H. Ahmadikia, A. Moradi, R. Fazlali, and A. Parsa, “Analytical solution of non-Fourier and Fourier bioheat transfer analysis during laser irradiation of skin tissue,” *J. Mech. Sci. Technol.*, vol. 26, no. 6, pp. 1937–1947, Jun. 2012.
- [6] F. Xu, M. Lin, and T. J. Lu, “Modeling skin thermal pain sensation: Role of non-Fourier thermal behavior in transduction process of nociceptor,” *Comput. Biol. Med.*, vol. 40, no. 5, pp. 478–486, May 2010.
- [7] B. Vermeersch and G. Mey, “Non-Fourier thermal conduction in nano-scaled electronic structures,” *Analog Integr. Circuits Signal Process.*, vol. 55, no. 3, pp. 197–204, Apr. 2007.
- [8] L. Wang and X. Wei, “Equivalence between dual-phase-lagging and two-phase-system heat conduction processes,” *Int. J. Heat Mass Transf.*, vol. 51, no. 7–8, pp. 1751–1756, Apr. 2008.
- [9] D. S. Chandrasekharaiah, “Hyperbolic thermoelasticity: a review of recent literature,” *Appl. Mech. Rev.*, vol. 51, no. 12, pp. 705–729, 1998.

- [10] S. D. Bronson, J. G. Fujimoto, and E. P. Ippen, “Femtosecond electronic heat transport dynamics in thin gold films,” *Phys. Rev. Lett.*, vol. 59, no. 1962, 1987.
- [11] H. A. Stone, A. D. Stroock, and A. Ajdari, “Engineering Flows in Small Devices,” *Annu. Rev. Fluid Mech.*, vol. 36, no. 1, pp. 381–411, Jan. 2004.
- [12] X. B. Nie, S. Y. Chen, W. N. E, and M. O. Robbins, “A continuum and molecular dynamics hybrid method for micro- and nano-fluid flow,” *J. Fluid Mech.*, vol. 500, pp. 55–64, Jan. 2004.
- [13] S. Bhattacharyya, Z. Zheng, and A. T. Conlisk, “Electro-osmotic flow in two-dimensional charged micro- and nanochannels,” *J. Fluid Mech.*, vol. 540, p. 247, 2005.
- [14] M. Oliveira and L. Rodd, “Simulations of extensional flow in microrheometric devices,” *Microfluid. Nanofluidics*, vol. 5, no. 6, pp. 809–826, Apr. 2008.
- [15] G. Lebon and A. Clout, “Bénard-Marangoni instability in Maxwell–Cattaneo fluids,” *Phys. Lett. A*, vol. 105, no. 7, pp. 361–364, 1984.
- [16] D. Y. Tzou and K. S. Chiu, “Temperature-dependent thermal lagging in ultrafast laser heating,” *Int. J. Heat Mass Transf.*, vol. 44, no. 9, pp. 1725–1734, May 2001.
- [17] P. Haupt, *Continuum Mechanics and Theory of Materials*. New York: Springer Verlag, 2002.
- [18] C. I. Christov, “On frame indifferent formulation of the Maxwell–Cattaneo model of finite-speed heat conduction,” *Mech. Res. Commun.*, vol. 36, no. 4, pp. 481–486, Jun. 2009.
- [19] R. Khayat and M. Ostoja-Starzewski, “On the objective rate of heat and stress fluxes. Connection with micro/nano-scale heat convection,” *Discret. Contin. Dyn. Syst. - Ser. B*, vol. 15, no. 4, pp. 991–998, Mar. 2011.

- [20] P. Dauby, M. Nélis, and G. Lebon, “Generalized Fourier equations and thermoconvective instabilities,” *Rev. Mex. física*, no. 4, pp. 57–62, 2002.
- [21] B. Straughan and F. Franchi, “Benard convection and the Cattaneo law for heat conduction,” *Proc. R. Soc. Edinburgh Sect. A Math.*, vol. 96, no. 1–2, p. 175, 1984.
- [22] B. Straughan, “Tipping points in Cattaneo-Christov thermohaline convection,” *Proc. R. Soc. A Math. Phys. Eng. Sci.*, vol. 467, no. 2125, pp. 7–18, May 2010.
- [23] J. Buongiorno, “Convective Transport in Nanofluids,” *J. Heat Transfer*, vol. 128, no. 3, p. 240, 2006.
- [24] P. Vadasz, “Heat transfer augmentation in nanofluids via nanofins,” *Nanoscale Res. Letts.*, vol. 6, no. 154, 2011.
- [25] J. Garg, B. Poudel, M. Chiesa, J. B. Gordon, J. J. Ma, J. B. Wang, Z. F. Ren, Y. T. Kang, H. Ohtani, J. Nanda, G. H. McKinley, and G. Chen, “Enhanced thermal conductivity and viscosity of copper nanoparticles in ethylene glycol nanofluid,” *J. Appl. Physics*, vol. 103, no. 7, 2008.
- [26] A. Saha, S. Basu, and B. Kumar, “Effects of acoustic-streaming-induced flow in evaporating nanofluid droplets,” *J. Fluid Mech.*, vol. 692, no. 207, 2012.
- [27] D. Y. Tzou, *Macro-to-Microscale Heat Transfer: The Lagging Behaviour*. Washington: Taylor & Francis, 1997.
- [28] J. J. Vadasz and S. Govender, “Thermal wave effects on heat transfer enhancement in nanofluids suspensions,” *Int. J. Therm. Sci.*, vol. 49, no. 2, pp. 235–242, Feb. 2010.
- [29] R. B. Bird, R. C. Armstrong, and O. Hassager, *Dynamics of Polymeric Liquids Vol. 1*, 2nd ed. New York: John Wiley & Sons, 1987.
- [30] J. G. Oldroyd, “On the Formulation of Rheological Equations of State,” *Proc. R. Soc. A Math. Phys. Eng. Sci.*, vol. 200, no. 1063, pp. 523–541, Feb. 1950.



- [31] D. A. S. Rees, A. P. Bassom, and P. G. Siddheshwar, “Local thermal non-equilibrium effects arising from the injection of a hot fluid into a porous medium,” *J. Fluid Mech.*, vol. 594, pp. 379–398, 2008.
- [32] D. A. Nield, A. Barletta, and M. Celli, “The effect of viscous dissipation on the onset of convection in an inclined porous layer,” *J. Fluid Mech.*, vol. 679, pp. 544–558, 2011.
- [33] E. Spiegel and G. Veronis, “On the Boussinesq approximation for a compressible fluid,” *Astrophys. J.*, vol. 131, p. 442, 1960.
- [34] P. G. Drazin and W. H. Reid, *Hydrodynamic Stability*. Cambridge University Press, 1981.
- [35] A. V. Getling, *Rayleigh-Benard Convection: Structures and Dynamics*. World Scientific, 1998.
- [36] R. Khayat, “Finite-amplitude Taylor-vortex flow of viscoelastic fluids,” *J. Fluid Mech.*, vol. 400, pp. 33–58, 1999.
- [37] Z. Li and R. E. Khayat, “Finite-amplitude Rayleigh–Bénard convection and pattern selection for viscoelastic fluids,” *J. Fluid Mech.*, vol. 529, pp. 221–251, Apr. 2005.
- [38] H. Jones, “The properties of liquid helium,” *Rep Prog Phys*, vol. 280, 1939.
- [39] F. London, *Superfluid II: Macroscopic theory of superfluid Helium*. New York: Dover Publications, 1964.
- [40] R. J. Donnelly and C. F. Barenghi, “The observed properties of liquid helium at the saturated vapour pressure,” *J. Phys. Chem. Ref. Data*, vol. 27, 1998.
- [41] R. E. Khayat and B. C. Eu, “Generalized hydrodynamics and heat waves,” *Can. J. Phys.*, vol. 70, no. 1, pp. 62–71, Jan. 1992.
- [42] R. Khayat and B. Eu, “Nonlinear transport processes and fluid dynamics: Cylindrical Couette flow of Lennard-Jones fluids,” *Phys. Rev. A*, 1988.

- [43] D. Y. Tzou, "Thermal instability of nanofluids in natural convection," *Int. J. Heat Mass Transf.*, vol. 51, no. 11–12, pp. 2967–2979, Jun. 2008.
- [44] D. A. Nield and A. V. Kuznetsov, "The onset of convection in a horizontal nanofluid layer of finite depth," *Eur. J. Mech. - B/Fluids*, vol. 29, no. 3, pp. 217–223, May 2010.
- [45] Y. L. Joo and E. S. . Shaqfeh, "Observations of purely elastic instabilities in the Taylor-Dean flow of a Boger fluid," *J. Fluid Mech.*, vol. 262, pp. 27–73, 1994.
- [46] A. Oztekin and R. A. Brown, "Instability of a viscoelastic fluid between rotating parallel discs: analysis for the Oldroyd-B fluid," *J. Fluid Mech.*, vol. 255, pp. 473–502, 1993.
- [47] G. H. McKinley, A. Oztekin, J. A. Byars, and R. A. Brown, "Self-similar spiral instabilities in elastic flows between a cone and a plate," *J. Fluid Mech.*, vol. 285, pp. 123–164, 1995.
- [48] F. Franchi and B. Straughan, "Thermal convection at low temperature," *J. Non-Equilibrium Thermodyn.*, vol. 19, p. 368, 1994.
- [49] H. R. Brand and B. J. Zielinksa, "Tri-critical codimension-2 point near the onset of convection in viscoelastic liquids," *Phys. Rev. Lett.*, vol. 57, no. 25, p. 3167, 1986.
- [50] I. A. Eltayeb, "Non-linear thermal convection in an elasticoviscous layer heated from below," *Proc. R. Soc. Lond. A. Math. Phys. Sci.*, vol. 356, no. 1685, pp. 161–176, 1977.
- [51] R. E. Khayat and B. C. Eu, "Generalized hydrodynamics, normal stress effects and velocity slip in cylindrical Couette flow of Lennard-Jones fluids," *Phys. Rev. A*, vol. 39, no. 728, 1989.
- [52] G. Donzelli, R. Cerbino, and A. Vailati, "Bistable Heat Transfer in a Nanofluid," *Phys. Rev. Lett.*, vol. 102, no. 10, p. 104503, Mar. 2009.

- [53] P. Kolodner, "Oscillatory convection in viscoelastic DNA suspensions," *J. Nonnewton. Fluid Mech.*, vol. 75, no. 167, 1998.
- [54] P. Manneville, "From chaos to turbulence in fluid dynamics," in *Engineering Applications of Dynamics of Chaos*, W. Szemplinska-Stupnicka and I. Troger, Eds. Springer, 1991, pp. 67–138.
- [55] F. H. Busse, "Transition to turbulence in Rayleigh-Benard convection," in *Topics in Applied Physics, Hydrodynamic Instabilities and Transition to Turbulence*, H. L. Swinney and J. P. Gollup, Eds. Springer, 1985, pp. 97–133.

## Chapter 3

### 3 Thermal convection of fluids with non-Fourier heat transport

#### 3.1 Introduction

Heat transfer is typically described by Fourier's law, which is given by

$$\mathbf{Q} = -K\nabla T. \quad (3.1.1)$$

Here,  $\mathbf{Q}$  is the heat flux,  $K$  is the thermal conductivity of the medium, and  $T$  is the temperature. When combined with the First Law of Thermodynamics, Fourier's law predicts an infinite speed of heat propagation. Physically, however, a disturbance in  $T$  must travel at a finite speed that is determined by molecular interactions [1]. One approach to remedy this problem has been to add a partial time derivative to the left-hand side of Eq. (3.1.1), as in the case of the Maxwell-Cattaneo equation [2]. This results in a hyperbolic differential equation, implying wave-like heat transport. This does not necessarily solve the problem of instantaneous heat propagation, however [3]–[5], since the Maxwell-Cattaneo equation is not frame-invariant and, as such, its application is restricted to non-deformable media. Heat transport equations involving different objective derivatives have been introduced in attempts to remedy this situation. The most promising modification appears to be that of [6], recently revisited by [7], whose use of Oldroyd's upper-convected derivative [8] leads to the frame indifferent Cattaneo-Vernotte equation,

$$\tau \frac{\delta \mathbf{Q}}{\delta t} + \mathbf{Q} = -K\nabla T \quad (3.1.2)$$

where

$$\frac{\delta \mathbf{Q}}{\delta t} \equiv \frac{\partial \mathbf{Q}}{\partial t} + \mathbf{v} \cdot \nabla \mathbf{Q} - \mathbf{Q} \cdot \nabla \mathbf{v} - \mathbf{Q} \nabla \cdot \mathbf{v}. \quad (3.1.3)$$

$\tau$  is the thermal relaxation time of the medium and characterizes the relaxation of the heat flux to a new steady state following a perturbation of the temperature field.

Coupled with the energy equation, this constitutive equation yields a single equation for  $T(x,t)$ , an advantage that other frame-invariant formulations do not possess [6]. This equation replaces Fourier's law whenever non-Fourier effects are relevant, collapses back to Fourier's law when they are not, and can be applied to both deformable and non-deformable media. In this paper, we refer to fluids in which the effects of  $\tau$  are non-negligible as non-Fourier fluids, while those in which the relaxation time can be ignored are referred to as Fourier fluids.

Most practical problems involve materials with relaxation times on the order of picoseconds [9] and, in such cases, the Cattaneo-Vernotte equation reduces to the classical Fourier model. There are systems, however, in which the relaxation time is not negligible. Non-Fourier effects lead to thermal waves in superfluid liquid helium, referred to as second sound [10], [11], and have been increasingly observed in a variety of other systems as well. For example at small lengths scales, the heat transport properties of rarefied gases [12], [13] and convection around MEMS devices have been explained in terms of non-Fourier behaviour [14]–[16], and non-Fourier contributions to heat transport have been predicted in theories of granular flows [17], [18] as well as nanofluids [19].

The importance of non-Fourier effects is characterized by the ratio of the thermal relaxation time to the time scale for thermal diffusion. If  $D$  is a characteristic length scale

and  $\kappa$  the thermal diffusivity of the fluid, then the thermal diffusion time is  $\frac{D^2}{\kappa}$ . Non-

Fourier effects become significant when the ratio  $C = \frac{\tau\kappa}{D^2}$ , referred to as the Cattaneo number, becomes significant.  $C$  increases relatively rapidly as  $D$  decreases, and so non-Fourier effects are expected to be observable in very small systems such as micro- and nanometer devices that involve heat transport and flow [15], [20]–[28].

There has been a limited amount of work done on convection with non-Fourier heat transport [3], [29]–[31]. In this paper, we analytically investigate the linear stability of the

steady conduction state in a Rayleigh-Bénard configuration with  $C > 0$ , as well as the heat transport and stability of the steady convection state that bifurcates from the conduction state.

## 3.2 The Mathematical Model

### 3.2.1 Governing equations and boundary conditions

Consider a thin layer of a Newtonian non-Fourier liquid of infinite extent in the  $(x,y)$  directions, confined between isothermal plates at  $Z = 0$  and  $Z = D$ . The fluid layer is heated from below, with the plates maintained at temperatures  $T_0 + \delta T$  and  $T_0$ , respectively. When  $\delta T$  is small, there is no flow and the heat transport across the layer is solely due to conduction. As  $\delta T$  is increased, thermal expansion causes the density of the liquid near the lower plate to decrease. When the decrease in gravitational potential energy, which results from raising the less-dense fluid to the top of the layer, becomes larger than the energy dissipated by viscosity and thermal diffusion, a convective flow develops.

The fluid density  $\rho$  is assumed to depend linearly on the temperature  $T$  according to

$$\rho = \rho_0 [1 - \alpha_T (T - T_0)], \quad (3.2.1)$$

where  $\alpha_T$  is the coefficient of thermal expansion and  $\rho_0$  is the density of the fluid at  $T_0$ .

The fluid is assumed to be incompressible, with specific heat at constant pressure  $c_p$ , thermal conductivity  $K$  and viscosity  $\mu$ . The fluid behavior is described by equations for the conservation of mass, linear momentum and energy, as well as the constitutive equation for the non-Fourier heat flux. In this case, the conservation equations are given by

$$\nabla \cdot \mathbf{V} = 0, \quad (3.2.2)$$

$$\rho_0 (\mathbf{V}_t + \mathbf{V} \cdot \nabla \mathbf{V}) = -\nabla P - \rho g \hat{\mathbf{z}} + \mu \Delta \mathbf{V}, \quad (3.2.3)$$

$$\rho_0 c_p (T_t + \mathbf{V} \cdot \nabla T) = -\nabla \cdot \mathbf{Q}, \quad (3.2.4)$$

where  $\Delta$  is the Laplacian operator and the subscript  $t$  denotes partial differentiation with respect to time. Here  $\mathbf{V} = (U, 0, W)$  is the velocity vector,  $P$  is the pressure,  $g$  is the acceleration due to gravity, and  $\hat{z}$  is a unit vector in the  $z$ -direction. In writing Eqs. (3.2.2)-(3.2.4) we have used the Boussinesq approximation, which states that the effect of the variations in density are negligible everywhere in the conservation equations except in the buoyancy term of Eq. (3.2.3) [32]. We take the heat flux to be governed by the Cattaneo-Vernotte equation introduced above, re-written here as

$$\tau(\mathbf{Q}_t + \mathbf{V} \cdot \nabla \mathbf{Q} - \mathbf{Q} \cdot \nabla \mathbf{V}) = -\mathbf{Q} - K \nabla T. \quad (3.2.5)$$

We use free-free boundary conditions and perfectly conducting upper and lower plates, such that the boundary conditions are

$$W(X, Z = 0, t) = W(X, Z = D, t) = 0,$$

$$W_{zz}(X, Z = 0, t) = W_{zz}(X, Z = D, t) = 0. \quad (3.2.6)$$

$$T(X, Z = 0, t) = T_0 + \delta T, \quad T(X, Z = D, t) = T_0.$$

While other boundary conditions could be adopted, the free-free conditions are convenient due to the mathematical simplicity of the corresponding solutions for  $\mathbf{V}$  and  $T$  [33].

The base state of the system of Eqs. (3.2.2)-(3.2.5) with the boundary conditions in Eq. (3.2.6) corresponds to no flow. Both the transient and upper convective terms in Eq. (3.2.5) vanish in this state, and transport of heat occurs simply by conduction. Consequently, the temperature, pressure gradient and heat flux in this state are given by

$$T_B = -(Z/D)\delta T + T_0 + \delta T,$$

$$dP_B / dZ = -\rho_0 [1 - \alpha_T \delta T (1 - Z/D)] g, \quad (3.2.7)$$

$$\mathbf{Q}_B = \left( 0, K \frac{\delta T}{D} \right),$$

respectively, where the subscript B refers to the base state. The problem is conveniently cast in dimensionless form by taking the length, time and velocity scales as  $D$ ,  $\frac{D^2}{\kappa}$  and  $\frac{\kappa}{D}$ , respectively. Let  $p = \frac{D^2}{\kappa\mu}(P - P_B)$ ,  $\mathbf{q} = \frac{D}{K\delta T}(\mathbf{Q} - \mathbf{Q}_B)$  and  $\theta = \frac{T - T_B}{\delta T}$  be the dimensionless deviations of the pressure, heat flux and temperature from their values in the base state. Substituting these into Eqs. (3.2.2)-(3.2.5) the dimensionless equations for these deviations are

$$\nabla \cdot \mathbf{v} = 0, \quad (3.2.8)$$

$$\text{Pr}^{-1}(\mathbf{v}_t + \mathbf{v} \cdot \nabla \mathbf{v}) = -\nabla p + \text{Ra}\theta \mathbf{e}_z + \Delta \mathbf{v}, \quad (3.2.9)$$

$$\theta_t + \mathbf{v} \cdot \nabla \theta = -\nabla \cdot \mathbf{q} + w, \quad (3.2.10)$$

$$C(\mathbf{q}_t - \mathbf{v}_z + \mathbf{v} \cdot \nabla \mathbf{q} - \mathbf{q} \cdot \nabla \mathbf{v}) = -\mathbf{q} - \nabla \theta, \quad (3.2.11)$$

where  $\mathbf{v} = (u, 0, w)$  is the dimensionless velocity vector. There are two linear terms of non-Fourier origin in Eq. (3.2.11): the transient term proportional to  $\mathbf{q}_t$  and the term involving  $\mathbf{v}_z$ . The non-dimensional Prandtl number, Rayleigh number, and Cattaneo number are given by

$$\text{Pr} = \frac{\nu}{\kappa}, \quad \text{Ra} = \frac{\delta T \alpha_T g D^3}{\nu \kappa}, \quad C = \frac{\tau \kappa}{D^2}, \quad (3.2.12)$$

respectively, where  $\kappa = \frac{K}{\rho_0 c_p}$  is the thermal diffusivity.



The heat flux can be eliminated from Eqs. (3.2.10) and (3.2.11) by taking the divergence of Eq. (3.2.11), using the identity  $\nabla \cdot (\mathbf{a} \cdot \nabla \mathbf{b}) = \nabla \mathbf{a} : \nabla \mathbf{b} + \mathbf{a} \cdot \nabla (\nabla \cdot \mathbf{b})$ , where  $\mathbf{a}$  and  $\mathbf{b}$  are two general vectors, and using (3.2.8) and (3.2.10). We obtain

$$C[\theta_{tt} + 2\mathbf{v} \cdot \nabla \theta_t + \mathbf{v}_t \cdot \nabla \theta - w_t + \mathbf{v} \cdot \nabla (\mathbf{v} \cdot \nabla \theta)] + \theta_t + \mathbf{v} \cdot \nabla \theta - w = \nabla^2 \theta. \quad (3.2.13)$$

Since the problem is two-dimensional, we introduce the stream function  $\psi(x, z, t)$ , such that

$$\mathbf{u} = \psi_z, \quad w = -\psi_x.$$

Finally, taking the curl of Eq. (3.2.9) eliminates of the pressure term from the momentum equation. The resulting system of equations for the two unknowns  $\psi$  and  $\theta$  is

$$\text{Pr}^{-1} [\Delta \psi_t + \psi_z \psi_{xxx} - \psi_x \psi_{zzz} + \psi_z \psi_{xxx} - \psi_x \psi_{xxz}] = \Delta^2 \psi - \text{Ra} \theta_x \quad (3.2.14)$$

$$\begin{aligned} C[\theta_{tt} + \psi_{zt} \theta_x - \psi_{xt} \theta_z + 2(\psi_z \theta_{xt} - \psi_x \theta_{zt}) + \psi_{xt} + \psi_z \psi_{xx} - \psi_x \psi_{xz} + \psi_z \psi_{xz} \theta_x \\ - \psi_z \psi_{xx} \theta_z - \psi_x \psi_{zz} \theta_x + \psi_x \psi_{xz} \theta_z + \psi_z^2 \theta_{xx} - 2\psi_x \psi_z \theta_{xz} + \psi_x^2 \theta_{zz}] \\ + \theta_t + \psi_z \theta_x - \psi_x \theta_z + \psi_x - \theta_{xx} - \theta_{zz} = 0 \end{aligned} \quad (3.2.15)$$

The non-dimensional boundary conditions on  $\psi$  and  $\theta$  are

$$\begin{aligned} \psi_x(x, z=0, t) &= \psi_x(x, z=1, t) \\ &= \psi_{zz}(x, z=0, t) = \psi_{zz}(x, z=1, t) \\ &= \theta(x, z=0, t) = \theta(x, z=1, t) = 0. \end{aligned} \quad (3.2.16)$$

Eqs. (3.2.14) and (3.2.15) reduce to the usual equations for Rayleigh-Bénard convection with Fourier heat transport if  $C = 0$ .

### 3.2.2 Development of the Dynamical System

The solution to Eqs. (3.2.14) and (3.2.15), subject to boundary conditions in Eq. (3.2.16), can be represented by an infinite Fourier series in  $x$  and  $z$  with time dependent Fourier

coefficients. This yields an infinite set of coupled ordinary differential equations. In the spirit of Lorenz [34], we truncate this Fourier series to obtain a finite system of ordinary differential equations, keeping only the minimum number of terms required to include the necessary physics. The truncated system must still satisfy the boundary conditions.

Additionally, we require that the truncated equations for the non-Fourier system reduce to the well-known Lorenz model [34] in the absence of non-Fourier effects, i.e., when  $C \rightarrow 0$ . As in the case of Fourier fluids, we keep only the first term in the Fourier series for the stream function, which satisfies the boundary conditions in Eq. (3.2.16):

$$\psi(x, z, t) = \psi_1(t) \sin(\pi z) \sin(kx). \quad (3.2.17)$$

Here,  $k$  is the wave number of the flow in the  $x$ -direction. As with a Fourier fluid, more than one term must be kept in the expression for the temperature field to retain some part of the original system's essential nonlinearity. Again, following Lorenz [34], we write the temperature field as

$$\theta(x, z, t) = \theta_1(t) \sin(\pi z) \cos(kx) + \theta_2(t) \sin(2\pi z). \quad (3.2.18)$$

Projecting Eqs. (3.2.14)-(3.2.15) onto the modes in Eqs. (3.2.17)-(3.2.18), we obtain, after some algebra, a system of five coupled first-order ordinary differential equations:

$$\dot{X} = -\text{Pr}(X + \text{Ra}Y) \quad (3.2.19)$$

$$\dot{Y} = A \quad (3.2.20)$$

$$\dot{A} = X^2Y - 2XB + \text{Pr}(X + \text{Ra}Y)Z + \frac{\text{Pr}}{\text{Ra}_{\text{cF}}}(X + \text{Ra}Y) - a \left( A + XZ + \frac{X}{\text{Ra}_{\text{cF}}} + Y \right) \quad (3.2.21)$$

$$\dot{Z} = B \quad (3.2.22)$$

$$\dot{B} = \frac{X^2}{\text{Ra}_{\text{cF}}} + 2XA - \text{Pr}(X + \text{Ra}Y)Y + 2X^2Z + a(XY - B - bZ) \quad (3.2.23)$$

Here, time has been rescaled has been rescaled by  $\beta = \pi^2 + k^2$ , and the scaled mode amplitudes are

$$X = \frac{\pi k}{\sqrt{2}b} \psi_1, \quad Y = \frac{\pi k^2}{\sqrt{2}\beta^3} \theta_1, \quad Z = \frac{\pi k^2}{\beta^3} \theta_2. \quad (3.2.24)$$

The parameters

$$a = \frac{1}{C\beta}, \quad b = \frac{4\pi^2}{\beta}, \quad \text{Ra}_{cF} = \frac{\beta^3}{k^2} \quad (3.2.25)$$

have also been introduced. When  $C = 0$ , Eqs. (3.2.19)-(3.2.23) reduce to the usual Lorenz Model [34].

### 3.3 Linear Stability Analysis of the Conduction State

The linear stability of the conduction state for a fluid with a single relaxation time was examined previously [35]. The results will be summarized here for completeness and to provide the background information necessary to properly discuss the transition from conduction to steady convection expected for non-Fourier fluids.

As for any fluid, once a critical value of the Rayleigh number has been exceeded, the stability of the conduction state of a non-Fourier fluid is lost to convection. We introduce an infinitesimal perturbation to the steady conduction state defined by

$$\begin{aligned} X(x, z, t) &= X'(z)e^{\sigma t + ikx}, & Y(x, z, t) &= Y'(z)e^{\sigma t + ikx}, & A(x, z, t) &= A'(z)e^{\sigma t + ikx}, \\ Z(x, z, t) &= Z'(z)e^{\sigma t + ikx}, & B(x, z, t) &= B'(z)e^{\sigma t + ikx}, \end{aligned} \quad (3.3.1)$$

where  $\sigma$  describes the growth rate of the perturbation. The dispersion relation is given by

$$0 = \left( \sigma^2 + a\sigma + ab \right) \left( \sigma^3 + (a + \text{Pr})\sigma^2 + \left( a \text{Pr} - \frac{\text{Ra Pr}}{\text{Ra}_{cF}} + a \right) \sigma + a \text{Pr} - a \frac{\text{Ra Pr}}{\text{Ra}_{cF}} \right) \quad (3.3.2)$$

The non-Fourier conduction state can lose stability to either steady or unsteady convection, and to allow for this possibility,  $\sigma$  is taken to be complex, i.e.,

$$\sigma = \sigma_r + i\omega.$$

$\omega$  is the dimensionless frequency of oscillation of the convective flow. If the real part  $\sigma_r$  is negative (positive), then the conduction state is stable (unstable) to these infinitesimal perturbations. The quadratic portion of this Eq. (3.3.2) yields only stable values for  $\sigma$ . To obtain the marginal stability boundary, we thus set the cubic factor in Eq. (3.3.2) equal to zero and then set  $\sigma_r = 0$ .

For steady convection,  $\omega = 0$ , and the Rayleigh number  $Ra_c$  at the onset of convection is the same as for Fourier transport, i.e.,

$$Ra_c = Ra_{cF} = \frac{\beta^3}{k^2}, \quad (3.3.3)$$

where the subscript F indicates the Fourier result. In this case,  $Ra_c$  has a minimum of

$$Ra_{mF} = \frac{27\pi^4}{4} \text{ at a wave number } k_{mF} = \frac{\pi}{\sqrt{2}}.$$

For the case of oscillatory convection,  $Ra_c$  and  $\omega$  are given by

$$Ra_c = aRa_{cF} \left( \frac{Pr^2 + a(Pr+1)}{Pr^2} \right) \quad (3.3.4)$$

and

$$\omega = a - \frac{a^2(Pr+1)}{Pr}, \quad (3.3.5)$$

respectively. An oscillatory solution to Eq. (3.3.2) is only possible if the right-hand-side of Eq. (3.3.5) is positive. This requires  $a < \frac{Pr}{Pr+1}$  or, using Eq. (3.2.25a),

$$C > \frac{Pr+1}{Pr\beta}. \quad (3.3.6)$$

Similarly, oscillatory convection can only occur if

$$k > \sqrt{\frac{1 + \text{Pr}}{\text{Pr} C} - \pi^2}. \quad (3.3.7)$$

Eq. (3.3.6) indicates that oscillatory convection is only possible if either  $C$  or the wave number is large enough. There are thus two distinct regions of the marginal stability curve, as shown in Fig. 3.1. One is the weakly non-Fourier fluid region, defined as  $C < 0.0651$ . Here, the stability boundary is comprised of the Fourier curve (shown as a heavy line in Fig. 3.1) splitting off into the oscillatory non-Fourier branch at their intersection point. Since the minimum of this curve is at the same values of  $Ra$  and  $k$  as in the Fourier case, the conduction state still loses stability at  $Ra_{cF}$  with no oscillatory behaviour. The other region is strongly non-Fourier, corresponding to  $C > 0.0651$ . Here, the minimum of the non-Fourier branch is less than  $Ra_{cF}$  and convection sets in earlier than for a Fourier fluid. On this branch, the loss of stability is via a Hopf bifurcation to an oscillatory convection state.

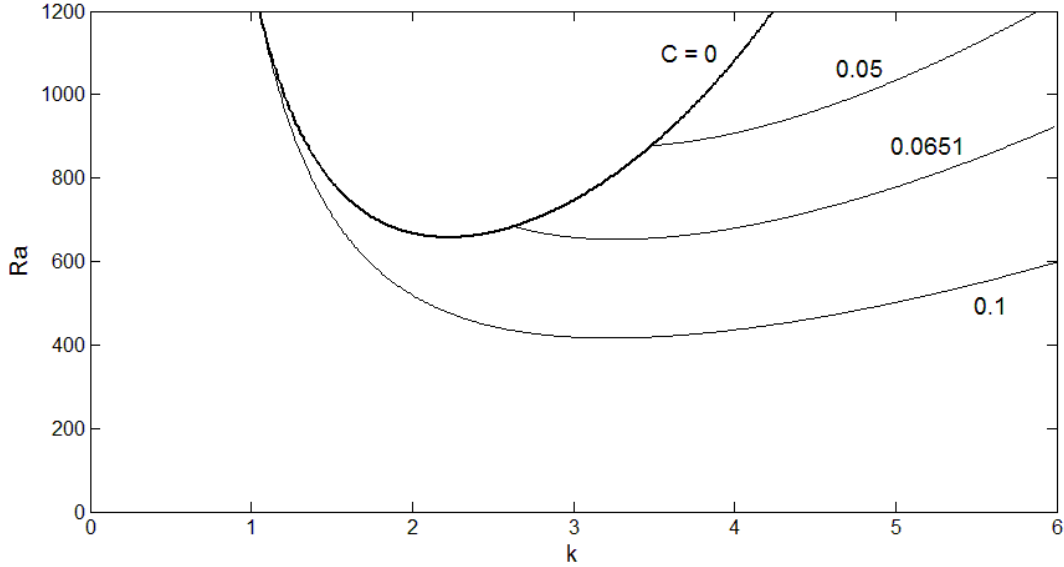


**Figure 3.1 - Marginal stability curves for the onset of convection in a non-Fourier fluid for several values of the Catteneo number  $C$ .  $Pr = 10$  in all cases. The Fourier stability boundary ( $C = 0$ ) is shown by a heavier line. The weakly non-Fourier region corresponds to  $C < 0.0651$ , and the strongly non-Fourier region to  $C > 0.0651$ .**

The Fourier and non-Fourier branches intersect at

$$k_i = \sqrt{\frac{1 + Pr}{Pr C} - \pi^2}, \quad (3.3.8)$$

where the frequency  $\omega$  vanishes. It can be easily verified that

$$Ra_c(k = k_i) = Ra_i = Ra_{cF}(k = k_i).$$

Eq. (3.3.8) indicates that as  $C$  increases,  $k_i$  decreases and eventually goes to zero, at which point oscillatory convection is expected to occur at all wave numbers.

As shown previously [35],  $Pr$  does not affect the Fourier curve, however, an increase in the Prandtl number drives the non-Fourier branch of the stability boundary downward, promoting instability. Conversely, lower  $Pr$  fluids require stronger non-Fourier effects to change the instability conditions from the standard Lorenz model.

When the system becomes unstable by crossing the strongly non-Fourier stability boundary, it is predicted to do so via a Hopf Bifurcation. One can show numerically that there is only one pair of purely imaginary roots, where all other roots have non-zero real parts. At a Hopf Bifurcation, the transversality condition,

$$\left. \frac{d}{dRa} \operatorname{Re}(\sigma_{1,2}) \right|_{Ra=Ra_c} \neq 0, \quad (3.3.9)$$

must also be satisfied [36]. Here,  $\sigma_{1,2}$  represents the pair of purely imaginary eigenvalues. The derivative of the cubic portion of the dispersion relation is taken and isolated for

$$\frac{d\sigma}{dRa} = \frac{\operatorname{Pr}(a + \sigma)}{Ra \left[ 3\sigma^2 + 2(a + \operatorname{Pr})\sigma + \left( a \operatorname{Pr} - \frac{Ra \operatorname{Pr}}{Ra_{cF}} + a \right) \right]}. \quad (3.3.10)$$

The transversality condition Eq. (3.3.9) is clearly satisfied since the ‘a’ term in the numerator ensures a non-zero real part.

In the analysis that follows, we investigate weakly non-Fourier steady state solutions to Eq. (3.2.19)-(3.2.23). This will limit the analysis to  $C < 0.0651$  where the minimum of the stability boundary occurs at  $Ra \approx 657$  and  $k = \pi / \sqrt{2}$ .

### 3.4 Steady State Solutions

We first find the steady state solutions and study their linear stability analytically. The goal is to shed light on the key differences between convection in fluids with Fourier and non-Fourier heat transport. Although the value of  $Ra_{cF}$  does not change, weak non-Fourier effects are still expected to alter the stability of the steady convection state due to the additional non-linear terms, of non-Fourier origin, that come into the energy equation. For small relaxation times (or equivalently, for large  $a$ ), one expects that for  $Ra$  close to  $Ra_{cF}$ , the flow will be similar to that in a Fourier fluid.

The nonlinear terms in Eq. (3.2.15) that come from the upper-convective derivative alter the steady state solution from that of the standard Lorenz model. As in the Fourier case, the trivial solution  $X = Y = Z = A = B = 0$  still exists, and corresponds to pure thermal

conduction with no flow. As  $Ra$  becomes greater than  $Ra_{cF}$ , two branches bifurcate from the conduction state, corresponding to the onset of convective rolls. These two branches are symmetric with respect to a change in sign of  $X$ , which corresponds physically to reversing the direction of rotation of the rolls. For simplicity, we consider only solutions with  $X \geq 0$  here. The steady state solution is found by setting

$$\dot{X} = \dot{Y} = \dot{Z} = \dot{A} = \dot{B} = 0.$$

In this case, the momentum equation Eq. (3.2.19) gives,

$$Y = -\frac{X}{Ra}, \quad (3.4.1)$$

as in the original Lorenz model. Making this substitution in Eq. (3.2.21) we get

$$Z = \frac{-Ra_{cF}X^2 + a(Ra_{cF} - Ra)}{aRaRa_{cF}}. \quad (3.4.2)$$

Finally, using Eq. (3.4.1) and Eq. (3.4.2) in Eq. (3.2.23), we obtain

$$0 = 2Ra_{cF}X^4 + a(Ra + Ra_{cF}(a - 2 - b))X^2 + a^2b(Ra_{cF} - Ra). \quad (3.4.3)$$

This equation is quadratic in  $X^2$ . It can be rearranged to give  $Ra$  as a function of the convective amplitude  $X$ :

$$Ra = Ra_{cF} \left[ \frac{-2X^4 + (2a - a^2 + ab)X^2 - a^2b}{aX^2 - a^2b} \right]. \quad (3.4.4)$$

We will denote the solution to Eq. (4.4) for  $C > 0$  by  $X_{NF}$ , and the Fourier solution at the same  $Ra$  by  $X_F$ .



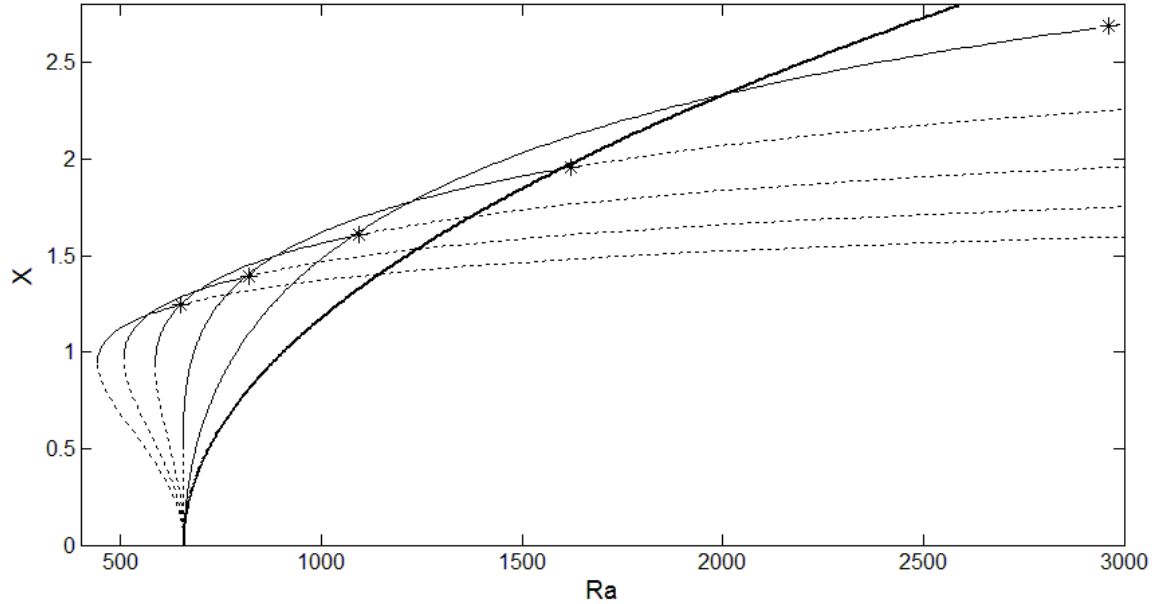


**Figure 3.2 – Steady state convection amplitude as a function of Ra. The heavier curve represents  $C = 0$ , and the fine curves are, from right to left:  $C = 0.01, 0.02, 0.03, 0.04$  and  $0.05$ . Solid lines are linearly stable states, and dashed lines are linearly unstable. The stars indicate the point of at which the steady convection state becomes unstable, as discussed in the text.**

Eq. (3.4.4) indicates that the steady state solution is independent of  $Pr$ . This expression is plotted for weakly non-Fourier fluids with different values of  $C$  in Fig. 3.2, allowing a comparison of the convection amplitude in the Fourier and weakly non-Fourier cases. For all  $C$ , the bifurcation occurs at  $Ra = Ra_{cF}$ , where the conduction state  $X = 0$  becomes unconditionally unstable in favour of convection ( $X \neq 0$ ). The critical Rayleigh number is

$$Ra_c = Ra_{cF} = \frac{(\pi^2 + k^2)^3}{k^2} = \frac{\beta^3}{k^2}, \quad (3.4.5)$$

with the critical wave number also equal to its Fourier value,

$$k_c = k_{cF} = \frac{\pi}{\sqrt{2}}. \quad (3.4.6)$$

Fig. 3.2 shows that for  $C$  less than about 0.02, the bifurcation to the convecting state remains supercritical. Close to the onset of convection,  $X_{NF}$  is larger than in the Fourier case, and increases as  $C$  increases. This indicates that even a small amount of non-Fourier character increases the convective flow velocity close to the onset.

As  $Ra$  is increased for a given value of  $C$ , however,  $X_{NF}$  flattens out and eventually crosses and then falls below the curve for  $C = 0$ . At high  $Ra$ ,  $X_{NF}$  approaches a horizontal asymptote due to the vanishing of the denominator in Eq. (3.4.4). Equating this denominator to zero gives the maximum steady state roll amplitude,

$$X_{\text{inf}} = \sqrt{ab} = \sqrt{\frac{4\pi^2}{C(\pi^2 + k^2)^2}}. \quad (3.4.7)$$

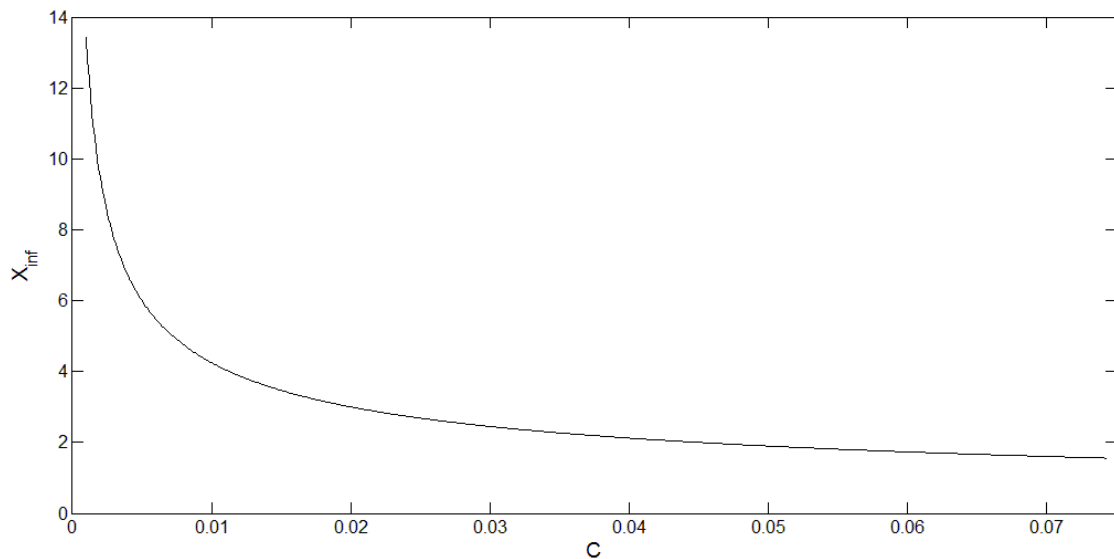


**Figure 3.3 - The limiting amplitude of the steady state convection branch as  $Ra$  goes to infinity plotted as a function of  $C$ .**

As shown in Fig. 3.3, the value of this asymptote decreases from infinity as  $C$  increases from zero. Although these results suggest that  $X_F$  will always eventually surpass  $X_{NF}$ , we show below that for large enough  $C$ , the non-Fourier convection state loses stability before this happens. In addition, when  $C$  is sufficiently large, the steady conduction state becomes unstable to large perturbations even for  $Ra < Ra_{cF}$ .

The value of  $X$  at the intersection of the Fourier and non-Fourier solutions is found by equating the expressions for  $Ra$  in the two cases:

$$Ra_{cF} \left( \frac{X^2}{b} + 1 \right) = Ra_{cF} \left[ \frac{-2X^4 + (2a - a^2 + ab)X^2 - a^2b}{aX^2 - a^2b} \right].$$

Solving for  $X$  and excluding the trivial intersection at  $Ra = Ra_{cF}$  gives the amplitude at the intersection as

$$X = \sqrt{\frac{ab(1+b)}{a+2b}} \quad (3.4.8)$$

for finite  $a$  ( $C > 0$ ). Note that when  $a = \infty$  ( $C = 0$ ), the two solutions overlap for all  $Ra$ .

As  $C$  increases, the bifurcation to convection becomes subcritical. To find where this occurs, we set  $Ra = Ra_{cF}$  in Eq. (3.4.4), obtaining

$$0 = -2X^4 + a(1-a+b)X^2. \quad (3.4.9)$$

A real, non-trivial solution appears when the coefficient of  $X^2$  becomes positive. This occurs when

$$a_{\text{sub}} = 1 + b, \quad (3.4.10)$$

or from (3.2.25a),

$$C = C_{\text{sub}} = \frac{1}{\beta}. \quad (3.4.11)$$

Fig. 3.2 shows the transition from a supercritical bifurcation to a subcritical bifurcation. The fact that the bifurcation becomes subcritical demonstrates that in sufficiently non-Fourier fluids, convection can occur at much lower  $Ra$  than in Fourier fluids. Note that the backward portion of the subcritical bifurcation curves shown in Fig. 3.2 is unstable. The minimum value of  $Ra$  for which the convection state exists, and the corresponding

value of the roll amplitude  $X_m$  can be found from Eq. (3.4.4) by setting  $dRa/dX = 0$ . The result for  $X_m$  is

$$X_m = \pm \frac{1}{2} \sqrt{4ab - 2a\sqrt{2b^2 + 2ab - 2b}}, \quad (3.4.12)$$

where the two possible solutions correspond to the branches above and below the x-axis. The value of  $Ra$  at the minimum of the subcritical branch is found by substituting Eq. (3.4.12) into Eq. (3.4.4), giving

$$Ra_m = \sqrt{2}Ra_{cF} \left( 4\sqrt{b(b+a-1)} + \sqrt{2}(2-a-3b) \right) \quad (3.4.13)$$

Eq. (3.4.13) applies only in the weakly non-Fourier regime, and so breaks down for  $C > 0.0651$ . Fig. 3.4 shows the behaviour of  $X_m$  and  $Ra_m$  as functions of  $C$ .

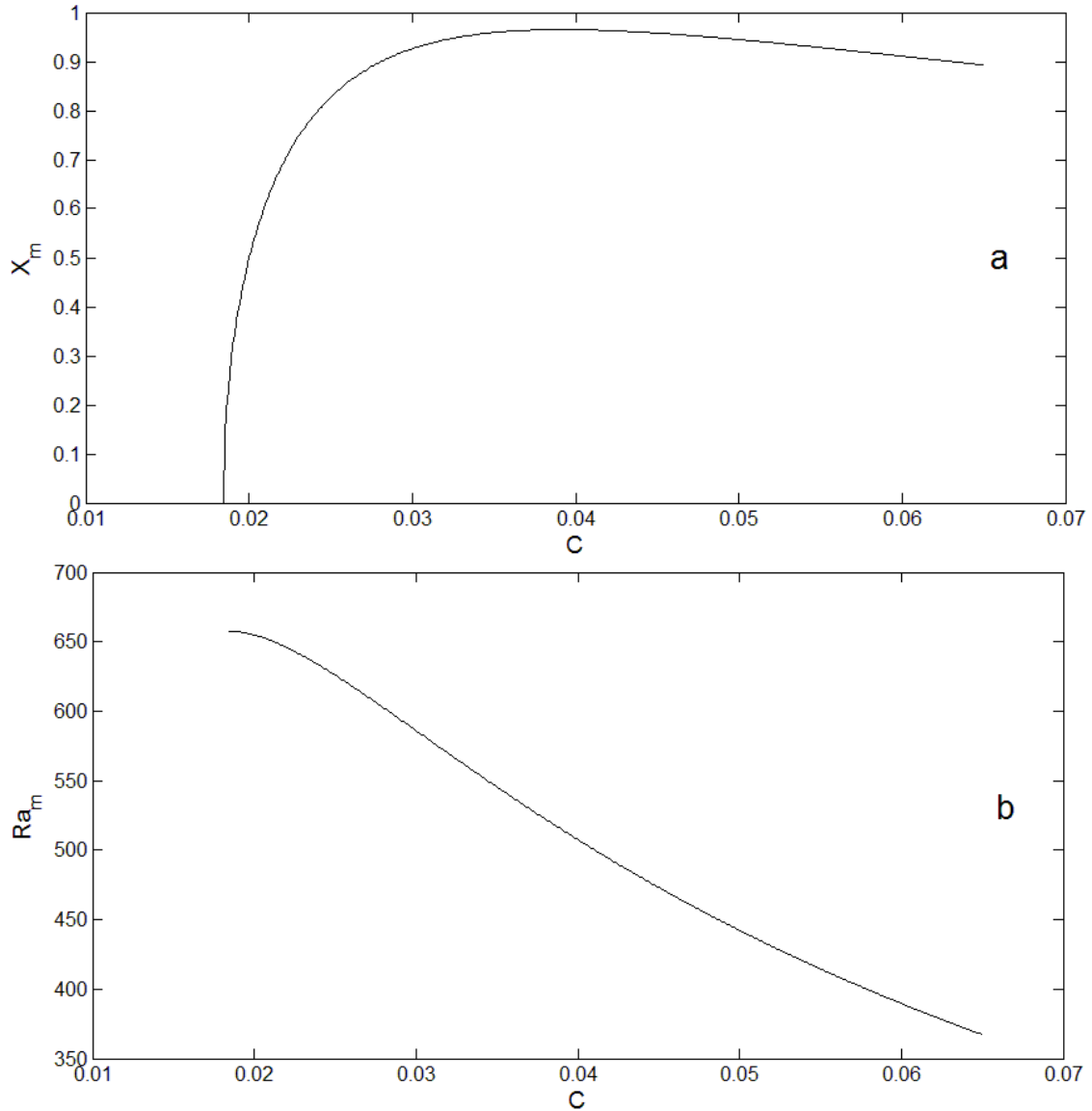


**Figure 3.4 – a) The minimum value of  $X$  and b)  $Ra_m$  on the subcritical bifurcation curves for values of  $C$  in the weakly non-Fourier regime**

### 3.5 Linear Stability Analysis of the Steady State Convection

In the absence of non-Fourier effects, the steady convection state discussed in Sect. 3.4 loses stability to chaos at  $Ra/Ra_{cF} \approx 24.74$  [34]. The stability behaviour changes for weakly non-Fourier fluids, however. A linear stability analysis of the steady convection state leads to a dispersion relation that is fifth order in the complex growth rate  $\sigma$ . The point at which the real part of  $\sigma$  changes sign and the steady convection state becomes unstable must be found numerically. Fig. 3.5 shows the Rayleigh number  $Ra^*$  at which this instability appears as a function of  $C$ .

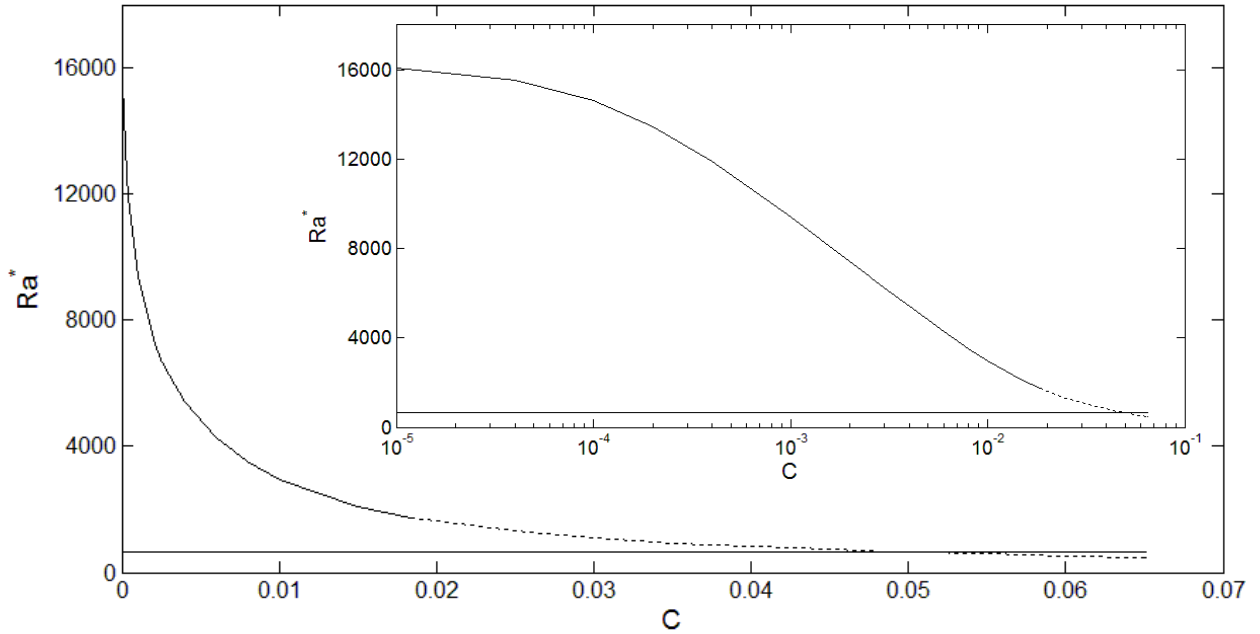


**Figure 3.5 –  $Ra^*$  vs  $C$ . The solid line represents the region in which the bifurcation from conduction to convection is supercritical and dotted line represents the subcritical bifurcation regime. The horizontal line represents  $Ra_{cF}$ . The inset shows the same data, but with a logarithmic x-axis.**

As  $C$  is increased, the range of existence of the steady convection state decreases, approaching 0 asymptotically as  $C \rightarrow \infty$ . When  $C \approx 0.05$ , the instability of the steady convection state occurs for  $Ra^* = Ra_{cF}$  as indicated in Fig. 3.5. In this regime, there is no direct transition from conduction to steady convection as  $Ra$  is increased through  $Ra_{cF}$ .

As discussed above,  $X_{NF}$  is always larger than  $X_F$  close to  $Ra_c$ , but becomes smaller for large  $Ra$ . As  $C$  increases, the stable range of the steady convection state decreases. We find that the non-Fourier convection state may lose stability before  $X_{NF}$  is surpassed in magnitude by  $X_F$ . This is illustrated in Fig. 3.6, which shows the steady Fourier and non-Fourier convection amplitudes  $X_F$  and  $X_{NF}$  at the Rayleigh number  $Ra^*$  at which the non-Fourier convection state loses stability. The inset shows the difference  $X_{NF} - X_F$  at the same Rayleigh number.

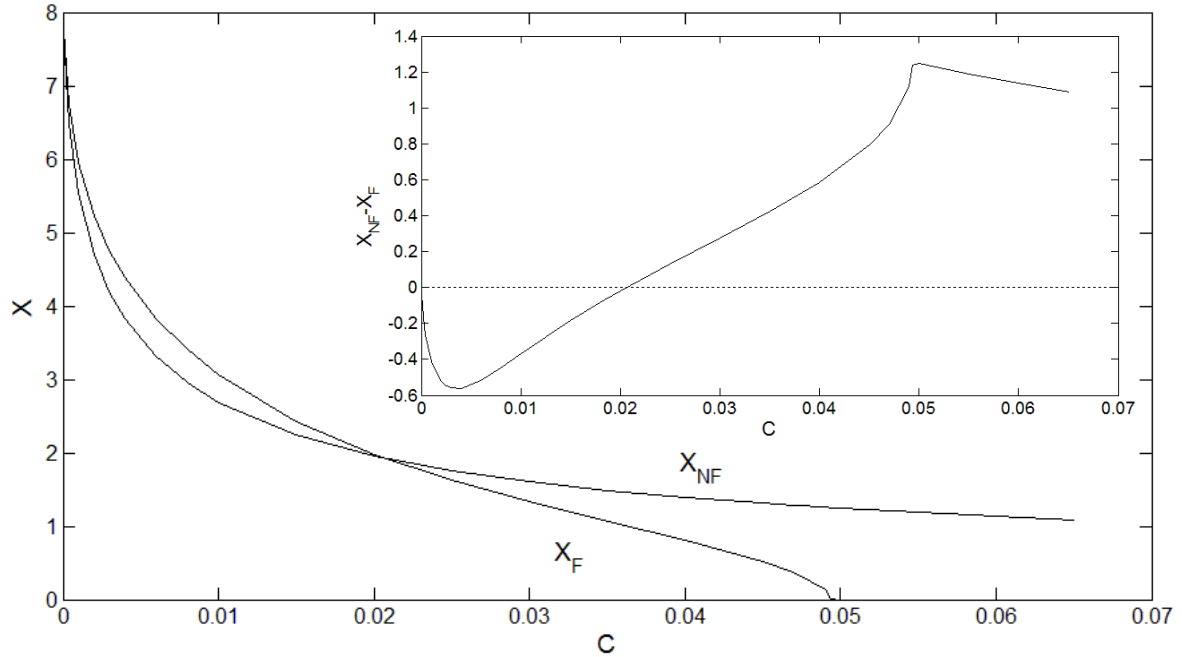


**Figure 3.6 – The convection amplitude,  $X$ , for a Fourier and a non-Fourier fluid at the Rayleigh number  $Ra^*$  at which the steady convection state becomes unstable. The inset shows the difference  $X_{NF}-X_F$  at  $Ra^*$ .**

As  $C$  increases from zero,  $X_{NF} < X_F$  at  $Ra^*$ . As the stability limit of the non-Fourier convection state decreases, the value of  $X_{NF}-X_F$  at  $Ra^*$  initially decreases as well, approaching a minimum at  $C \approx 0.004$ . The difference then increases until  $C \approx 0.02$ , where  $X_F$  and  $X_{NF}$  become equal. At higher  $C$ , non-Fourier convection amplitude is always greater than  $X_F$  at  $Ra^*$ , reaching a maximum  $C \approx 0.05$  where  $Ra^* \approx Ra_{cF}$ , and thus  $X_F = 0$ .

The loss of stability of the steady convection state occurs via a Hopf Bifurcation. Numerical solution of the fifth-order polynomial dispersion relation at the bifurcation point yields one pair of purely imaginary roots with all other roots having strictly negative real parts. The transversality condition, Eq. (3.3.9), is also satisfied, as illustrated in Fig. 3.7, which shows that the slope of  $\sigma_r$  as a function of  $Ra$  is non-zero at  $Ra^*$ .

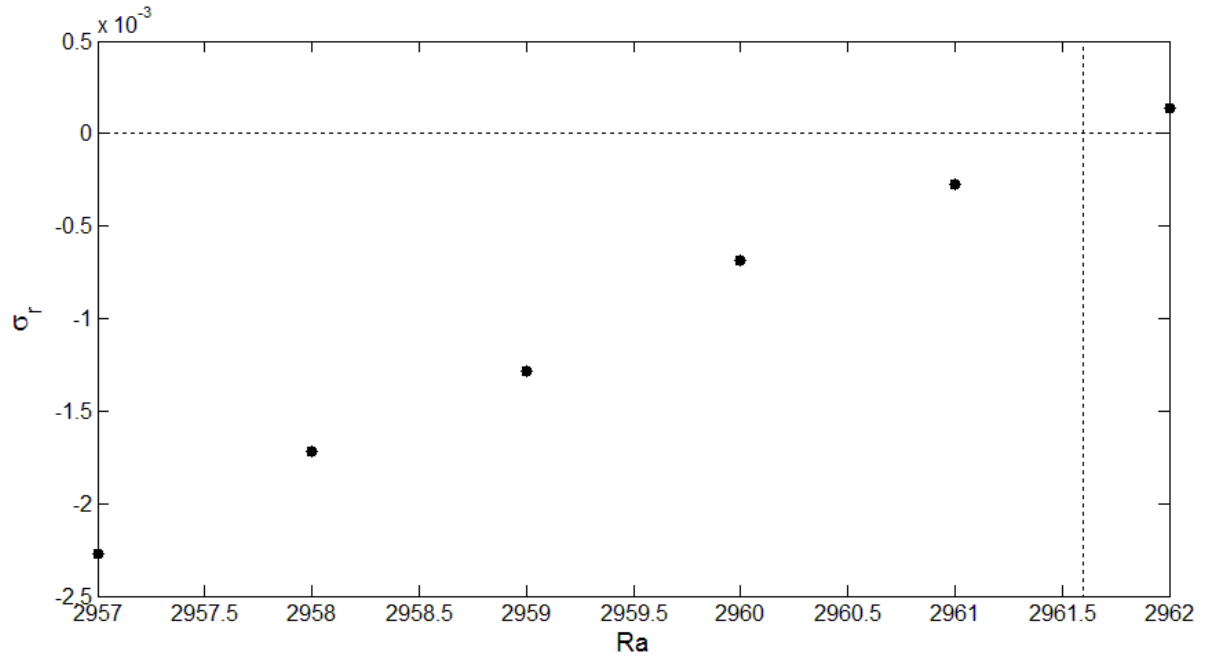


**Figure 3.7 –  $\sigma_r$  vs Ra near the loss of stability of the steady convection state at  $Ra^*$  for  $C = 0.01$ . The vertical line shows  $Ra^*$ , at which  $\sigma_r = 0$ .**

Pr has no effect on the steady convection state itself, but it does affect its linear stability. As Pr increases, the steady convection state becomes more unstable, similar to the effect of Pr on the linear stability of the conduction state for a non-Fourier fluid [35]. Fig. 3.8 shows  $Ra^*$  as a function of Pr.



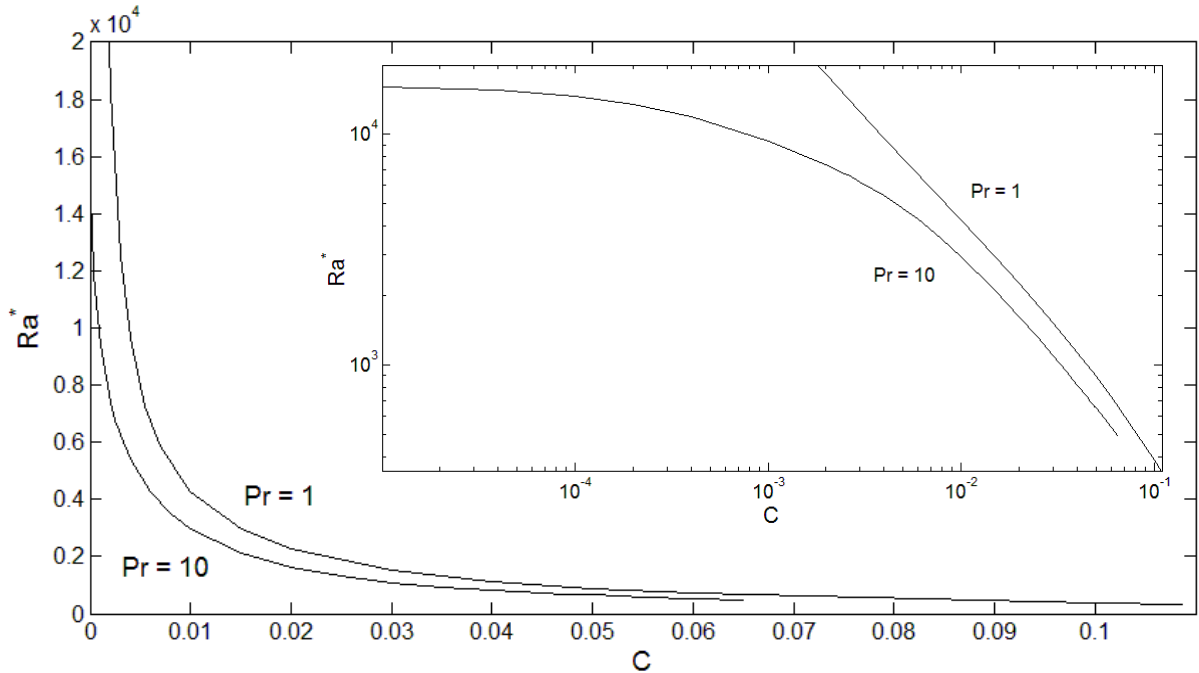


**Figure 3.8 -  $Ra^*$  as a function of  $C$  for two values of  $Pr$ . The inset is a log-log plot of the same data.**

Decreasing  $Pr$  increases  $Ra^*$ , increasing the stability range of the convection state. This effect is more pronounced at low  $C$ . For example, for  $C = 0.0001$ , the Rayleigh number at the instability for  $Pr = 1$  is over 23 times that of  $Pr = 10$ . In addition, the range of  $C$  over which steady convection exists is larger for low  $Pr$ . This reflects the results of [35] showing that lowering the Prandtl number inhibits non-Fourier effects.

### 3.6 Heat Transport

Convective heat transfer is described by the Nusselt number,  $Nu$ , defined as the ratio of total heat transport to the conductive heat transport that would exist in the absence of convection. In our dimensionless units,  $Nu$  is given by

$$Nu = 1 + Q_z \quad (3.6.1)$$

Averaging this horizontally over one convection cell gives

$$\overline{Nu} = 1 + \overline{Q_z} = 1 + \int_0^{\frac{2\pi}{k}} Q_z dx \quad (3.6.2)$$

In general,  $Q_z$  will include contributions due to convective heat transport as well as thermal gradients. At  $z = 0$  and  $z = 1$ , however, the flow vertical velocity is zero, so  $Q_z$  will simply be proportional to  $\nabla T$ . In this case, we can write  $Q_z$  as

$$Q_z(x, z, t) = q_{z1}(t) \cos(\pi z) \cos(kx) + q_{z2}(t) \cos(2\pi z) \quad (3.6.3)$$

with  $z = 0$  or  $z = 1$ .

Integrating this over  $x$  as in Eq. (3.6.2) we get

$$\overline{Nu} = 1 + q_{z2}. \quad (3.6.4)$$

By conservation of energy,  $Nu$  is independent of  $z$  under steady state conditions, so this expression holds for all  $z$ .

Substituting the truncated Fourier expansions for the stream function, temperature, and heat flux into Eq. (3.2.11) and projecting over  $x = [0, 2\pi/k]$  gives

$$q_{z2} = -2\pi\theta_2, \quad (3.6.5)$$

and thus

$$\overline{Nu} = 1 - 2\pi\theta_2. \quad (3.6.6)$$

Scaling this expression as above, we can find the cell averaged Nusselt number in terms of  $X$ :

$$\overline{Nu} = 1 + 2 \left[ \frac{Ra_{cF} X^2 - a(Ra_{cF} - Ra)}{aRa} \right]. \quad (3.6.7)$$

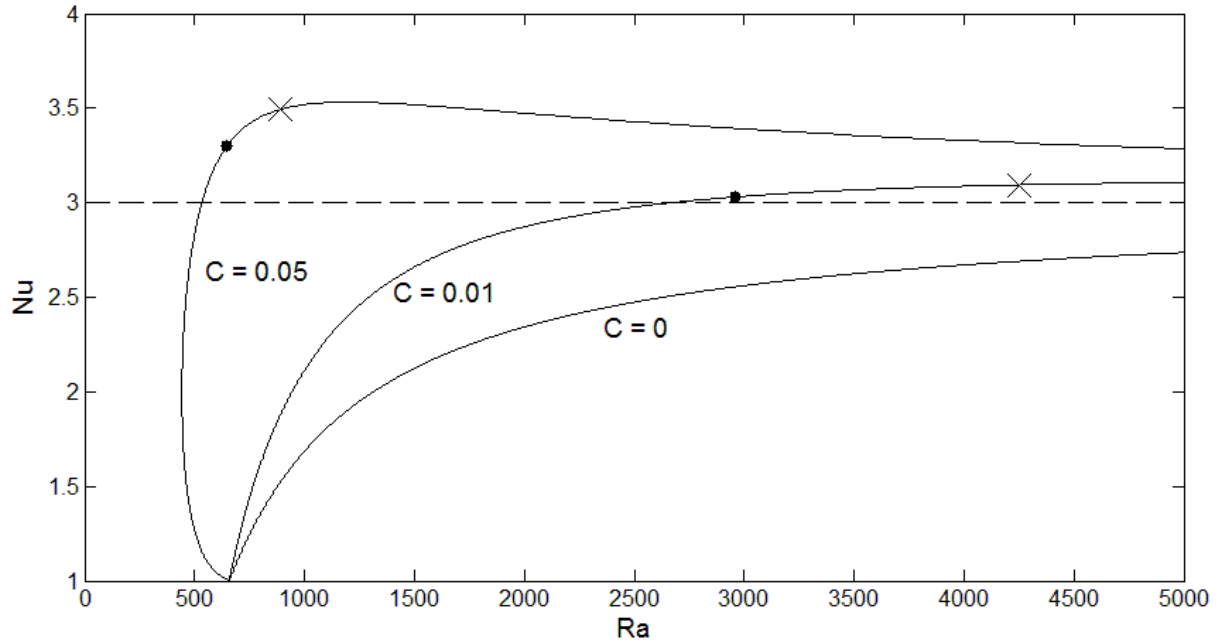


**Figure 3.9 - Nu vs Ra showing the point of instability for Pr = 10 (•) and Pr = 1 (x).**

Fig. 3.9 depicts the effects of non-Fourier heat transport on Nu. In the Fourier case ( $C = 0$ ), Nu increases monotonically as Ra is increased, and approaches  $Nu = 3$  as  $Ra \rightarrow \infty$  [37]. As  $C$  is increased, the Nusselt number at any particular value of Ra increases monotonically even though  $X_{NF}$  may not be larger than  $X_F$ . When  $C > 0$ , Nu reaches a maximum value that is higher than the asymptotic Fourier limit, then decreases to approach  $Nu = 3$  from above. When  $C$  is large enough that the bifurcation to convection is subcritical, Nu jumps discontinuously at the onset of convection, as shown by Figure 3.9 for  $C = 0.05$ .

The Prandtl number does not affect the value of the Nusselt number directly, but, as discussed above, it does influence the point at which the steady convective state becomes unstable. As Pr decreases, the Rayleigh number at the point of instability increases, as shown in Fig. 3.9. As a result, Nu may not always be an increasing function of Ra, although as explained above, Nu will always increase as  $C$  increases for a given value of Ra.

### 3.7 Discussion

Non-Fourier heat transport was previously shown to affect the stability boundary of the steady conduction state and the onset of Rayleigh-Bénard convection [35]. Our present results demonstrate that they will also lead to changes in the properties and stability of the steady convection state. For  $C$  close to zero, the amplitude of non-Fourier steady state convection is larger than for a Fourier fluid close to onset, however for all values of  $C$ ,  $X_{NF}$  becomes smaller than  $X_F$  at large  $Ra$ . As  $C$  increases through a critical value, the bifurcation to convection becomes subcritical, yielding the possibility of convection at values of  $Ra$  less than  $Ra_{cF}$ . We have also shown that  $Nu$  is expected to be larger for non-Fourier convection at all  $C > 0$ , regardless of the value of  $Ra$ , suggesting that non-Fourier effects could lead to higher heat transfer than in the Fourier case. The linear stability of the steady convection state is also affected by the presence of non-Fourier effects. As  $C$  increases from zero, the value of  $Ra$  at which the steady convection state loses stability decreases quickly and at large  $C$  approaches zero asymptotically.

As discussed in the introduction, non-Fourier effects are expected to become important at small length scales. This point has been considered in the last decade [15], [25] as the importance of nano-structured devices has grown. Experimentally, increased heat transfer has been observed in small scale natural convection around MEMS devices [15] and it was pointed out that conventional models could underestimate the heat transfer in such microscale flows. It has also been suggested that the efficiency of applications making use of Polymerase Chain Reactions (PCR) could be enhanced by further characterization of the small-scale convective flow fields [28]. PCR utilizes Rayleigh-Bénard convection at a scale on the order of  $10^{-3}$  m where non-Fourier effects could be significant.

The dimensional analysis of [15] can provide some insight into the behaviour of the Nusselt number. We define the Grashof number by

$$Gr = \frac{\delta T \alpha_T g D^3}{\nu^2} = \frac{Ra}{Pr}. \quad (3.7.1)$$

For natural convection on macroscopic scales, the buoyancy force is balanced by the fluid inertia, in which case it can be shown by dimensional analysis that

$$\text{Nu} \sim \text{Gr}^{0.5} \text{Pr} . \quad (3.7.2)$$

As the length scale of the problem decreases, the inertial force becomes dominated by viscosity. In this case, buoyancy is balanced by viscous forces and dimensional analysis gives

$$\text{Nu} \sim \text{Gr} \text{Pr} . \quad (3.7.3)$$

As long as Gr remains larger than 1, this analysis predicts that Nu should increase for microscale heat transfer at a given value of Gr. This is consistent with our predictions for the effect of non-Fourier heat transfer, which indeed is expected to be important in small scale problems.

Eq. (3.6.7) shows that as  $\text{Ra} \rightarrow \infty$ , the Nusselt number tends to  $\text{Nu} = 3$ , just as in the Fourier case. Interestingly, Fig. 12 in [15] also shows that the influence of the small length scale on the convective heat transfer disappears at large Ra as the Nusselt number predicted from macroscale correlations merges with the experimental results. This behaviour is again consistent with our analysis.

Non-Fourier effects have also been recognized in nanofluids [19] and rarefied gases [12], [13]. Experimentally, nanofluids have exhibited oscillatory convection [38] which we have shown to be a characteristic of non-Fourier effects. Nanofluids have also shown to have increased heat transport capabilities with increasing volume fraction of nanoparticles [39].

From kinetic theory pertaining to rarefied gases, we can relate the Cattaneo number to the Knudsen number,  $\text{Kn} = \lambda / D$ , where  $\lambda$  is the mean free path. For a rarefied gas, [40] equivalently describes the kinematic viscosity as

$$\nu = \frac{\bar{c}\lambda}{3} , \quad (3.7.4)$$

where  $\bar{c}$  is the mean molecular velocity. Further, from Eq. (3.11) and Eq. (3.15) in [40], the relaxation time can be defined as

$$\tau = \frac{3\mu}{2p}, \quad (3.7.5)$$

where  $p$  is the mean pressure. From [41], the pressure is approximately given by

$$p = \frac{\rho\bar{c}^2}{3} \quad (3.7.6)$$

and thus, substituting into Eq. (3.7.5), writing  $\nu = \mu / \rho$ , and substituting Eq. (3.7.4), the relaxation time becomes

$$\tau = \frac{3\lambda}{2\bar{c}}. \quad (3.7.7)$$

Next, we recall the Cattaneo number and substitute  $\kappa = \nu / \text{Pr}$  to obtain

$$C = \frac{\tau\nu}{\text{Pr}D^2}. \quad (3.7.8)$$

Here, we can insert Eq. (3.7.4) and (3.7.7) as well as make use of the Knudsen number, to give the following relationship:

$$C = \frac{\text{Kn}^2}{2\text{Pr}}. \quad (3.7.9)$$

Eq. (3.7.9) shows that an increase in  $\text{Kn}$  leads to larger non-Fourier effects and allows us to estimate the relationship between the importance of small scale effects, typically described by the Knudsen number, and non-Fourier heat transfer. For gas microflows, where the mean free path of the fluid and the length scale may be of similar order, the validity of Fourier's law becomes questionable as it is valid only for small  $\text{Kn}$  [40]. Using this relationship, we can attempt to envelope both the effects of non-Fourier heat transfer and partial slip in small scale applications using the Knudsen number. The table below

uses Eq. (3.7.9) to estimate the Cattaneo number for some common gases at 20°C and standard atmospheric pressure, assuming the Prandtl number to be 2/3.

**Table 1 - Cattaneo number for some common gases (mean free paths are from [42])**

Fluid	Cattaneo Number (C)		
	D=10 <sup>-5</sup> m	D=10 <sup>-6</sup> m	D=10 <sup>-7</sup> m
Air	3.47×10 <sup>-5</sup>	3.47×10 <sup>-3</sup>	3.47×10 <sup>-1</sup>
Argon	3.89×10 <sup>-5</sup>	3.89×10 <sup>-3</sup>	3.89×10 <sup>-1</sup>
CO <sub>2</sub>	1.52×10 <sup>-5</sup>	1.52×10 <sup>-3</sup>	1.52×10 <sup>-1</sup>
Hydrogen	1.17×10 <sup>-4</sup>	1.17×10 <sup>-2</sup>	1.17
Water Vapour	1.32×10 <sup>-5</sup>	1.32×10 <sup>-3</sup>	1.32×10 <sup>-1</sup>
Helium	2.88×10 <sup>-4</sup>	2.88×10 <sup>-2</sup>	2.88
Nitrogen	3.37×10 <sup>-5</sup>	3.37×10 <sup>-3</sup>	3.37×10 <sup>-1</sup>
Neon	1.47×10 <sup>-4</sup>	1.47×10 <sup>-2</sup>	1.47
Oxygen	3.89×10 <sup>-5</sup>	3.89×10 <sup>-3</sup>	3.89×10 <sup>-1</sup>

Table 1 shows that with advancements in micro- and nano-scale technologies, the scale length can approach the mean free path even at standard pressures, which is expected to lead to significant non-Fourier and partial slip effects [43]. Previously, vacuum pressures were required to achieve such effects.

Finally, there is a strong analogy between the Cattaneo-Vernotte equation used to describe non-Fourier heat transfer and Maxwell's equation for a viscoelastic fluid. We have shown that the steady conduction state for non-Fourier fluids can lose stability to

either steady or oscillatory convection, and that at a certain value of  $C$ , the bifurcation from steady conduction to convection changes from supercritical to subcritical.

Analogous behaviour is seen in the case of a viscoelastic fluid when the elasticity number is sufficiently large [37], [44]. The stress and strain in the viscoelastic case play the role of the temperature and heat transport in the heat transfer problem, and the relaxation time in the viscoelastic case is equivalent to  $\tau$  here.

### 3.8 Conclusion

This study has examined the steady state Rayleigh-Bénard convection of non-Fourier fluids. We have investigated the case in which there is a single relaxation time  $\tau$  governing the response of the heat flux to changes in the temperature gradient. Non-Fourier effects are expected to become important when the dimensionless Cattaneo number,  $C = \frac{\tau\kappa}{D^2}$ , is significant.

We have shown by steady state analysis that near the onset of convection, the convection amplitude is always greater in the presence of non-Fourier effects than for a Fourier fluid. As  $Ra$  increases, however, there is a point at which the Fourier convection amplitude becomes greater than the non-Fourier convection amplitude. As  $C$  increases, the bifurcation to convection becomes subcritical, making the conduction state unstable to large perturbations at values of  $Ra$  below the Fourier bifurcation point.

We also performed a linear stability analysis of the steady convective state showing that it loses stability at a Hopf bifurcation at a Rayleigh number lower than the stability limit of a Fourier fluid. For large enough  $C$ , the steady convection state loses stability for  $Ra$  lower than the bifurcation from the conduction state. In such a case, a steady convection state cannot be reached via small perturbations of the conduction state. We find that the Nusselt number calculated for a non-Fourier fluid is always larger than that for a Fourier fluid, even though the convection amplitude may not be greater. Our results are in qualitative agreement with experimental results and dimensional analysis for natural convection around MEMS devices.



### 3.9 Acknowledgements

This research was supported by the Natural Sciences and Engineering Research Council of Canada.

### 3.10 References

- [1] D. Joseph and L. Preziosi, “Heat waves,” *Rev. Mod. Phys.*, vol. 61, no. 1, pp. 41–73, 1989.
- [2] D. E. Glass, M. N. Özışık, D. S. McRae, and B. Vick, “Hyperbolic heat conduction with temperature-dependent thermal conductivity,” *J. Appl. Phys.*, vol. 59, no. 6, p. 1861, 1986.
- [3] G. Lebon and A. Clout, “Bénard-Marangoni instability in Maxwell–Cattaneo fluids,” *Phys. Lett. A*, vol. 105, no. 7, pp. 361–364, 1984.
- [4] D. Y. Tzou and K. S. Chiu, “Temperature-dependent thermal lagging in ultrafast laser heating,” *Int. J. Heat Mass Transf.*, vol. 44, no. 9, pp. 1725–1734, May 2001.
- [5] P. Haupt, *Continuum Mechanics and Theory of Materials*. New York: Springer Verlag, 2002.
- [6] C. I. Christov, “On frame indifferent formulation of the Maxwell–Cattaneo model of finite-speed heat conduction,” *Mech. Res. Commun.*, vol. 36, no. 4, pp. 481–486, Jun. 2009.
- [7] R. Khayat and M. Ostoja-Starzewski, “On the objective rate of heat and stress fluxes. Connection with micro/nano-scale heat convection,” *Discret. Contin. Dyn. Syst. - Ser. B*, vol. 15, no. 4, pp. 991–998, Mar. 2011.
- [8] J. G. Oldroyd, “On the Formulation of Rheological Equations of State,” *Proc. R. Soc. A Math. Phys. Eng. Sci.*, vol. 200, no. 1063, pp. 523–541, Feb. 1950.

- [9] D. S. Chandrasekharaiah, "Hyperbolic thermoelasticity: a review of recent literature," *Appl. Mech. Rev.*, vol. 51, no. 12, pp. 705–729, 1998.
- [10] H. Liepmann and G. Laguna, "Nonlinear interactions in the fluid mechanics of helium II," *Annu. Rev. Fluid Mech.*, p. 34, 1984.
- [11] R. Donnelly, "The two-fluid theory and second sound in liquid helium," *Phys. Today*, no. October, p. 34, 2009.
- [12] L. S. Pan, D. Xu, J. Lou, and Q. Yao, "A generalized heat conduction model in rarefied gas," *Europhys. Lett.*, vol. 73, no. 6, pp. 846–850, Mar. 2006.
- [13] Z. Wang, L. Bao, and B. Tong, "Rarefaction criterion and non-Fourier heat transfer in hypersonic rarefied flows," *Phys. Fluids*, vol. 22, no. 12, p. 126103, 2010.
- [14] D. Y. Tzou and J. Xu, "Nonequilibrium Transport: The Lagging," in *Advances in Transport Phenomena*, 2011, pp. 93–170.
- [15] Z. Y. Guo and Z. X. Li, "Size effect on microscale single-phase flow and heat transfer," *Int. J. Heat Mass Transf.*, vol. 46, no. 1, pp. 149–159, Jan. 2003.
- [16] Z. Y. Guo and Z. X. Li, "Size effect on single-phase channel flow and heat transfer at microscale," *Int. J. Heat Fluid Flow*, vol. 24, no. 3, pp. 284–298, Jun. 2003.
- [17] N. Sela and I. Goldhirsch, "Hydrodynamic equations for rapid flow of smooth inelastic spheres, to Burnett order," *J. Fluid Mech.*, vol. 361, pp. 41–74, 1998.
- [18] J. J. Brey, J. W. Dufty, C. S. Kim, and A. Santos, "Hydrodynamics for granular flow at low density," *Phys. Rev. E*, vol. 58, no. 4638, 1998.
- [19] L. Wang and X. Wei, "Equivalence between dual-phase-lagging and two-phase-system heat conduction processes," *Int. J. Heat Mass Transf.*, vol. 51, no. 7–8, pp. 1751–1756, Apr. 2008.

- [20] H. A. Stone, A. D. Stroock, and A. Ajdari, "Engineering Flows in Small Devices," *Annu. Rev. Fluid Mech.*, vol. 36, no. 1, pp. 381–411, Jan. 2004.
- [21] X. B. Nie, S. Y. Chen, W. N. E, and M. O. Robbins, "A continuum and molecular dynamics hybrid method for micro- and nano-fluid flow," *J. Fluid Mech.*, vol. 500, pp. 55–64, Jan. 2004.
- [22] S. Bhattacharyya, Z. Zheng, and A. T. Conlisk, "Electro-osmotic flow in two-dimensional charged micro- and nanochannels," *J. Fluid Mech.*, vol. 540, p. 247, 2005.
- [23] M. Oliveira and L. Rodd, "Simulations of extensional flow in microrheometric devices," *Microfluid. Nanofluidics*, vol. 5, no. 6, pp. 809–826, Apr. 2008.
- [24] S. G. Kandlikar, S. Colin, Y. Peles, S. Garimella, R. F. Pease, J. J. Brandner, and D. B. Tuckerman, "Heat Transfer in Microchannels—2012 Status and Research Needs," *J. Heat Transfer*, vol. 135, no. 9, Jul. 2013.
- [25] X. J. Hu, A. Jain, and K. E. Goodson, "Investigation of the natural convection boundary condition in microfabricated structures," *Int. J. Therm. Sci.*, vol. 47, no. 7, pp. 820–824, Jul. 2008.
- [26] X. G. Liang and Z. Y. Guo, "The Scaling Effect on the Thermal Processes at Mini/Microscale," *Heat Transf. Eng.*, vol. 27, no. 4, pp. 30–40, May 2006.
- [27] B. Vermeersch and G. Mey, "Non-Fourier thermal conduction in nano-scaled electronic structures," *Analog Integr. Circuits Signal Process.*, vol. 55, no. 3, pp. 197–204, Apr. 2007.
- [28] M. Krishnan, V. Ugaz, and M. Burns, "PCR in a Rayleigh-Bénard convection cell," *Science (80-. )*, vol. 298, p. 793, 2002.
- [29] P. Dauby, M. Nélis, and G. Lebon, "Generalized Fourier equations and thermoconvective instabilities," *Rev. Mex. física*, no. 4, pp. 57–62, 2002.

- [30] B. Straughan, “Tipping points in Cattaneo-Christov thermohaline convection,” *Proc. R. Soc. A Math. Phys. Eng. Sci.*, vol. 467, no. 2125, pp. 7–18, May 2010.
- [31] B. Straughan and F. Franchi, “Benard convection and the Cattaneo law for heat conduction,” *Proc. R. Soc. Edinburgh Sect. A Math.*, vol. 96, no. 1–2, p. 175, 1984.
- [32] E. Spiegel and G. Veronis, “On the Boussinesq approximation for a compressible fluid,” *Astrophys. J.*, vol. 131, p. 442, 1960.
- [33] A. V. Getling, *Rayleigh-Benard Convection: Structures and Dynamics*. World Scientific, 1998.
- [34] E. Lorenz, “Deterministic nonperiodic flow,” *J. Atmos. Sci.*, vol. 20, p. 130, 1963.
- [35] D. F. Stranges, R. E. Khayat, and B. Albaalbaki, “Thermal convection of non-Fourier fluids. Linear stability,” *Int. J. Therm. Sci.*, vol. 74, pp. 14–23, Dec. 2013.
- [36] J. E. Marsden and M. McCracken, *The Hopf Bifurcation and its applications*. New York: Springer-Verlag, 1976, p. 20.
- [37] R. E. Khayat, “Chaos and overstability in the thermal convection of viscoelastic fluids,” *J. Nonnewton. Fluid Mech.*, vol. 53, pp. 227–255, Jul. 1994.
- [38] G. Donzelli, R. Cerbino, and A. Vailati, “Bistable Heat Transfer in a Nanofluid,” *Phys. Rev. Lett.*, vol. 102, no. 10, p. 104503, Mar. 2009.
- [39] A. G. A. Nnanna and M. Routhu, “Transport Phenomena in Buoyancy-Driven Nanofluids – Part II,” in *2005 ASME Summer Heat Transfer Conference*, 2005, pp. 1–8.
- [40] H. Struchtrup and P. Taheri, “Macroscopic transport models for rarefied gas flows: a brief review,” *IMA J. Appl. Math.*, vol. 76, no. 5, pp. 672–697, Feb. 2011.
- [41] F. Reif, *Fundamentals of Statistical and Thermal Physics*. Long Grove: Waveland Press, 2009, pp. 479–480.

- [42] A. Krutina, “The mean free path for some gases at 20C and different pressures.” [Online]. Available: <http://www.leakdetection-technology.com/science/introduction-to-the-gas-laws/the-mean-free-path-for-some-gases-at-20-c-and-different-pressures>.
- [43] E. Arkilic, “Slip in microchannels,” in *Proceedings of Rarefied Gas Dynamics Symposium*, 1994.
- [44] Z. Li and R. E. Khayat, “Finite-amplitude Rayleigh–Bénard convection and pattern selection for viscoelastic fluids,” *J. Fluid Mech.*, vol. 529, pp. 221–251, Apr. 2005.

## Chapter 4

### 4 The influence of second order partial slip boundary conditions on thermal convection

#### 4.1 Introduction

Macroscopic fluid flow over solid surfaces is regularly modeled using the no-slip boundary condition. This assumes that the fluid velocity at the boundary is equal to the velocity of the boundary. Similarly, no-jump refers to the temperature boundary condition, assuming that the temperature of the fluid at the liquid-solid interface is equal to that of the solid; however, in this paper the term no-slip will serve to encompass both velocity slip and temperature jump conditions. From a microscopic point of view, these assumptions may no longer be accurate. The validity of the no-slip boundary conditions are a function of the Knudsen number,  $Kn = \lambda/D$ , where  $\lambda$  is the mean free path of the fluid particles, and  $D$  is a physically relevant length scale. For most practical circumstances to date,  $Kn \ll 1$ , and the no-slip boundary condition is suitable. At large  $Kn$ , fluid velocity and temperature at the boundary differ from that of the solid, a phenomena typically associated with incompressible liquids at small scales [1] and gases, especially rarified gases [2], [3], where  $\lambda$  can easily be on the order of the length scale. Polymer flows [4], [5] have also exhibited slip at the solid-liquid interface. With the advent of micro-electromechanical systems (MEMS) and nanotechnology, the length scale has begun to approach the mean free path of ordinary fluids as well.

The slip flow regime is defined by  $0.01 < Kn < 0.1$  [6]–[8]. As the Knudsen number increases into this regime and higher such as for micro- and nanodevices, no-slip ceases to be an appropriate boundary condition. Further increase of the Knudsen number may also cause the breakdown of other approximations such as Fourier's law, Newtonian stress and the Boussinesq approximation, which have previously been examined separately in terms of their effect on linear stability of the steady conduction state in natural convection [9]–[11].

When Kn is sufficiently large such that the no-slip boundary condition is no longer suitable, the slip at the boundary must be taken into account. This means that the tangential component of the velocity and temperature of the fluid immediately in contact with a solid surface are not equal to the velocity and temperature of the solid surface, respectively [8], [12], [13]. When the effects of slip are accounted for, this will be referred to as partial slip.

The non-dimensional first-order hydrodynamic slip boundary condition proposed by Maxwell [8], [14] which governs the velocity at the boundary is

$$\mathbf{V} - \mathbf{V}_{\text{wall}} = \frac{2-\zeta}{\zeta} \text{Kn} \left( \frac{\partial \mathbf{V}}{\partial \mathbf{n}} \right)_{\text{wall}} \quad (4.1.1)$$

where  $\mathbf{V}$  is the velocity,  $\zeta$  is the tangential momentum accommodation coefficient [15] and  $\mathbf{n}$  is the normal to the boundary facing into the fluid. The coefficient on the partial derivative is known as the slip length  $l_s$ , which is related to the mean free path [16]. This is the theoretical distance outside of the boundary for which the tangential velocity would be zero, as shown by Fig. 4.1.

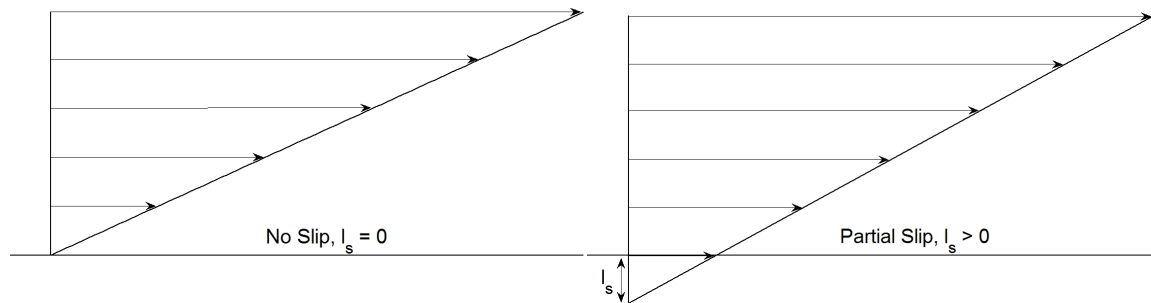


**Figure 4.1 - Slip length for no-slip and first-order partial slip boundary conditions**

First-order boundary conditions assume that the extrapolated velocity profile is linear. Higher-order approximations to the slip conditions relax this assumption. The first-order non-dimensional temperature jump boundary condition [8], [17] is described by

$$T - T_{\text{wall}} = \frac{2-\zeta}{\zeta} \frac{2\gamma}{\gamma+1} \frac{\text{Kn}}{\text{Pr}} \left( \frac{\partial T}{\partial \mathbf{n}} \right)_{\text{wall}} \quad (4.1.2)$$

where  $T$  is the temperature,  $\gamma$  is the specific heat ratio and  $Pr$  is the Prandtl number. Again, the coefficient on the partial derivative indicates a distance toward the outside of the boundary for which the temperature would be equal to that of the wall.

Slip effects are expected to be important in small length scale Rayleigh-Bénard convection where two infinite horizontal plates with separation  $D$  confine a thin layer of fluid. These plates are at fixed temperatures, where the lower plate is maintained at a temperature  $\delta T$  greater than the upper plate. When the temperature difference between the plates is low enough, the fluid layer remains motionless and conduction is the only method of heat transport between them. As  $\delta T$  increases through a critical value, thermal expansion causes the lower layers to become less dense and buoyancy effects induce a transition to convective rolls. This critical value is generally described by the Rayleigh number, which is proportional to the temperature difference between the plates. Due to its natural occurrence in macroscale systems such as the ocean, weather, and the Earth's mantle, Rayleigh-Bénard convection possesses physical relevance as well as theoretical and experimental simplicity [18], [19]. Convective rolls have also been observed in the molecular-dynamics studies of microscopic Rayleigh-Bénard convection [20], [21]. It is a well-suited platform for analyzing the effects of partial slip boundary conditions.

When the no-slip boundary condition is applied at both the top and bottom plates, the critical Rayleigh number at which the loss of the stability of the steady conduction state occurs is  $Ra_c \approx 1708$ . By incorporating hydrodynamic slip at the boundary, the stress, and thus the viscous dissipation are reduced. As a result, viscous forces are less able to balance buoyancy forces, and convection sets in more easily. For  $Kn \rightarrow \infty$  in Maxwell's first-order approximation, the boundaries become stress free and  $Ra_c \approx 657.5$ . The first-order boundary conditions proposed by Maxwell [14] have been studied previously [13], however, second-order effects are expected to be important near what is called the transition regime, where  $Kn > 0.1$  [22], [23], and will be discussed further in the following sections. Second-order boundary conditions include the effects of the second derivative normal to the boundary on the velocity and temperature and thus would not add any new slip to Fig. 4.1 due to its linear profile at the boundary.



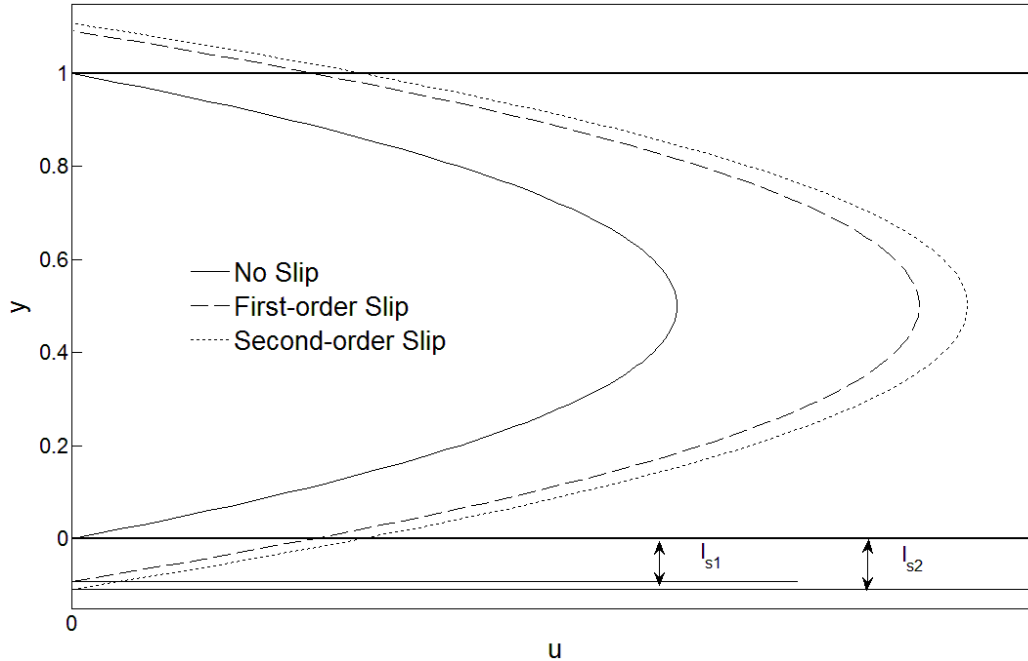


**Figure 4.2 - Comparison of first- and second-order slip effects on Poiseuille flow.  $l_{s1}$  and  $l_{s2}$  denote the slip length for first- and second-order slip, respectively.**

In the case of Poiseuille flow however, second-order effects alter the flow conditions as shown by Figure. 4.2. Second-order slip changes the slip length and thus the slip velocity from the first order approximation, as shown by  $l_{s2}$  and  $l_{s1}$ , respectively. Boundary conditions with second-order effects have been reported to give high accuracy in microchannel flows up to  $Kn = 0.25$  [24] and are expected to be necessary for flows in the transition regime where  $Kn > 0.1$  [25].

In this paper, we analyze the linear stability of Rayleigh-Bénard convection with  $Kn > 0$  using both first and second-order slip boundary conditions in velocity and temperature, showing their effect on the onset of convection. Results calculated using values of the coefficients proposed in references [12] and [8] are compared, and the difference between first- and second-order boundary conditions are highlighted.

## 4.2 Governing equations and boundary conditions

Consider a thin layer of a Newtonian liquid of infinite extent in the  $(x,y)$  directions, confined between two perfectly conducting isothermal plates at  $z = -D/2$  and  $z = D/2$ . The

fluid layer is heated from below, with the plates maintained at temperatures  $T_0 + \delta T$  and  $T_0$ , respectively.

The fluid density  $\rho$  is assumed to depend linearly on the temperature  $T$  according to

$$\rho = \rho_0 [1 - \alpha_T (T - T_0)], \quad (4.2.1)$$

where  $\alpha_T$  is the coefficient of thermal expansion and  $\rho_0$  is the density of the fluid at  $T_0$ .

The fluid is assumed to be incompressible, and to have specific heat at constant pressure  $C_p$ , thermal conductivity  $K$  and viscosity  $\mu$ . The fluid behavior is described by equations for the conservation of mass, linear momentum and energy, as well as the constitutive equation for Fourier heat flux. In this case, these equations are given by

$$\nabla \cdot \mathbf{V} = 0, \quad (4.2.2)$$

$$\rho_0 (\mathbf{V}_t + \mathbf{V} \cdot \nabla \mathbf{V}) = -\nabla P - \rho g \hat{\mathbf{z}} + \mu \Delta \mathbf{V}, \quad (4.2.3)$$

$$\rho_0 c_p (\mathbf{T}_t + \mathbf{V} \cdot \nabla \mathbf{T}) = -\nabla \cdot \mathbf{Q}, \quad (4.2.4)$$

$$\mathbf{Q} = -K \nabla T \quad (4.2.5)$$

where  $\Delta$  is the Laplacian operator and the subscript  $t$  denotes partial differentiation with respect to time. Here the flow is assumed to be two dimensional such that  $\mathbf{V} = (U, 0, W)$  is the velocity vector,  $P$  is the pressure,  $g$  is the acceleration due to gravity and  $\hat{\mathbf{z}}$  is a unit vector in the  $z$ -direction. In writing Eqs. (4.2.3) and (4.2.4) we have used the Boussinesq approximation, which states that the effect of the variations in density is negligible everywhere except in the buoyancy term of Eq. (4.2.3) [26].

The second-order slip boundary condition for the fluid velocity is given by Eq. (4.2.6) [8].

$$\mathbf{V} - \mathbf{V}_{\text{wall}} = a_1 \lambda \left( \frac{\partial \mathbf{V}}{\partial \mathbf{n}} \right)_{\text{wall}} + a_2 \lambda^2 \left( \frac{\partial^2 \mathbf{V}}{\partial \mathbf{n}^2} \right)_{\text{wall}} + a_3 \lambda^2 \left( \frac{\partial \mathbf{T}}{\partial \mathbf{m}} \right)_{\text{wall}}, \quad (4.2.6)$$

where  $\mathbf{m}$  is the unit vector in the direction tangential to the wall. In our case, it reduces to

$$\mathbf{V} - \mathbf{V}_{\text{wall}} = a_1 \lambda \left( \frac{\partial \mathbf{V}}{\partial \mathbf{n}} \right)_{\text{wall}} + a_2 \lambda^2 \left( \frac{\partial^2 \mathbf{V}}{\partial \mathbf{n}^2} \right)_{\text{wall}}, \quad (4.2.7)$$

since the plates are assumed to be isothermal and thus no horizontal temperature gradient exists along the boundary. In the case of 2-dimensional Rayleigh-Bénard convection in an infinitely horizontal plane, with fixed impenetrable boundaries,  $\mathbf{V}_{\text{wall}} = \mathbf{W}_{\text{wall}} = 0$ , and thus

$$\mathbf{U} = a_1 \lambda \left( \frac{\partial \mathbf{U}}{\partial \mathbf{n}} \right)_{\text{wall}} + a_2 \lambda^2 \left( \frac{\partial^2 \mathbf{U}}{\partial \mathbf{n}^2} \right)_{\text{wall}}. \quad (4.2.8)$$

In our geometry,  $\frac{\partial}{\partial \mathbf{n}} = \frac{\partial}{\partial Z}$ , so

$$\begin{aligned} U \left( \mathbf{X}, Z = -\frac{D}{2}, t \right) &= a_1 \lambda \left. \frac{\partial U}{\partial Z} \right|_{Z=-\frac{D}{2}} + a_2 \lambda^2 \left. \frac{\partial^2 U}{\partial Z^2} \right|_{Z=-\frac{D}{2}}, \\ U \left( \mathbf{X}, Z = \frac{D}{2}, t \right) &= -a_1 \lambda \left. \frac{\partial U}{\partial Z} \right|_{Z=\frac{D}{2}} + a_2 \lambda^2 \left. \frac{\partial^2 U}{\partial Z^2} \right|_{Z=\frac{D}{2}}. \end{aligned} \quad (4.2.9)$$

The second-order boundary condition on the temperature [8] is

$$\mathbf{T} - \mathbf{T}_{\text{wall}} = b_1 \lambda \left( \frac{\partial \mathbf{T}}{\partial \mathbf{n}} \right)_{\text{wall}} + b_2 \lambda^2 \left( \frac{\partial^2 \mathbf{T}}{\partial \mathbf{n}^2} \right)_{\text{wall}} \quad (4.2.10)$$

which again due to geometry becomes

$$\begin{aligned}
T\left(X, Z = -\frac{D}{2}, t\right) &= T_0 + \delta T + b_1 \lambda \left. \frac{\partial T}{\partial Z} \right|_{Z=-\frac{D}{2}} + b_2 \lambda^2 \left. \frac{\partial^2 T}{\partial Z^2} \right|_{Z=-\frac{D}{2}} \\
T\left(X, Z = \frac{D}{2}, t\right) &= T_0 - b_1 \lambda \left. \frac{\partial T}{\partial Z} \right|_{Z=\frac{D}{2}} + b_2 \lambda^2 \left. \frac{\partial^2 T}{\partial Z^2} \right|_{Z=\frac{D}{2}}
\end{aligned} \tag{4.2.11}$$

The constants  $a_n$  and  $b_n$  depend on the properties of the system and are generally determined by experiment. These boundary conditions are all encompassing as they embody slip ( $\lambda = \infty$ ) and strictly no slip ( $\lambda = 0$ ), allowing exploration of the limits as well as everything in between.

The base state of the system of Eqs. (4.2.2)-(4.2.5) corresponds to no flow where transport of heat occurs simply by conduction. Consequently, the temperature, pressure gradient, heat flux and velocity in this state are given by

$$\begin{aligned}
T_B &= \frac{-\delta T}{(2b_1 \lambda + 1)} Z + T_H - \frac{\delta T}{2}, \\
dP_B / dZ &= -\rho_0 \left[ 1 - \alpha_T \delta T (1 - Z/D) \right] g, \\
Q_B &= \left( 0, K \frac{\delta T}{D} \right), \\
\mathbf{v}_B &= (0, 0, 0),
\end{aligned} \tag{4.2.12}$$

respectively, where the subscript B refers to the base state. The problem is conveniently

cast in dimensionless form by taking the length, time and velocity scales as  $D$ ,  $\frac{D^2}{\kappa}$  and  $\frac{\kappa}{D}$ ,

respectively. Let  $p = \frac{D^2}{\kappa \mu} (P - P_B)$ ,  $\mathbf{q} = \frac{D}{K \delta T} (\mathbf{Q} - \mathbf{Q}_B)$ ,  $\mathbf{v} = \frac{D}{\kappa} \mathbf{V}$ , and  $\theta = \frac{T - T_B}{\delta T}$  be the

dimensionless deviations of the pressure, heat flux, velocity and temperature from their values in the base state. Substituting these into Eqs. (4.2.2)-(4.2.5) the dimensionless equations for these deviations are:

$$\nabla \cdot \mathbf{v} = 0 \tag{4.2.13}$$

$$\text{Pr}^{-1}(\mathbf{v}_t + \mathbf{v} \cdot \nabla \mathbf{v}) = -\nabla p + \text{Ra}\theta \mathbf{e}_z + \Delta \mathbf{v} \quad (4.2.14)$$

$$\theta_t + \mathbf{v} \cdot \nabla \theta = -\nabla \cdot \mathbf{q} + w \quad (4.2.15)$$

$$\mathbf{q} = -\nabla \theta \quad (4.2.16)$$

The non-dimensional Prandtl number and Rayleigh number are given by

$$\text{Pr} = \frac{\nu}{\kappa}, \quad \text{Ra} = \frac{\delta T \alpha_T g D^3}{\nu \kappa}, \quad (4.2.17)$$

respectively, where  $\kappa = \frac{K}{\rho_0 c_p}$  is the thermal diffusivity.

The heat flux can be eliminated from Eqs. (4.2.15) and (4.2.16), and since the problem is two dimensional, we introduce the stream function  $\psi(x, z, t)$ , such that

$$u = \psi_z, \quad w = -\psi_x.$$

Finally, taking the curl of Eq. (4.2.14) eliminates of the pressure term from the momentum equation. The resulting system of equations for the two unknowns  $\psi$  and  $\theta$  is

$$\text{Pr}^{-1}[\Delta \psi_t + \psi_z \psi_{xxx} - \psi_x \psi_{zzz} + \psi_z \psi_{xxx} - \psi_x \psi_{xxz}] = \Delta^2 \psi - \text{Ra} \theta_x, \quad (4.2.18)$$

$$\theta_t + \psi_z \theta_x - \psi_x \theta_z + \psi_x - \theta_{xx} - \theta_{zz} = 0. \quad (4.2.19)$$

The non-dimensional boundary conditions on  $\psi$  and  $\theta$  for all  $x$  and  $t$  are,

$$\begin{aligned}
\psi\left(z = -\frac{1}{2}\right) &= \psi\left(z = \frac{1}{2}\right) = 0 \\
\psi_z\left(z = -\frac{1}{2}\right) - a_1 \text{Kn} \psi_{zz}\left(z = -\frac{1}{2}\right) - a_2 \text{Kn}^2 \psi_{zzz}\left(z = -\frac{1}{2}\right) \\
&= \psi_z\left(z = \frac{1}{2}\right) + a_1 \text{Kn} \psi_{zz}\left(z = \frac{1}{2}\right) - a_2 \text{Kn}^2 \psi_{zzz}\left(z = \frac{1}{2}\right) = 0 \\
\theta\left(z = -\frac{1}{2}\right) - b_1 \text{Kn} \theta_z\left(z = -\frac{1}{2}\right) - b_2 \text{Kn}^2 \theta_{zz}\left(z = -\frac{1}{2}\right) \\
&= \theta\left(z = \frac{1}{2}\right) + b_1 \text{Kn} \theta_z\left(z = \frac{1}{2}\right) - b_2 \text{Kn}^2 \theta_{zz}\left(z = \frac{1}{2}\right) = 0
\end{aligned} \tag{4.2.20}$$

Eqs. (4.2.18) and (4.2.19) are the usual equations for Rayleigh-Bénard convection with Fourier heat transport, yet the solution will depend heavily on the nature of the boundary conditions in Eqs. (4.2.20).

#### 4.2.1 Development of the Dynamical System

The solution to Eqs. (4.2.18)-(4.2.19) with boundary conditions Eqs. (4.2.20) is represented by a truncated Fourier series in  $x$  and  $z$  with time dependent Fourier coefficients. We have truncated this Fourier series to the same order as that of Lorenz [27], such that the stream function is represented by

$$\psi(x, z, t) = \psi_1(z, t) \sin(kx) \tag{4.2.21}$$

and the temperature field by

$$\theta(x, z, t) = \theta_1(z, t) \cos(kx) + \theta_2(z, t). \tag{4.2.22}$$

The  $z$ -dependence is left undefined to allow for the possibility of different boundary conditions. The following dynamical system is developed by projecting Eqs. (4.2.18)-(4.2.19) onto the modes in Eqs. (4.2.21)-(4.2.22):

$$\text{Pr}^{-1} \left[ -k^2 \dot{\psi}_1 + \dot{\psi}'' \right] = k^4 \psi_1 - 2k^2 \psi_1'' + \psi_1^{iv} + k \text{Ra} \theta_1 \tag{4.2.23}$$

$$\dot{\theta}_1 - k\psi_1\theta_2' + k\psi_1 + k^2\theta_1 - \theta_1'' = 0 \quad (4.2.24)$$

$$\dot{\theta}_2 - \frac{1}{2}k\psi_1'\theta_1 - \frac{1}{2}k\psi_1\theta_1' - \theta_2'' = 0 \quad (4.2.25)$$

Here, the over dot represents a derivative with respect to time and the prime denotes a partial derivative with respect to  $z$ . If the  $z$ -dependence for both  $\psi$  and  $\theta$  was described by  $\cos(n\pi z)$ , then Eqs. (4.2.23)-(4.2.25) becomes the Lorenz model.

### 4.3 Linear Stability Analysis of the Conduction State

The linear stability of the conduction state for a fluid with first-order partial slip boundary conditions has been examined previously [13]. The results will be summarized and expanded on here by including second order slip conditions as well as slip coefficients,  $a_n$  and  $b_n$ , from [12] and [8] in Eq. (4.2.20). We substitute the following infinitesimal perturbation to the steady conduction state into Eqs. (4.2.23)-(4.2.25):

$$\begin{aligned} \psi_1 &= e^{\sigma t}\psi_1(z) \\ \theta_1 &= e^{\sigma t}\theta_1(z) \\ \theta_2 &= e^{\sigma t}\theta_2(z) \end{aligned} \quad (4.3.1)$$

Here,  $\sigma$  characterizes the growth rate of the perturbation. By neglecting nonlinear terms and isolating for the highest derivatives in  $z$ , we obtain the following set of ODEs:

$$\begin{aligned} \psi_1^{iv} &= -k^4\psi_1 + 2k^2\psi_1'' - kRa\theta_1 + Pr^{-1}\left(-k^2\sigma\psi_1 + \sigma\psi_1''\right) \\ \theta_1'' &= \sigma\theta_1 + k\psi_1 + k^2\theta_1 \\ \theta_2'' &= \theta_2 \end{aligned} \quad (4.3.2)$$

Only the trivial solution exists for the third equation, which is decoupled from the remainder of the system. Setting  $\sigma = 0$  to obtain the critical stability condition ( $Ra = Ra_c$ ) leaves

$$\begin{aligned}\psi_1^{iv} &= -k^4\psi_1 + 2k^2\psi_1'' - kRa\theta_1, \\ \theta_1'' &= k\psi_1 + k^2\theta_1\end{aligned}, \quad (4.3.3)$$

showing that linear stability will be independent of the Prandtl number. Combined with Eqs. (4.2.20) and the condition

$$\psi''' \left( z = \frac{1}{2} \right) = 1,$$

which is required for the solution of the extra parameter  $Ra$ , this boundary value problem (BVP) can be solved numerically.

Regarding the temperature jump boundary condition, upon analysis of the linearized Eq. (4.2.19) with  $\sigma = 0$  we obtain,

$$\psi_x - \theta_{xx} - \theta_{zz} = 0. \quad (4.3.4)$$

At each of the boundaries  $\psi_x$  and  $\theta_{xx}$  are zero since there is no flow through the plate and since the plate is isothermal, respectively. As a result,  $\theta_{zz}$  is also zero at the boundaries, causing the second-order temperature jump term to become irrelevant for Rayleigh-Bénard convection with isothermal plates. Thus, only second-order hydrodynamic slip and first-order temperature jump will be considered henceforth.

The numerical solution of the BVP for the critical Rayleigh number is very sensitive to the initial guess and thus the linear stability method employed by [28] was used to provide an accurate initial guess to the BVP. Neglecting the non-linear terms, the linearized versions of Eq. (4.2.18)-(4.2.19) are

$$0 = \Delta^2\psi - Ra\theta_x \quad (4.3.5)$$

$$0 = \psi_x - \nabla^2\theta \quad (4.3.6)$$

Expressing the perturbations as



$$\begin{aligned}\psi &= e^{ikx+\sigma t} \psi_k(z) \\ \theta &= e^{ikx+\sigma t} \theta_k(z) \end{aligned} \quad (4.3.7)$$

and setting  $\sigma = 0$  for critical stability, we can express  $\theta$  as a function of  $\psi$ , leading to

$$\theta_k = \frac{-i}{k} D_z^2 \psi_k. \quad (4.3.8)$$

Substituting this into the energy equation yields

$$\left[ D_z^3 + k^2 \text{Ra} \right] \psi_k = 0 \quad (4.3.9)$$

where  $D_z = \partial_z^2 - k^2$ . The  $z$ -dependence is then assumed to take the form

$$\psi_k(z) = \sum_{n=1}^3 M_n \sin(q_n z) \quad (4.3.10)$$

where the  $M_n$  are unknown coefficients and  $q_n$  are the three solutions of

$$q_n = \sqrt{-k^2 + \sqrt[3]{k^2 \text{Ra}_c(k)} (1)^{1/3}} \quad (4.3.11)$$

where  $1^{1/3} = 1, 1/2 \pm 1/2\sqrt{3}$ . The coefficients  $M_n$  are determined by the three boundary conditions on  $\psi$  and  $\theta$  at  $z = 1/2$ , listed in Eq. (4.2.20), giving

$$\begin{aligned} \sum_{n=1}^3 \left( M_n \cos\left(\frac{1}{2} q_n\right) \right) &= 0 \\ \sum_{n=1}^3 \left( M_n q_n \sin\left(\frac{1}{2} q_n\right) \right) + a_1 \text{Kn} \sum_{n=1}^3 \left( M_n q_n^2 \cos\left(\frac{1}{2} q_n\right) \right) + a_2 \text{Kn}^2 \sum_{n=1}^3 \left( M_n q_n^3 \sin\left(\frac{1}{2} q_n\right) \right) &= 0 \\ \sum_{n=1}^3 \left[ M_n (q_n^2 + k^2)^2 \cos\left(\frac{1}{2} q_n\right) \right] - b_1 \text{Kn} \sum_{n=1}^3 M_n q_n (q_n^2 + k^2)^2 \sin\left(\frac{1}{2} q_n\right) &= 0 \end{aligned}$$

These equations can be written as a matrix  $\tilde{\mathbf{A}}$  times the vector  $\mathbf{M} = [M_1 \ M_2 \ M_3]^T$ . For a non-trivial solution, the determinant of  $\tilde{\mathbf{A}}$  must be zero. The real and imaginary parts of the determinant are plotted with respect to  $\text{Ra}$  and the conditions for critical stability are

found wherever both intersect with zero. This solution is then used in the BVP to ensure the fastest and most correct solution. The BVP solver is used to generate the figures in the following sections due to its ability to output a numerical result.

Suggested values for  $a_1$ ,  $a_2$  and  $b_1$  from Deissler and Karniadakis & Beskok ([8], [12] respectively) are shown in Table 2.

**Table 2 - Slip coefficients developed by [8] and [12] for second-order hydrodynamic slip and first-order temperature jump.**

	$a_1$	$a_2$	$b_1$
Deissler	1	-9/8	1
Karniadakis and Beskok	1	1/2	1

The coefficient  $a_1$  is defined as  $(2-\zeta)/\zeta$  from Eq. (4.1.1) where  $\zeta$  is the tangential momentum accommodation coefficient [15]. It is generally considered to be close to 1 for most engineering applications [3], explaining the choice for  $a_1$  by the authors depicted in the above table. For the results in this chapter,  $\zeta$  will continue be chosen as 1. The

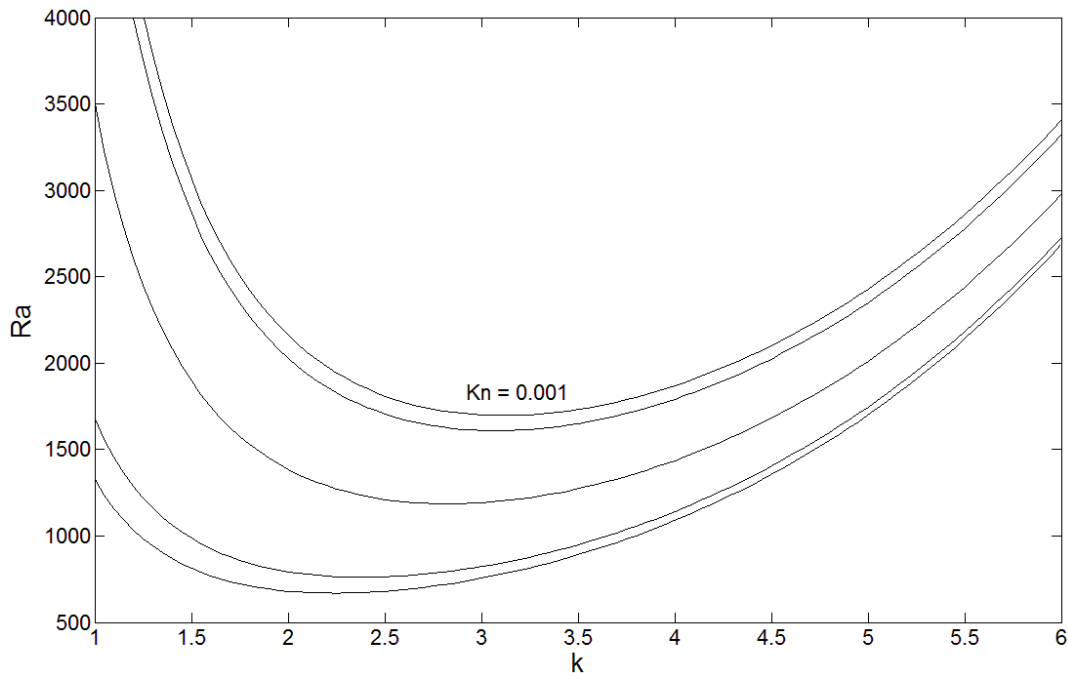
temperature coefficient  $b_1$  is defined as  $\frac{2-\zeta}{\zeta} \frac{2\gamma}{\gamma+1} \frac{1}{Pr}$  from Eq. (4.1.2) [8], [13], [14], [29],

where  $\gamma$  is also assumed to be 1 [25]. The Prandtl number used in the following calculation is also 1, which is its value for many gases. Thus, it is reasonable that  $b_1$  was chosen to equal one for the first-order temperature jump coefficient by both authors.

## 4.4 Results and Discussion

### 4.4.1 First-Order Slip

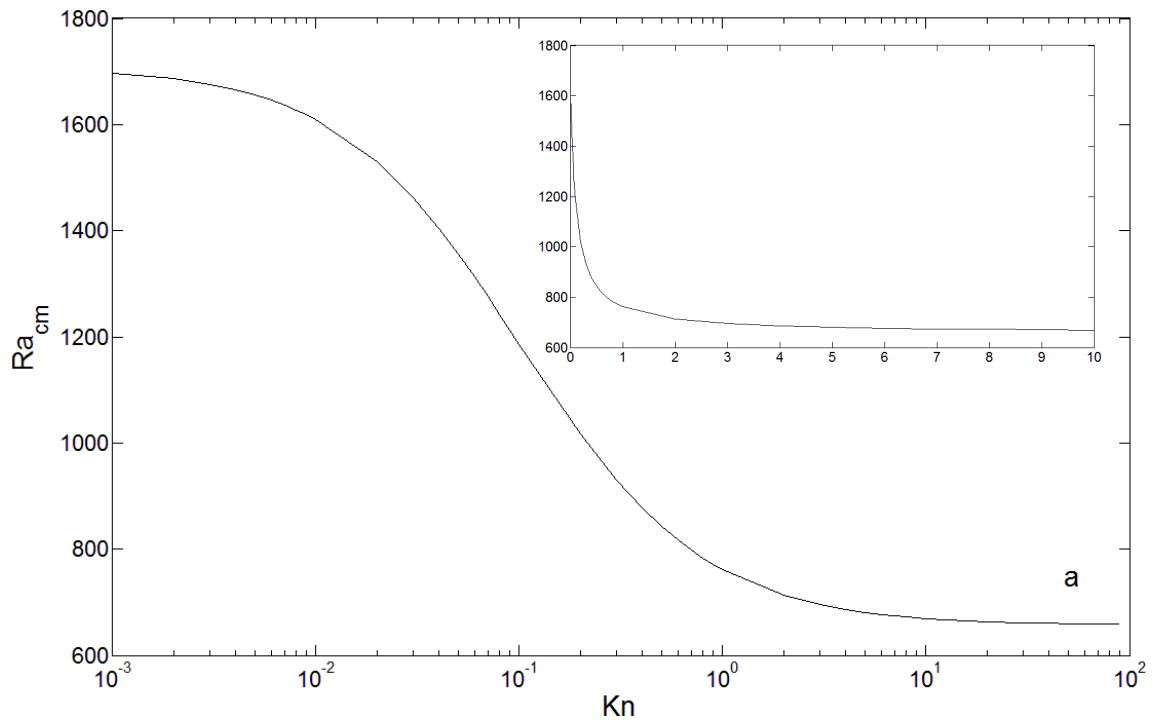
We will first evaluate the case where only first-order hydrodynamic slip is considered, as shown in Fig. 4.3 and Fig. 4.4. In this case, both [8] and [12] suggest that  $a_1 = 1$ .



**Figure 4.3 – The influence of first-order hydrodynamic slip on the Rayleigh number,  $Ra_c$ , vs wave number,  $k_c$ , for varying  $Kn$  and  $a_1 = 1$ . From top to bottom,  $Kn = 0.001, 0.01, 0.1, 1$  and  $10$ .**

For  $Kn \ll 1$ , the stability boundary in the  $Ra$ - $k$  plane is very close to the known solution for no-slip boundary conditions. As  $Kn$  increases from zero, the minimum critical Rayleigh number,  $Ra_c$ , and the critical wave number,  $k_c$ , both decrease from their no-slip values of 1707.76 and 3.117, respectively. This is due to the reduced stress at the boundaries which reduces the effect of viscous dissipation, allowing convection to begin at lower  $Ra$ . As one might expect from quick analysis of the first-order hydrodynamic slip boundary conditions, the critical Rayleigh number and critical wave number decrease to the known values for stress free boundaries as the Knudsen number becomes large. Fig. 4.4 shows the minimum critical Rayleigh number,  $Ra_{cm}$ , and the corresponding

critical wave number,  $k_{cm}$ , as a function of  $Kn$ , as the boundary conditions change from stick boundary conditions (small  $Kn$ ) to stress free boundary conditions (large  $Kn$ ).



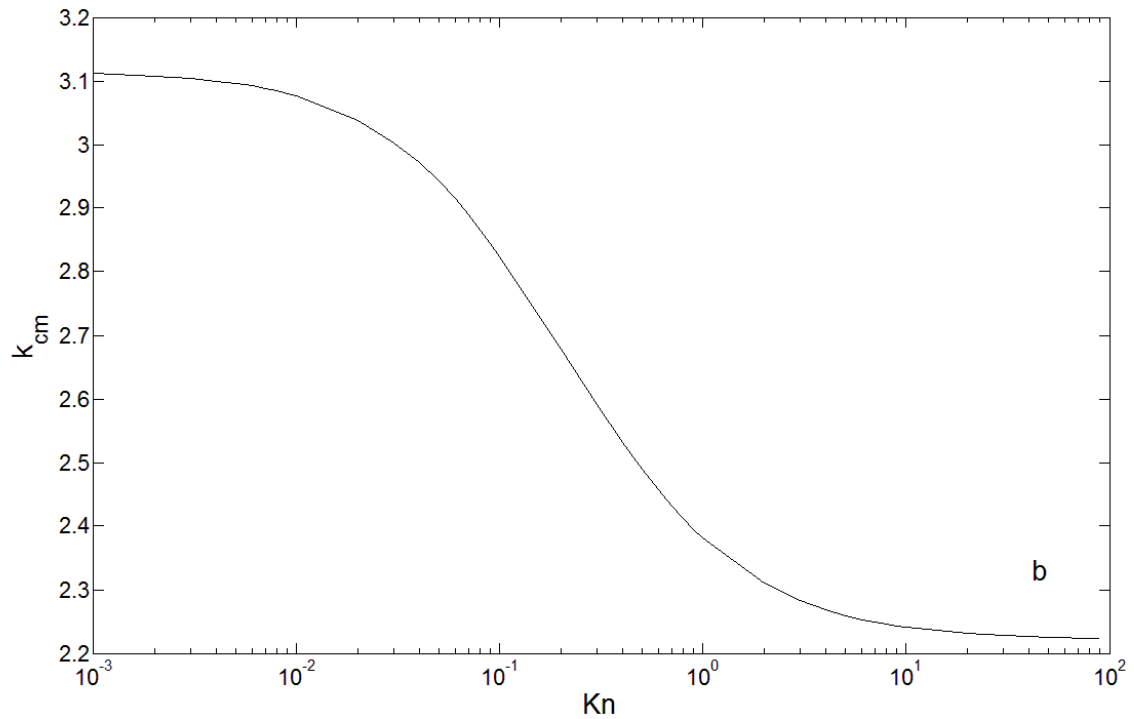


**Figure 4.4 – The effect of first-order hydrodynamic slip with  $a_1 = 1$  on a) the minimum critical Rayleigh number and b) the corresponding critical wave number vs Kn. The inset to (a) shows the same results for  $Ra_{cm}$  but with a linear scale on the Knudsen axis.**

When plotted with a logarithmic Kn axis, as in Fig. 4.4, the values of  $Ra_{cm}$  and  $k_{cm}$  appear to change most rapidly in range  $0.01 < Kn < 10$ . This however is an artifact of the logarithmic axis. The inset show that slope is most negative for small Kn and the magnitude decreases monotonically as Kn increases. For  $Kn < 0.01$ , the no-slip boundary condition should be sufficient, predicting instability to occur close to  $Ra = 1708$  at a wave number near 3.117. When  $Kn > 10$ , the boundaries may be considered stress free since the partial derivative in the boundary condition is required to go to zero as Kn becomes large in order to keep the velocity well behaved. Thus, for large Kn the first-order boundary conditions predict instability to occur close to  $Ra = 657.5$  at a wave number near 2.22.

The effect of first-order temperature jump is shown by Fig. 4.5.

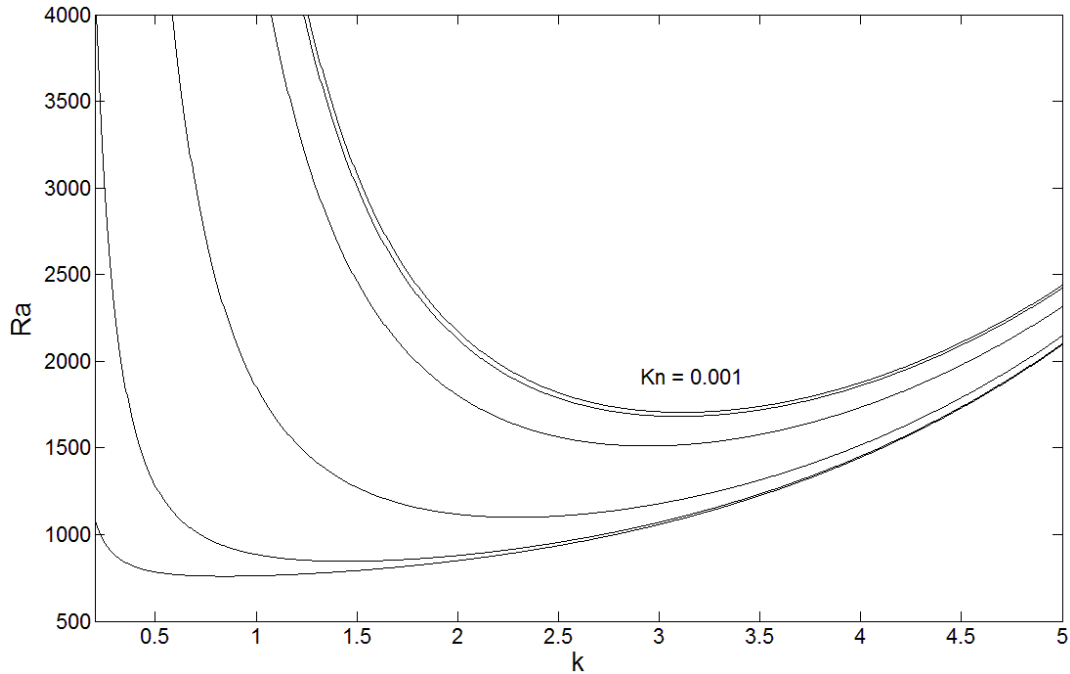


**Figure 4.5 – The influence of first-order temperature jump on the Rayleigh number,  $Ra_c$ , vs wave number,  $k_c$ , for varying  $Kn$  and  $b_1 = 1$ . From top to bottom,  $Kn = 0.001, 0.01, 0.1, 1$  and  $10$ .**

Interestingly, this too has the effect of lowering the critical Rayleigh number. One might expect that since the temperature jump brings the temperature at the boundaries closer to each other over the same distance this effect may inhibit the transition to convection by lowering the temperature gradient. In order to understand this behaviour, consider an extrapolated fluid cell with plate separation equal to  $D + 2l_s$  as shown in Fig. 4.6.

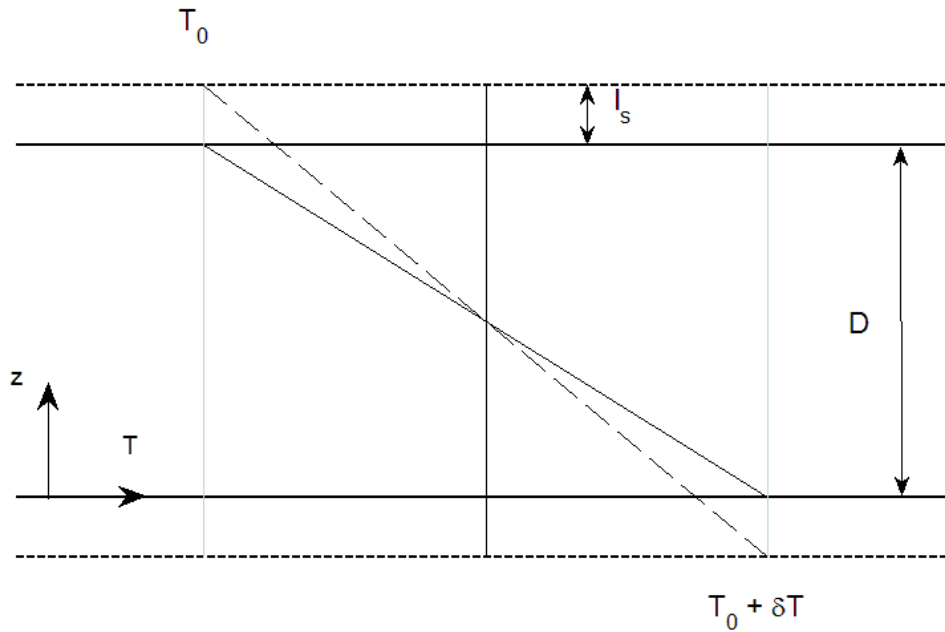


**Figure 4.6 - Real convection cell (solid horizontal lines) and no-slip linear temperature profile (solid line). Temperature profile with jump (dashed line) is extrapolated by a slip length  $l_s$  to either side such that it has no temperature jump at the extrapolated cell (dashed horizontal lines).**

The thick solid horizontal lines represent the real fluid cell containing a no-slip temperature profile which has also been drawn with a solid line. The dashed line represents a real temperature profile with a temperature jump in the real cell. This temperature jump profile is extrapolated out to the virtual cell (dashed horizontal lines) by a slip length on either side. By doing so, the temperature jump there is equal to zero. The Rayleigh number for the extrapolated cell can then be defined as

$$Ra = \frac{\delta T \alpha_T g (D + 2l_s)^3}{\nu \kappa}.$$

When  $\delta T$  reaches the critical temperature difference for the extrapolated cell such that  $Ra_E = 1708$ , the real cell's  $Ra$  (Eq. 4.2.17) is still be below this critical limit. At this point, convection would begin to set in for the extrapolated cell as shown by the solid curve representing the infinitesimal velocity perturbation in Fig. 4.7.

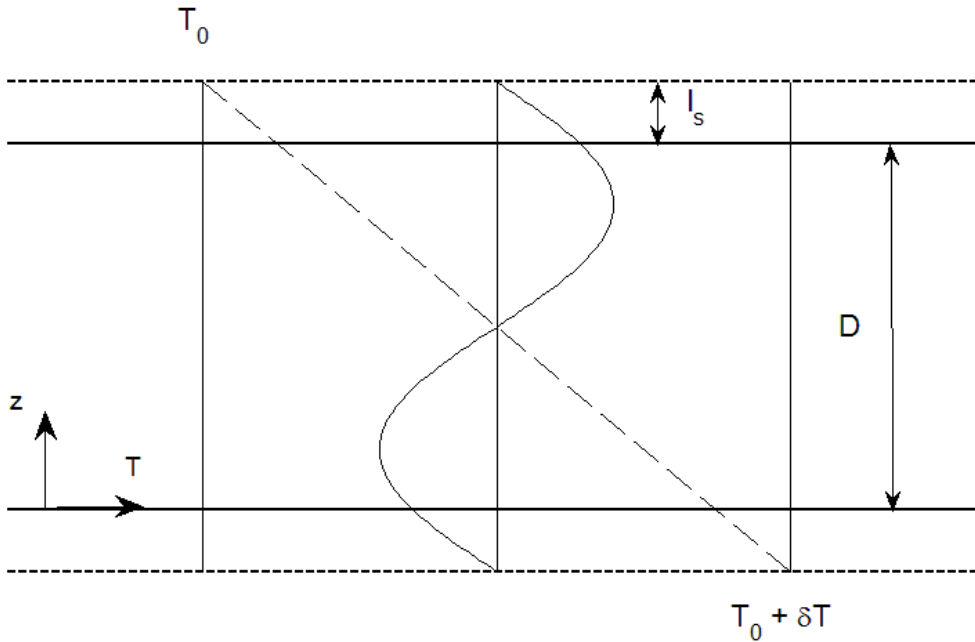


**Figure 4.7 - Onset of convection for the extrapolated cell. The temperature is shown by the dashed line and the infinitesimal velocity profile is shown by the solid line. Both temperature and velocity profile are no-slip for the extrapolated cell but not the real fluid cell.**

At the onset, both the temperature and velocity profile are no-slip at the extrapolated cell boundaries. However, the profiles are not no-slip at the boundary of the real fluid cell. Thus, a temperature jump boundary condition may also imply a partial slip boundary condition on the velocity, or that they are at least mathematically equivalent.



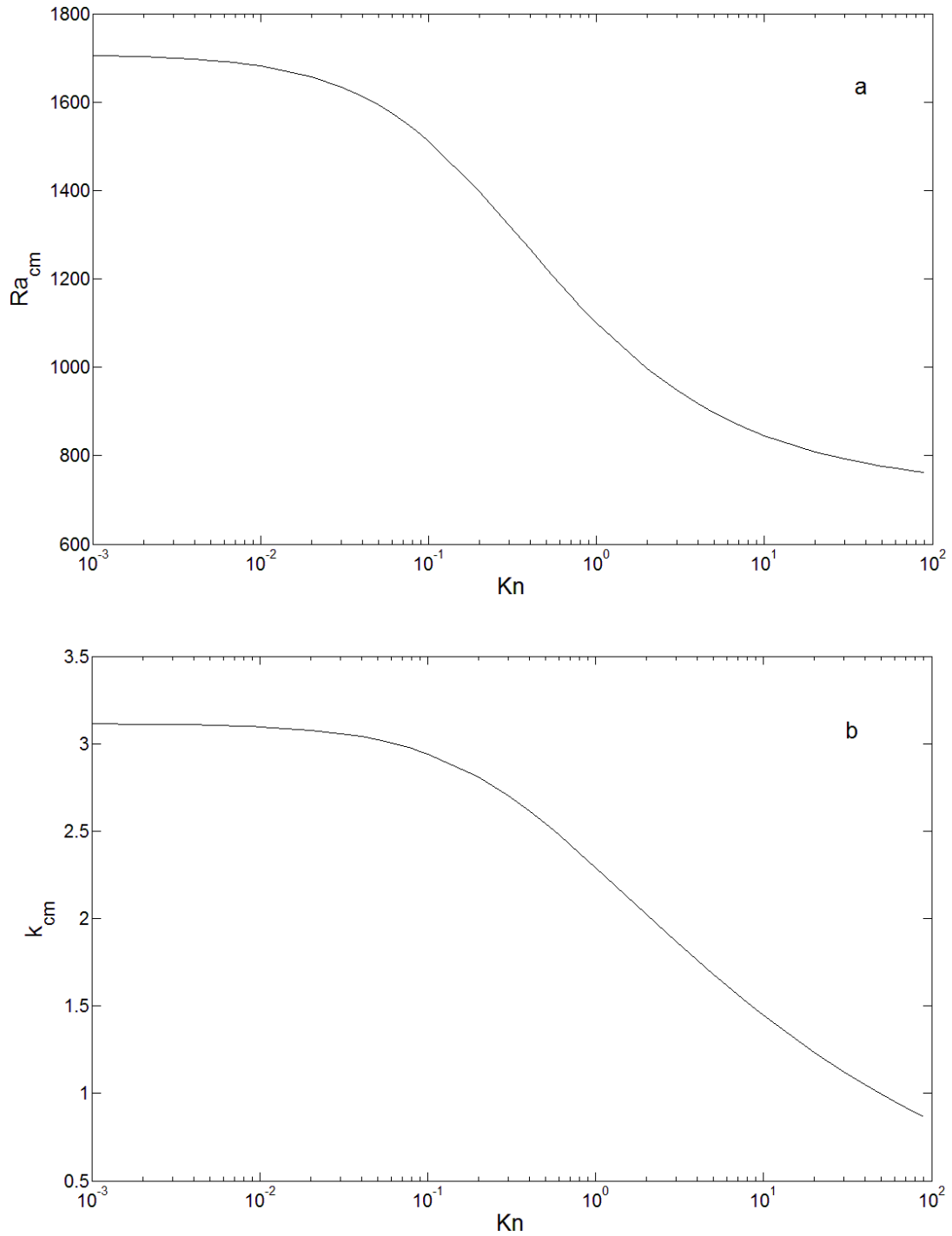
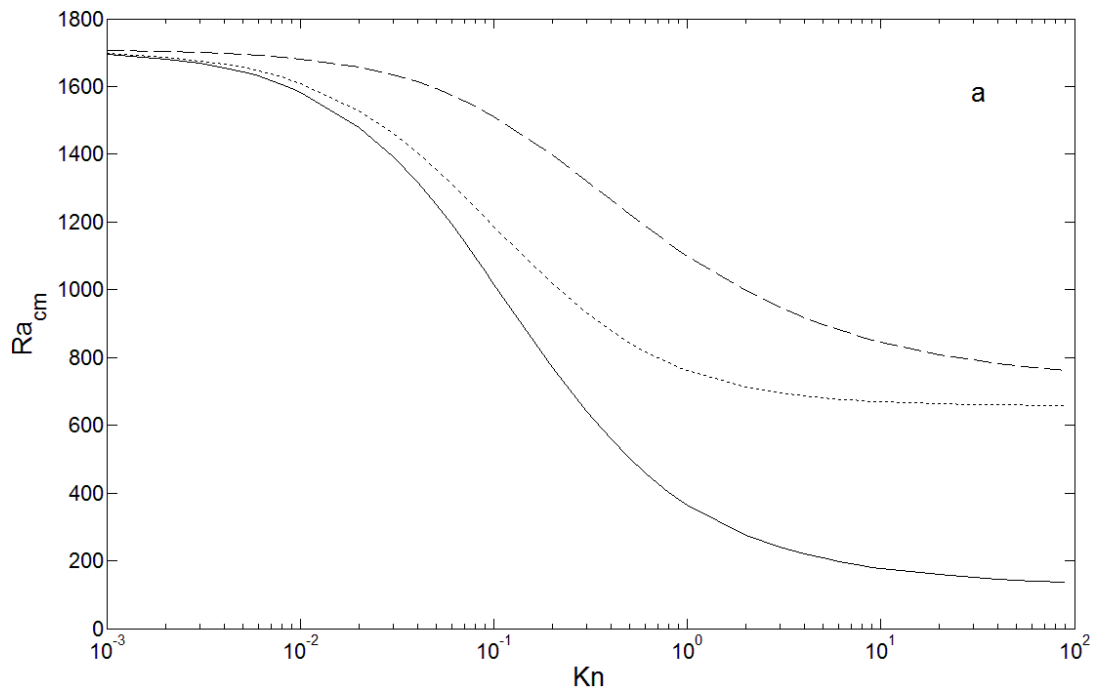


**Figure 4.8 – The effect of first-order temperature jump on a) the minimum critical Rayleigh number and b) the corresponding critical wave number vs Kn for  $b_1 = 1$ .**

The relationship between  $Ra_{cm}$  and  $k_{cm}$  as the Knudsen number increases is shown in Fig. 4.8. As the Knudsen number increases past 0.01, the critical Rayleigh number begins to

exhibit significant changes. Significant changes continue to occur in  $Ra$  until  $Kn \approx 100$ , at which point it asymptotically approaches approximately 700. At this magnitude of Knudsen number, however, the continuum assumption will break down since the random motion of particles will need to be considered. Considerable change still occurs for  $Kn < 1$ , which may well be within the realm of applicability.

Change in the critical wave number is small until  $Kn > 0.1$ , where it continues to decrease throughout the remainder of the domain. Again, one would not expect the continuum approximation to hold in the region of  $Kn = 100$ , but considerable change does still occur for  $Kn < 1$ . The first-order temperature jump can still greatly affect the critical conditions for instability and could even be more significant than first-order hydrodynamic slip for some values of  $\gamma$  and  $Pr$ . At least for the coefficients chosen, it appears as though a first-order temperature jump has more of an effect on the critical wave number, whereas first-order hydrodynamic slip as more of an effect on the critical Rayleigh number.



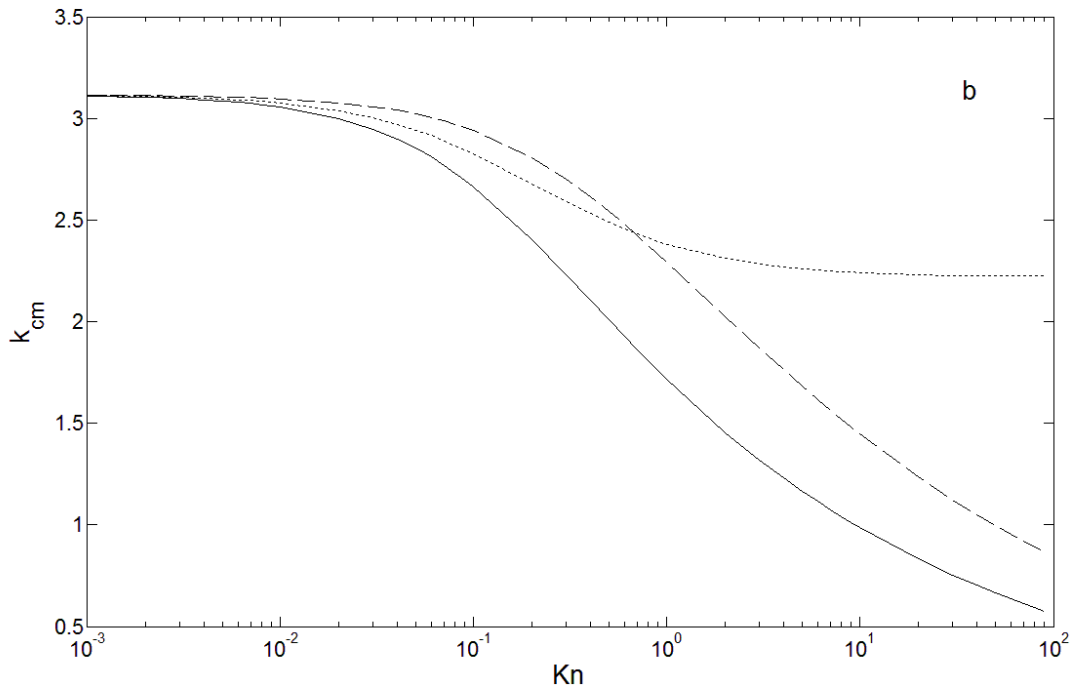
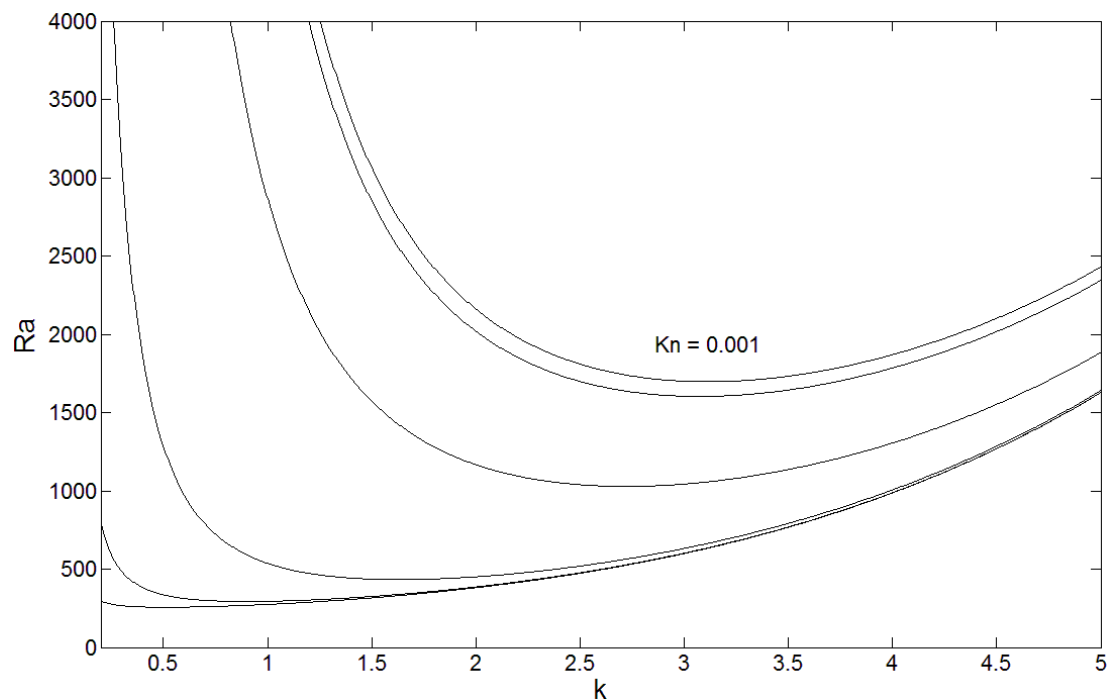


**Figure 4.9 – The effect of both first-order hydrodynamic slip and first-order temperature jump (solid line) on a) the minimum critical Rayleigh number and b) the corresponding critical wave number vs  $Kn$ . The short dashed line shows the results for first-order hydrodynamic slip only and the long dashed line is for a first-order temperature jump only.**

Fig. 4.9 shows the critical Rayleigh number and critical wave number calculated for a system with both first-order hydrodynamic slip and a temperature jump. We can see that the minimum critical Rayleigh number decreases faster when both first-order effects are included and asymptotically approaches a lower  $Ra$ . The same effect is seen for the minimum critical wave number. It appears as though the velocity slip has a greater effect on  $Ra_{cm}$  since the solution for first-order velocity slip (short dashed curve) is similar to the solution obtained when both first-order effects are considered (solid curve). Concurrently, the temperature jump has a greater effect on  $k_{cm}$  since the solution for first-order temperature jump (long dashed curve) is very similar to the solid curve. The changes in the stability boundary shows that partial slip boundary conditions are expected to play a significant role in Rayleigh-Bénard convection at the microscale where  $Kn$  enters the slip-flow regime and beyond.

#### 4.4.2 Second-Order Slip

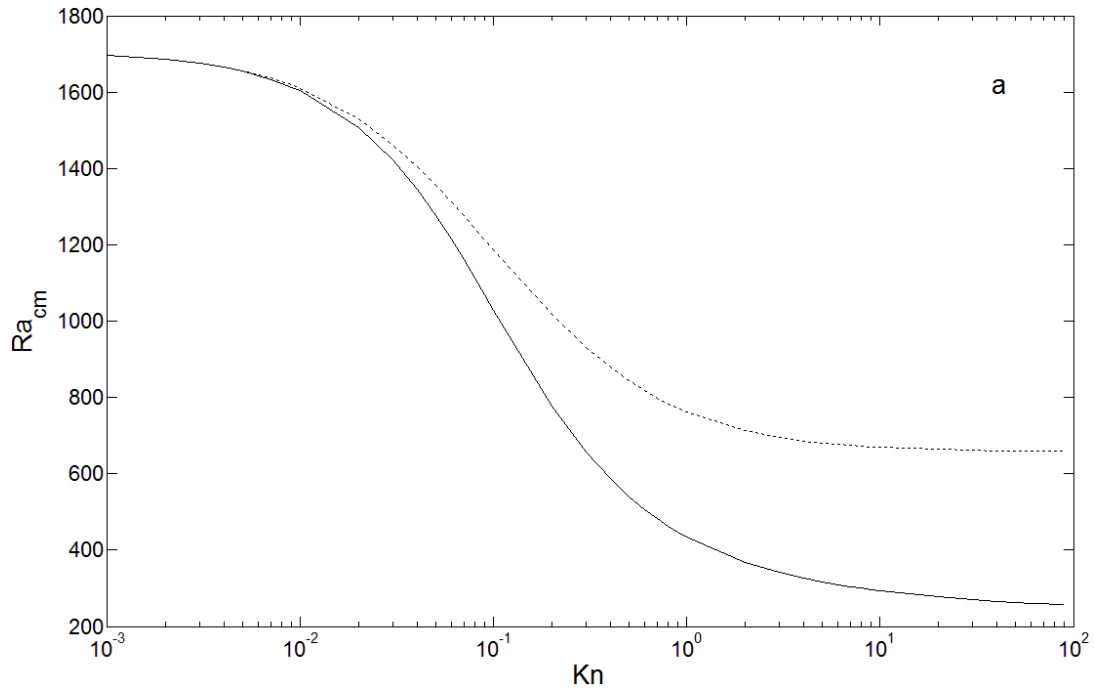
According to [22], [23], the first-order slip conditions become insufficient near  $Kn = 0.1$ . After this point, second-order slip boundary conditions are necessary. Second-order hydrodynamic slip conditions have been reported to give results in good agreement with experiment up to  $Kn = 1.5$  [22]. Different values of  $a_2$  have been proposed. We will first explore the effect of the sign of  $a_2$  by calculating with the values proposed by [12] and [8] and assuming no temperature jump. Beginning with  $a_1 = 1$  and  $a_2 = -9/8$  as proposed by [12], the general picture is again described using the  $Ra$ - $k$  plane as in Fig. 4.10.



**Figure 4.10 – The influence of second-order hydrodynamic slip effects on the critical Rayleigh number,  $Ra_c$ , vs wave number,  $k$ , for varying  $Kn$  with  $a_1 = 1$  and  $a_2 = -9/8$ . From top to bottom,  $Kn = 0.001, 0.01, 0.1, 1$  and  $10$ .**

By inspection of the boundary condition with the coefficients chosen by [12], second-order hydrodynamic slip causes further slip for  $a_2 < 0$  compared with first-order effects. As depicted by Fig. 4.10, both the critical Rayleigh number and wave number are smaller than for stick boundary conditions. In the limit that  $Kn$  becomes large, the stress-free limit of  $Ra_c \approx 657$  and  $k_c \approx 2.22$  no longer occurs since, in order for the boundary

condition to be well behaved, both the first and second derivative of the velocity in Eq. (4.2.20) are required to go to zero as  $\text{Kn} \rightarrow \infty$ . Otherwise, the slip velocity would become infinite. Fig. 4.11 shows the minimum critical Rayleigh number and corresponding critical wave number, compared with the results for first-order hydrodynamic slip.



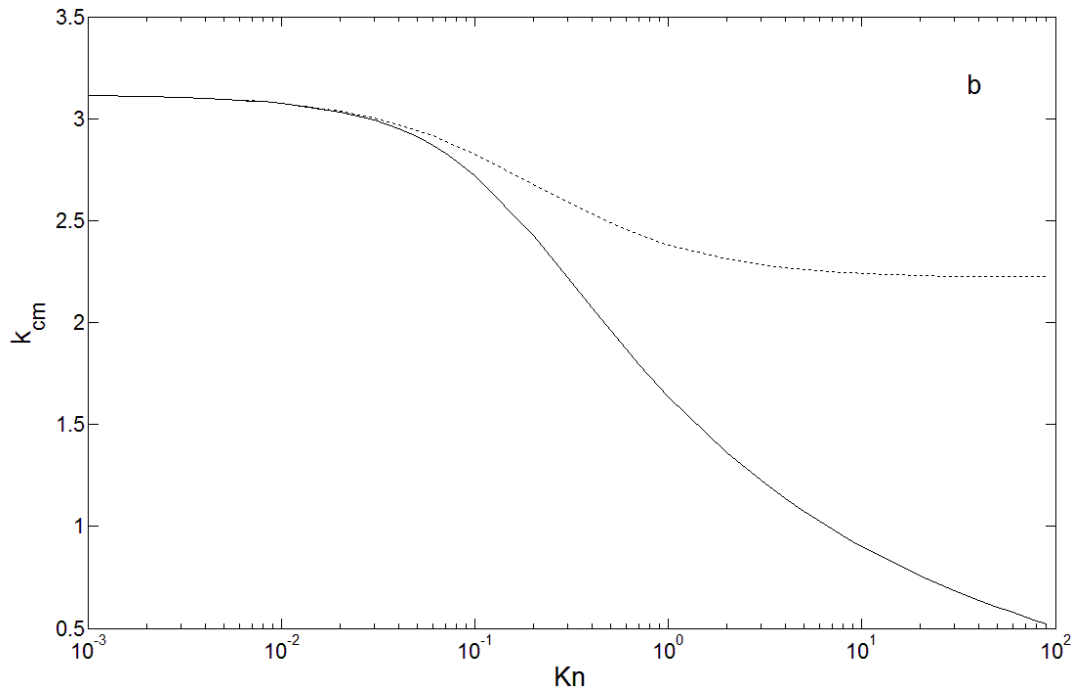


**Figure 4.11 – The effect of second-order hydrodynamic slip effects (solid line) with coefficients proposed by [12] on a) the minimum critical Rayleigh number and b) the corresponding critical wave number vs  $Kn$  with  $a_1 = 1$  and  $a_2 = -9/8$ . Dashed line indicates solution for first-order hydrodynamic slip.**

Both  $Ra_{cm}$  and  $k_{cm}$  are significantly affected by the inclusion of second-order hydrodynamic slip for the value of  $a_2$  chosen. The difference becomes very apparent in the transition regime where  $Kn > 0.1$  which has been suggested previously [25]. Here,  $Ra_{cm}$  decreases faster and its asymptotic behaviour approaches a value approximately a third of that for first-order effects. This is due to the rate of change of the stress with respect to  $z$  (second-order effects) also approaching zero at the boundary, causing the stress to increase more slowly into the fluid. Concurrently,  $k_{cm}$  decreases much more quickly than for first-order slip and approaches zero for large Knudsen number. Although second-order effects largely depend on the value of  $Kn$ , experimental analysis will be required to determine appropriate coefficients for second-order effects in a Rayleigh-Bénard configuration since it is clear that their inclusion can yield drastic changes.

When considering second-order slip proposed by [8] where  $a_2 = 0.5$ , the solution for  $Ra_{cm}$  and  $k_{cm}$  yields a vertical asymptote near  $Kn = 0.5$  as shown by Fig. 4.12.

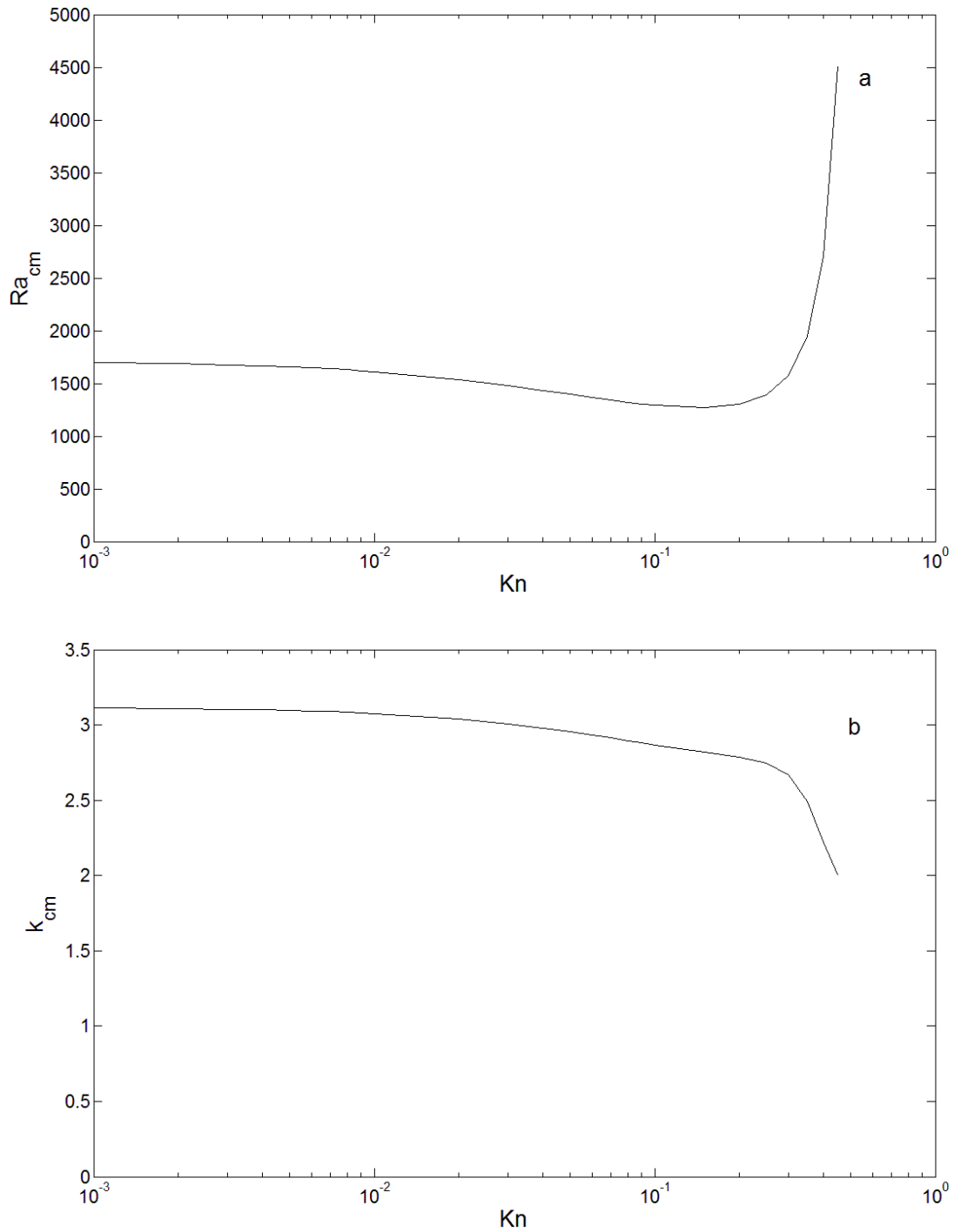
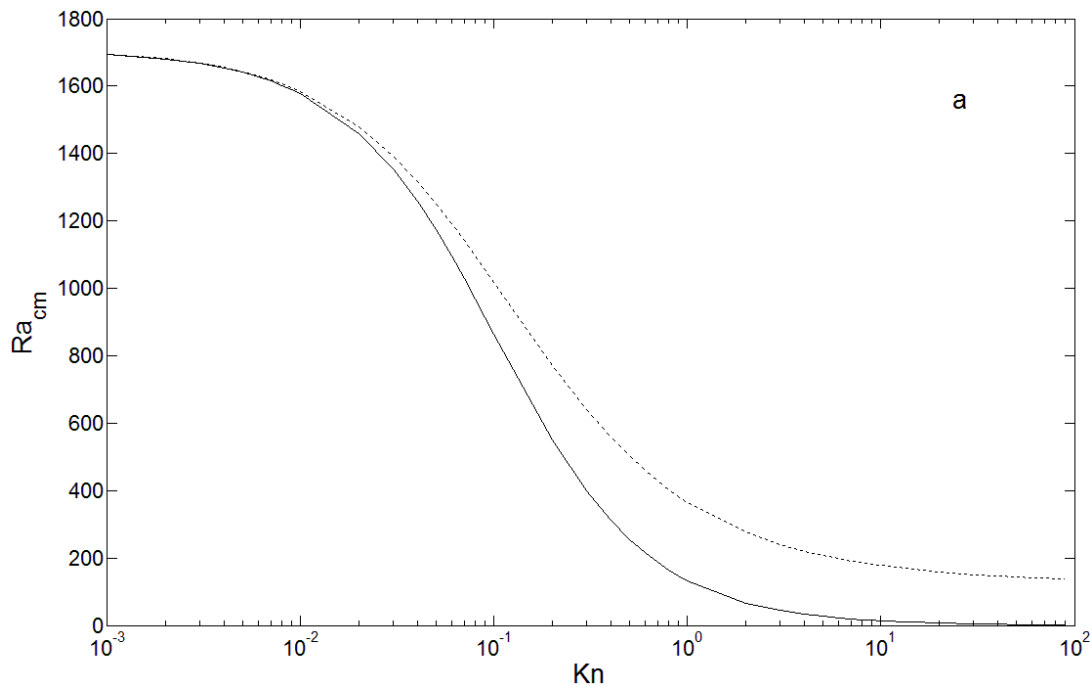


**Figure 4.12 – The effect of second-order hydrodynamic slip effects with coefficients proposed by [8] where  $a_1 = 1$  and  $a_2 = 0.5$  on a) the minimum critical Rayleigh number and b) the corresponding critical wave number vs Kn**

By inspection of the boundary condition Eq. (4.2.20) for  $a_2 > 0$ , there will exist a  $\text{Kn}$  that causes first- and second-order hydrodynamic slip effects to cancel out, numerically creating asymptotic behaviour. Due to the vertical asymptote, the decreases in both  $\text{Ra}_{\text{cm}}$  and  $k_{\text{cm}}$  are much slower than for  $a_2 < 0$ . The critical Rayleigh number is predicted to be greater than that for first-order effects. As a result, it looks doubtful that  $a_2 > 0$  is a physically realistic boundary condition for Rayleigh-Bénard convection. A preference to the coefficient proposed by Deissler [12] where  $a_2 = -9/8$  was also communicated by Colin et al [24].

Finally, now that we've investigated the effects of velocity slip and temperature jump separately, we will explore the combination of both second-order hydrodynamic slip and first-order temperature jump effects. Only the negative  $a_2 = -9/8$  suggested by [12] will be considered below as we will assume for now that the vertical asymptote encountered using  $a_2 > 0$  is non-physical.

Individual trends of  $\text{Ra}_{\text{cm}}$  and  $k_{\text{cm}}$  with respect to  $\text{Kn}$  are portrayed in Fig. 4.13 for first and second-order hydrodynamic slip as well as first-order temperature jump effects.





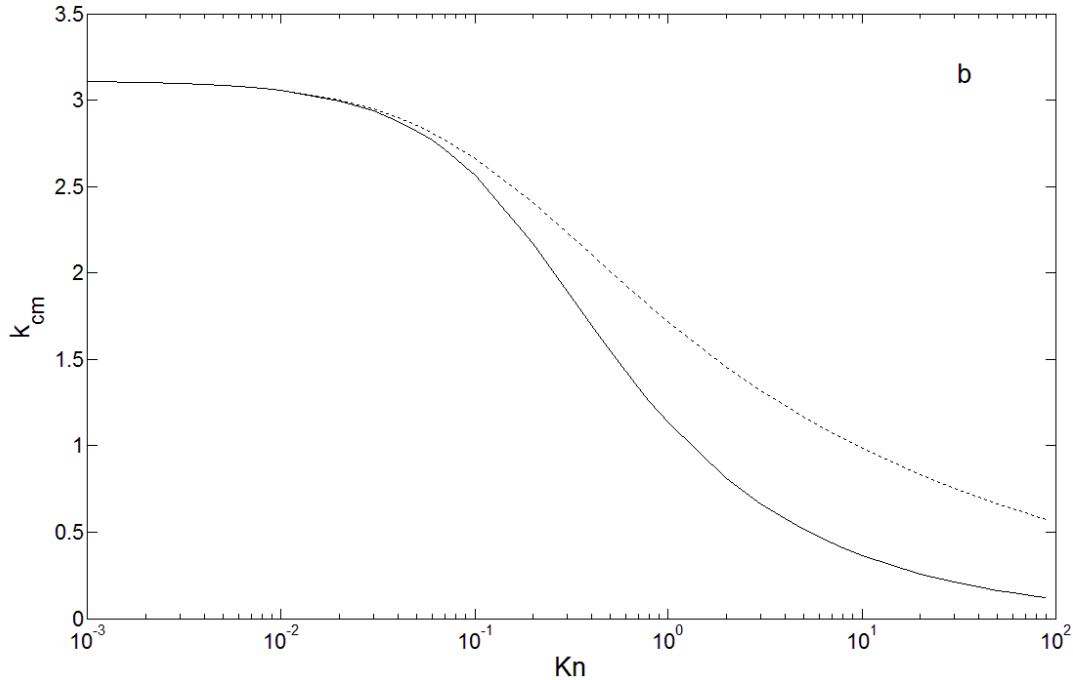


**Figure 4.13 - For the combined effects of  $a_1 = 1$ ,  $a_2 = -9/8$  and  $b_1 = 1$  (solid line), the a) minimum critical Rayleigh number vs  $Kn$  and b) corresponding critical wave number vs  $Kn$ . Dashed curve represents combined contribution from first-order velocity slip and temperature jump where  $a_1 = 1$  and  $b_1 = 1$ .**

Including second-order velocity slip and first-order temperature jump increases the amount of total slip and gives the greatest decrease in the stability boundary. The minimum critical Rayleigh number begins to decrease around  $10^{-2}$  and at a rate faster than when only first-order effects are considered. Little change is seen past  $10^1$ , decreasing asymptotically to just more than 20 for large  $Kn$ . The value of  $k_{cm}$  displays similar characteristics although the changes begin an order of magnitude later.

Second-order slip boundary conditions have a far greater effect on the conditions for instability in Rayleigh-Bénard convection than first-order slip boundary conditions. This is especially true in the transition regime where second-order effects are said to improve the accuracy of the solution [25], but also in the slip-flow regime there exists a difference between the first- and second-order solutions.

## 4.5 Conclusion

In this work, the effects of partial slip boundary conditions on the linear stability of Rayleigh-Bénard convection have been examined. Both first- and second-order effects on the hydrodynamic slip were studied; however, only a first-order temperature jump is explored since the second-order slip term in the temperature boundary condition was shown to vanish for isothermal plates. Linear stability is shown to be independent of  $Pr$  and the minimum critical Rayleigh number  $Ra_{cm}$  and corresponding wave number  $k_{cm}$  are calculated. Using first-order hydrodynamic slip, the microscale stability picture begins to change from that of the macroscale at the beginning of the slip-flow regime. This causes a significant reduction of the critical minimum Rayleigh number and, to a lesser extent, the corresponding wave number, approaching the known theoretical value for large  $Kn$  ( $Ra_{cm} \approx 657$  and  $k_{cm} \approx 2.22$ ). This change is most pronounced at small Knudsen number. The first-order temperature jump boundary condition also begins to show significant effects near  $Kn = 0.01$ , reducing both  $Ra_{cm}$  and  $k_{cm}$ . In this case, the boundary condition has a greater influence on the critical wave number than the Rayleigh number.

Interestingly, it can be argued that the temperature jump at the boundary is mathematically equivalent to velocity slip. The combination of first-order velocity and temperature slip leads to an even more unstable conduction state compared with either of the first-order effects independently. The inclusion of second-order hydrodynamic slip effects further promotes instability of the conduction state, depending on the value of the coefficient  $a_2$ . Analysis of two different conditions,  $a_2 < 0$  and  $a_2 > 0$  shows that a non-physical solution is obtained for the latter in a Rayleigh-Bénard configuration. More experimental work and numerical work solving for the full velocity field is necessary to understand whether positive or negative second-order coefficients are appropriate and to determine their magnitude. The difference between the solution for first- and second-order slip conditions increases drastically as the Knudsen number increases as both the minimum critical Rayleigh number and corresponding wave number approach zero for large  $Kn$  with second-order effects. As a result, any attempts to push a continuum solution of Rayleigh-Bénard convection near the transition regime should include second-order boundary conditions.

## 4.6 Acknowledgements

This research was supported by the Natural Sciences and Engineering Research Council of Canada.

## 4.7 References

- [1] T. Squires and S. Quake, “Microfluidics: Fluid physics at the nanoliter scale,” *Rev. Mod. Phys.*, vol. 77, no. July, 2005.
- [2] E. Arkilic, “Slip in microchannels,” in *Proceedings of Rarefied Gas Dynamics Symposium*, 1994.
- [3] E. Arkilic, “Mass flow and tangential momentum accommodation in silicon micromachined channels,” *J. Fluid ...*, vol. 437, pp. 29–43, 2001.
- [4] W. B. Black and M. D. Graham, “Wall-Slip and Polymer-Melt Flow Instability,” 1996.
- [5] F. Brochard and P. G. De Gennes, “Shear-dependent slippage at a polymer/solid interface,” *Am. Chem. Soc.*, vol. 8, no. 12, pp. 3033–3037, Dec. 1992.
- [6] H. Struchtrup and P. Taheri, “Macroscopic transport models for rarefied gas flows: a brief review,” *IMA J. Appl. Math.*, vol. 76, no. 5, pp. 672–697, Feb. 2011.
- [7] N. Jeong, “Lattice Boltzmann approach for the simulation of rarefied gas flow in the slip flow regime,” *J. Mech. Sci. Technol.*, vol. 27, no. 6, pp. 1753–1761, Jul. 2013.
- [8] G. E. Karniadakis, A. Beskok, and N. Aluru, *Microflows and Nanoflows: Fundamentals and Simulation*. New York: Springer-Verlag, 2002.
- [9] D. F. Stranges, R. E. Khayat, and B. Albaalbaki, “Thermal convection of non-Fourier fluids. Linear stability,” *Int. J. Therm. Sci.*, vol. 74, pp. 14–23, Dec. 2013.

- [10] R. Khayat, “Fluid elasticity and the transition to chaos in thermal convection,” *Phys. Rev. E*, 1995.
- [11] A. Manela and I. Frankel, “On the Rayleigh–Bénard problem: dominant compressibility effects,” *J. Fluid Mech.*, vol. 565, p. 461, Sep. 2006.
- [12] R. G. Deissler, “An Analysis of Second-Order Slip Flow and Temperature-Jump Boundary Conditions for Rarefied Gases,” *Int. J. Heat Mass Transf.*, vol. 7, no. 6, pp. 681–694, 1964.
- [13] L. S. Kuo and P. H. Chen, “Effects of Slip Boundary Conditions on Rayleigh–Bénard Convection,” *J. Mech.*, vol. 25, no. 02, pp. 205–212, May 2011.
- [14] J. C. Maxwell, “On stresses in rarified gases arising from inequalities of temperature,” ... *Trans. R. Soc. ...*, vol. 170, no. 1879, pp. 231–256, 1879.
- [15] B.-Y. Cao, M. Chen, and Z.-Y. Guo, “Temperature dependence of the tangential momentum accommodation coefficient for gases,” *Appl. Phys. Lett.*, vol. 86, no. 9, p. 091905, 2005.
- [16] E. Lauga, M. Brenner, and H. Stone, “Microfluidics: the no-slip boundary condition,” in *Springer handbook of experimental fluid ...*, 2007, pp. 1219–1240.
- [17] N. G. Hadjiconstantinou, “The limits of Navier-Stokes theory and kinetic extensions for describing small-scale gaseous hydrodynamics,” *Phys. Fluids*, vol. 18, no. 11, p. 111301, 2006.
- [18] E. Bodenschatz, W. Pesch, and G. Ahlers, “Recent Developments in Rayleigh–Bénard Convection,” *Annu. Rev. Fluid Mech.*, vol. 32, pp. 709–778, 2000.
- [19] A. V. Getling, *Rayleigh-Benard Convection: Structures and Dynamics*. World Scientific, 1998.
- [20] D. C. Rapaport, “Molecular-Dynamics Study of Rayleigh–Bénard Convection,” *Phys. Rev. Lett.*, vol. 60, no. 24, pp. 2480–2483, 1988.

- [21] M. Mareschal and E. Kestemont, “Experimental evidence for convective rolls in finite two-dimensional molecular models,” *Nature*, vol. 329, pp. 427–429, 1987.
- [22] A. K. Sreekanth, “Slip flow through long circular tubes,” in *Proceedings of the Sixth International Symposium on Rarefied Gas Dynamics*, 1996, pp. 667–680.
- [23] E. S. Piekos and K. Breuer, “DSMC modeling of micromechanical devices,” in *AIAA Thermophysics Conference June 19-22*.
- [24] S. Colin, P. Lalonde, and R. Caen, “Validation of a Second-Order Slip Flow Model in Rectangular Microchannels,” *Heat Transf. Eng.*, vol. 25, no. 3, pp. 23–30, Apr. 2004.
- [25] B. Cetin and O. Bayer, “Evaluation of Nusselt Number for flow in a Microtube using Second-Order Slip Model,” vol. 15, pp. 103–109, 2011.
- [26] E. Spiegel and G. Veronis, “On the Boussinesq approximation for a compressible fluid,” *Astrophys. J.*, vol. 131, p. 442, 1960.
- [27] E. Lorenz, “Deterministic nonperiodic flow,” *J. Atmos. Sci.*, vol. 20, p. 130, 1963.
- [28] M. Cross, “Onset of Rayleigh-Bénard Convection : No-slip Boundaries,” 2006. .
- [29] N. G. Hadjiconstantinou, “The limits of Navier-Stokes theory and kinetic extensions for describing small-scale gaseous hydrodynamics,” *Phys. Fluids*, vol. 18, no. 11, p. 111301, 2006.

## Chapter 5

### 5 Conclusions

#### 5.1 Conclusion

This thesis has examined the effects of non-Fourier heat transfer on the natural convection of fluids in a Rayleigh-Bénard configuration. Single-phase-lagging effects were considered where a single relaxation time  $\tau$  governs the response of the heat flux to changes in the temperature gradient. Non-Fourier heat transfer has been discussed to have significance in a multitude of areas such as nanofluids [1], low temperature liquids [2], [3], and liquid metals [4]. Arguably the most natural application appears to be in gases at small length scales, large mean free path, or more specifically by large Knudsen number. Typically, non-Fourier heat transfer at small length scales is described by the extended transport equations for the heat flux from kinetic theory. These equations, such those developed from the Chapman-Enskog [5] method or Grad's 13 moment method [6], are highly non-linear and complex equations that are not always well behaved or well defined. In this thesis, we have employed the frame indifferent Cattaneo-Vernotte equation, derived through Oldroyd's upper-convected derivative, to represent non-Fourier effects. Use of this derivative has proven to be effective in the modeling of non-Newtonian behaviour in viscoelastic fluids which is also anticipated by kinetic theory. Parallels between non-Fourier and non-Newtonian heat transfer have been drawn in this work.

Through linear stability analysis, we show that non-Fourier fluids can lose the stability of their steady conduction state to either stationary or oscillatory convection. When the

Cattaneo number,  $C = \frac{\tau\kappa}{D^2}$ , is small, the neutral stability curve is comprised of a Fourier

branch and an oscillatory non-Fourier branch. In this case, the fluid is defined as weakly non-Fourier, and stability is lost via the minimum of the Fourier stability curve ( $Ra_{cF} \approx 657$ ), yielding stationary convection. As  $C$  increases to a critical value,  $C_H$ , both stationary and oscillatory convection become equally probable, leading to the existence of a bi-stable mode which has been observed in experiment [7], [8]. For  $C > C_H$ ,

oscillatory convection via a Hopf bifurcation is expected at a Rayleigh number that is less than that of a Fourier fluid. The oscillatory roll size is found to grow with the level of non-Fourier character. The frequency of oscillation decreases with roll size, however, a non-monotonic response is expected with respect to  $C$ . Unlike a Fourier fluid, the Prandtl number is expected to have an influence on the linear stability of non-Fourier fluids. An increase in  $Pr$  increases the likelihood of instability occurring via an oscillatory branch, however this effect becomes insignificant for  $Pr > 10$ .

By non-linear steady state analysis, we have shown that the convection amplitude of weakly non-Fourier fluids is greater than that of a Fourier fluid near the onset of convection. As  $Ra$  increases, however, the convection amplitude of a Fourier fluid can exceed that of a non-Fourier fluid. Despite this fact, we find that the Nusselt number calculated for a non-Fourier fluid is always larger than that of a Fourier fluid which is in agreement with experimental results and analysis for natural convection around MEMS devices [9]. Eventually, as  $C$  increases past a critical value, the bifurcation to convection changes from supercritical to subcritical. As a result, the conduction state is no longer stable to large perturbations at values of  $Ra$  below the Fourier bifurcation point.

A linear stability analysis of the steady convection state of a weakly non-Fourier fluid was also performed. This revealed that stability is lost via a Hopf bifurcation and at a Rayleigh number lower than the Fourier limit. If  $C$  is increased sufficiently, the steady convection state can lose its stability for  $Ra$  less than the bifurcation from the conduction state. As a result, there is no possible steady convection state that can be reached from small perturbations to the conduction state, which could not be predicted by linear stability analysis.

We have also examined the effects of partial-slip boundary conditions on linear stability of the Rayleigh-Bénard configuration. This too is a consequence of high  $Kn$ , affecting both the value of the velocity and temperature of the fluid at the boundaries. First- and second-order hydrodynamic slip and temperature jump were considered at the boundaries and different types of coefficients were explored, exclusive of non-Fourier effects.

First-order hydrodynamic slip and temperature jump were explored first, both leading to a reduction in the minimum critical Rayleigh number and corresponding critical wave number. The effects of the temperature jump boundary condition were analogously explained as a hydrodynamic slip in order to understand how they reduce the critical conditions for instability.

Second-order hydrodynamics slip effects were also explored. As the coefficients are largely empirical, both positive and negative values were analyzed. Although  $a_2 < 0$  was shown to further reduce the stresses at the boundary and reduce the criteria for instability,  $a_2 > 0$  yielded asymptotic behaviour which is assumed to be unphysical. The difference between first- and second-order effects became pronounced near the end of the slip flow regime where  $Kn \approx 0.1$ .

Second-order temperature jump was shown to be irrelevant to the problem when the assumption of isothermal plates is used.

## 5.2 Future Work

The combination of second-order boundary conditions with non-Fourier effects was not considered in this thesis, but is encouraged in order to push the applicability of continuum models into higher  $Kn$  territory, such as in the transition regime where  $Kn > 0.1$ . Here, the Cattaneo-Vernotte non-Fourier model should be considered as well. The breakdown of the Boussinesq approximation as well as the Newtonian stress assumption are also expected in smaller scale applications and thus it may be enlightening to combine as many of these effects as possible. Furthermore, the diffusion term has been left out of the conservation of energy equation. Although this assumption is appropriate for macroscale systems, as the length scale approaches the microscale and nanoscale, this term may need to be considered.

Additionally, an improvement to the relationship between a dual-phase fluid and a dual-phase-lagging fluid as proposed by Wang [1] should be attempted. Although this connection is enlightening, it is limited to the conduction of dual-phase and dual-phase-lagging fluids. It may be necessary to repeat this process for a nanofluid subject to



convection as well to see if the connection can still be made to non-Fourier fluids. Then, in order to more thoroughly explore non-Fourier effects in nanofluids, a dual-phase-lagging non-Fourier equation should be employed.

Finally, it may be of interest to explore the path to chaos and the attractors associated with non-Fourier heat transfer and partial slip boundary conditions. The modelling technique employed in this thesis is the same as was employed by Lorenz [10], where chaos was first investigated. This would also be interesting due to the similarities with viscoelastic models where exploration of the path to chaos and its attractors has been done [11], [12].

### 5.3 References

- [1] L. Wang and X. Wei, "Equivalence between dual-phase-lagging and two-phase-system heat conduction processes," *Int. J. Heat Mass Transf.*, vol. 51, no. 7–8, pp. 1751–1756, Apr. 2008.
- [2] H. Liepmann and G. Laguna, "Nonlinear interactions in the fluid mechanics of helium II," *Annu. Rev. Fluid Mech.*, p. 34, 1984.
- [3] R. Donnelly, "The two-fluid theory and second sound in liquid helium," *Phys. Today*, no. October, p. 34, 2009.
- [4] M. Niknami, R. E. Khayat, D. F. Stranges, and R. M. H. Khorasany, "On non-Fourier effects in macro- and micro-scale non-isothermal flow of liquids and gases," *Interfacial Phenom. Heat Transf.*
- [5] S. Chapman and T. . Cowling, *The Mathematical Theory of Non-Uniform Gases*. Cambridge: Cambridge University Press, 1970.
- [6] H. Grad, "On the kinetic theory of rarefied gases," *Commun. Pure Appl. Math.*, vol. 2, no. 4, pp. 331–407, 1949.

- [7] G. Donzelli, R. Cerbino, and A. Vailati, “Bistable Heat Transfer in a Nanofluid,” *Phys. Rev. Lett.*, vol. 102, no. 10, p. 104503, Mar. 2009.
- [8] Y. Yamanaka and K. Kakimoto, “Rayleigh–Benard oscillatory natural convection of liquid gallium heated from below,” *Chem. Eng. ...*, vol. 71, pp. 201–205, 1998.
- [9] Z. Y. Guo and Z. X. Li, “Size effect on microscale single-phase flow and heat transfer,” *Int. J. Heat Mass Transf.*, vol. 46, no. 1, pp. 149–159, Jan. 2003.
- [10] E. Lorenz, “Deterministic nonperiodic flow,” *J. Atmos. Sci.*, vol. 20, p. 130, 1963.
- [11] R. E. Khayat, “Chaos and overstability in the thermal convection of viscoelastic fluids,” *J. Nonnewton. Fluid Mech.*, vol. 53, pp. 227–255, Jul. 1994.
- [12] R. Khayat, “Fluid elasticity and the transition to chaos in thermal convection,” *Phys. Rev. E*, 1995.

## Curriculum Vitae

<b>Name:</b>	Daniel Stranges
<b>Post-secondary Education and Degrees:</b>	<p>The University of Western Ontario London, Ontario, Canada 2006-2010 B.E.Sc.</p> <p>The University of Western Ontario London, Ontario, Canada 2010-present Ph.D.</p>
<b>Honours and Awards:</b>	Honours Student 2006-2007, 2007-2008, 2008-2009, 2009-2010
<b>Related Work Experience</b>	<p>Teaching Assistant The University of Western Ontario 2010-2014</p> <p>Research Assistant The University of Western Ontario 2010-2014</p>

### **Publications:**

R.E. Khayat, D.F. Stranges, R. Khorasany, M. Niknami and B. Albaalbaki, Thermal Convection of Nanofluids: A Non-Fourier Perspective and Linear Stability Analysis, Proceedings of the World Congress on Engineering (2012)

D.F. Stranges, R.E. Khayat and B. Albaalbaki, "Thermal convection of non-Fourier fluids. Linear Stability," *Int. J. Thermal Sci.*, vol. 74, pp. 14-23, 2013.

D.F. Stranges, John R. de Bruyn, and R.E. Khayat, Thermal convection of fluids with non-Fourier heat transport, unpublished results.

D.F. Stranges, John R. De Bruyn and R.E. Khayat, The influence of second order partial slip boundary conditions on thermal convection, unpublished results.

M. Niknami, R.E. Khayat, D.F. Stranges and R.M.H. Khorasany, "On non-Fourier effects in macro and micro-scale non-isothermal flow of liquids and gases," *Interfacial Phenomena and Heat Transfer* (2014), in review.